CHALMERS
UNIVERSITY OF TECHNOLOGY

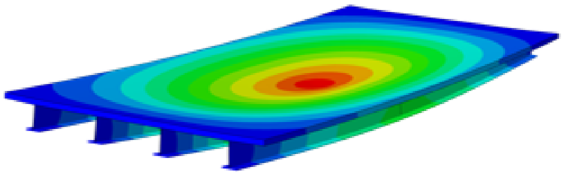

Structural Modeling for Preliminary Design of Steel-Concrete Composite Bridges

Master’s thesis in Master’s Programme Structural Engineering and Building Technology

Hugo Elmelid

Albin Bergh

DEPARTMENT OF ARCHITECTURE AND CIVIL ENGINEERING
Division of Structural Engineering

CHALMERS UNIVERSITY OF TECHNOLOGY
Master’s thesis ACEX30
Gothenburg, Sweden 2026

MASTER'S THESIS ACEX30

Structural Modeling for Preliminary Design of Steel-Concrete Composite Bridges

Master's Thesis in the Master's Programme Structural Engineering and Building Technology

Hugo Elmelid
Albin Bergh

Department of Architecture and Civil Engineering
Division of Structural Engineering
CHALMERS UNIVERSITY OF TECHNOLOGY
Gothenburg, Sweden 2026

Structural Modeling for Preliminary Design of Steel-Concrete Composite Bridges
Master's Thesis in the Master's Programme Structural Engineering and Building Technology

Hugo Elmelid

Albin Bergh

Supervisor: Ivar Nilsson, ELU Konsult AB
Co-supervisor and Examiner: Mohammad al-Emrani, Department of Architecture and Civil Engineering
Technical Guidance: Christoffer Svedholm, ELU Konsult AB

Examensarbete ACEX30
Institutionen för Arkitektur och Samhällsbyggnadsteknik
Chalmers Tekniska Högskola, 2026

Department of Architecture and Civil Engineering
Division of Structural Engineering
Chalmers University of Technology
SE-412 96 Göteborg
Sweden
Telephone +46 31 772 1000

Cover: Twin-girder steel-concrete composite bridge on the left and the deflected shape from the shell model analysis on the right.

Department of Architecture and Civil Engineering
Göteborg, Sweden, 2026

Structural Modeling for Preliminary Design of Steel-Concrete Composite Bridges
Master's thesis in the Master's Programme Structural Engineering and Building Technology

Hugo Elmelid

Albin Bergh

Department of Architecture and Civil Engineering
Division of Structural Engineering
Chalmers University of Technology

ABSTRACT

The preliminary design of steel-concrete composite bridges must be completed in a limited time frame, often representing a small fraction of the time allocated to the final design. This requires fast and accurate methods for estimating load effects, member dimensions, and material quantities. At the same time, preliminary estimates must remain consistent with the final design while being competitive in bidding.

This study evaluates modeling approaches for determining load effects using Brigade/-Plus and investigates methods for preliminary cross-section design. A literature study was conducted to identify relevant modeling approaches, followed by a case study of a steel-concrete composite bridge in Akalla. Three main modeling approaches were examined: a shell model, a grillage model, and three-beam-element-based models. The approaches were assessed with respect to accuracy, computational efficiency, and suitability for preliminary design.

The results show that a transverse beam model with vertical springs in combination with a longitudinal beam model is the most suitable modeling approach for preliminary design. Although conservative, the model provides a favorable balance between accuracy, simplicity, and computational efficiency. The study further demonstrates that the model could be improved by considering the spread of the load through the concrete slab using distribution angles. By updating the model by incorporating the resulting effective widths, material consumption was reduced by up to 17% compared to the original model. Furthermore, adjusting the slab strip width proved more effective than modifying the spring stiffness alone. The greatest improvements were observed in cases where fatigue governed the design.

The proposed modeling approach provides a practical workflow for preliminary design, enabling more accurate estimations of material quantities during the limited time frame.

Keywords: Steel-concrete composite bridges, preliminary design, load distribution factors, transverse beam model, structural modeling

Strukturmodellering för preliminär dimensionering av samverkansbroar i stål och betong
Examensarbete inom masterprogrammet konstruktionsteknik och byggnadsteknologi

Hugo Elmelid

Albin Bergh

Institutionen för arkitektur och samhällsbyggnadsteknik
Avdelningen för Konstruktionsteknik
Chalmers tekniska högskola

SAMMANFATTNING

Den preliminära dimensioneringen av samverkansbroar i stål och betong måste genomföras inom en begränsad tidsram och utgör ofta endast en liten del av den tid som avsätts för den slutliga dimensioneringen. Detta ställer krav på snabba och tillförlitliga metoder för att uppskatta lasteffekter, konstruktionsdimensioner och materialmängder. Samtidigt måste de preliminära uppskattningarna vara representativa för den slutliga konstruktionen och samtidigt möjliggöra konkurrenskraftiga anbud.

I denna studie utvärderas modelleringsmetoder för bestämning av snittkrafter i Brigade/-Plus samt metoder för preliminär tvärsnittsdimensionering. En litteraturstudie genomfördes för att identifiera relevanta modelleringsmetoder, följt av en fallstudie av en samverkansbro i stål och betong i Akalla. Tre huvudsakliga modelleringsmetoder undersöktes: en skalmodell, en balkrostmodell samt tre balkelement-baserade modeller. Metoderna utvärderades med avseende på noggrannhet, beräkningseffektivitet och lämplighet för preliminär dimensionering.

Resultaten visar att en transversell balkmodell med vertikala fjädrar i kombination med en longitudinell balkmodell är den mest lämpliga modelleringsmetoden för preliminär dimensionering. Trots att modellen är konservativ erbjuder den en gynnsam balans mellan noggrannhet, enkelhet och beräkningseffektivitet. Studien visar vidare att modellen kan förbättras genom att beakta lastens spridning genom betongplattan med hjälp av spridningsvinklar. Genom att inkludera de resulterande effektiva bredderna kunde modellen uppdateras och materialåtgången reduceras med upp till 17 % jämfört med den ursprungliga modellen. Vidare visade det sig att en anpassning av plattstrimlans bredd var mer effektiv än att enbart modifiera fjäderstyvheten. De största förbättringarna observerades i de fall där utmattning var dimensionerande.

Den föreslagna modelleringsmetoden erbjuder ett praktiskt arbetsflöde för preliminär dimensionering och möjliggör mer träffsäkra uppskattningar av materialmängder inom den begränsade tid som står till förfogande.

Nyckelord: Samverkansbroar i stål och betong, preliminär dimensionering, filfaktorer, transversella balkmodeller, strukturmodellering

Contents

Preface

In this thesis, a study of the structural modeling for the preliminary design of steel concrete composite bridges has been carried out. The project was done during the spring of 2026 at the Division of Structural Engineering at Chalmers University of Technology, Sweden, in collaboration with ELU Konsult AB.

First and foremost, we would like to thank our co-supervisor and examiner, Professor Mohammad al-Emrani at Chalmers University of Technology, for his valuable input and feedback throughout this project. We would also like to express our gratitude to our supervisor at ELU, Ivar Nilsson, for his patience and excellent supervision in our daily work. Furthermore, we extend our thanks to Christoffer Svedholm at ELU for his invaluable input and technical guidance. The feedback from all of you has been greatly appreciated, and your expertise in the field has had a significant positive impact on the project. Lastly, we wish to thank ELU Konsult for providing a supportive and inspiring working environment.

Gothenburg, June 2026
Hugo Elmelid
Albin Bergh

List of Figures

List of Tables

Notations

Abbreviations

B1-4	Beams 1 - 4
c/c	Center to center distance
CG	Center of Gravity
CSC	Cross-Section Class
EC	Eurocode
EN	European Standard
FEM	Finite Element Method
FLM	Fatigue Load Model
FLS	Fatigue Limit State
HPS	High Performance Steel
JASBC	Japan Association of Steel Bridge Construction
LDF	Load Distribution Factor
LM	Load Model
LT	Lateral Torsional
MS	Mild Steel
RH	Relative Humidity
SIS	Swedish Institute for Standards
SLS	Serviceability Limit State
SS	Swedish Standard
TSFS	Transportstyrelsens föreskrifter och allmänna råd om tillämpning av eurokoder
UDL	Uniformly Distributed Load
ULS	Ultimate Limit State

Greek letters

α	load spreading angle
α_T	expansion coefficient
γ	partial factor
δ	vertical deflection
$\Delta\sigma_E$	equivalent stress range
ΔT	temperature difference
ϵ_{cs}	shrinkage strain in concrete
η_b	utilization rate in bending
η_i	transverse influence line ordinate
η_v	utilization rate in shear
λ	damage equivalence factor
σ_c	concrete stress
σ_{steel}	steel stress
χ_{LT}	lateral torsional buckling reduction factor
ϕ	rebar diameter
ϕ_{studs}	studs diameter

Roman upper case letters

A_{post}	area of vertical posts
D	superstructure depth
D_{lower}	lower bound of upper sieve size
E	modulus of elasticity
EI	cross-section stiffness
G	modulus of rigidity
$G1.1$	construction stage 1 in structural analysis
$G1.2$	stage when formwork and construction loads are removed in structural analysis
$G2$	stage when pavement is applied in structural analysis
I_i	vertical moment of inertia
I_t	torsional moment of inertia
IF	intensity factor
J	torsional rigidity
L	span length
L_{eq}	equivalent span length
L_x	transverse element spacing
L_y	longitudinal element spacing
M	bending moment
N_{OBS}	number of heavy lorries per year
P	point load
P_{long}	point load applied in longitudinal model
Q_k	vehicle axle load
Q_{m1}	gross weight of one lorry
R	reaction force
S	girder spacing
V	shear force
$W_{roadway}$	roadway width

Roman lower case letters

b_c	width of concrete slab
b_{fo}	width of upper flange
b_{fu}	width of lower flange
e	eccentricity
e_D	distance between flange edge and stud
f_{ck}	characteristic cylinder compressive strength
$f_{ck,cube}$	characteristic cube compressive strength
f_{yd}	design yield strength of steel
g	gravitational acceleration
h_a	height of steel girder
h_c	height of concrete slab
h_w	height of web
k	spring stiffness
k_t	torsional spring stiffness
k_v	vertical spring stiffness

n	number of girders
n_L	long-term modular ratio
q	distributed load
q_{long}	distributed load applied in longitudinal model
s	spacing
t_c	concrete slab thickness
t_{fo}	thickness of upper flange
t_{fu}	thickness of lower flange
t_w	thickness of web
x_i	distance to center of gravity of girders

1 Introduction

1.1 Background

A steel-concrete composite bridge is a structural concept in which the advantages of steel and concrete are utilized to create a bridge that is both lightweight and robust. As concrete exhibits high compressive strength and steel offers high tensile strength, the structural system is arranged so that each material resists the forces for which it is best suited. The arrangement consists of steel girders with a concrete slab on top that is connected via shear connectors to ensure interaction.

The bridge design process begins with procurement, during which tenders submit their design bids. The design process at this stage usually only lasts for a few days, representing just a fraction of what is used in the final design, where all the details are thoroughly reviewed. The purpose of preliminary sizing is to determine rough dimensions that can be used as a basis for cost estimates. However, despite the limited time for these early design stages, the material quantities must align with those of the final design while being as low as possible to ensure competitive bidding and a successful project.

There are different approaches to structural modeling in preliminary design to determine the load effects, leading to a wide range of cost estimates. This highlights the need for an optimized process to minimize material quantities, thus reducing costs and environmental footprint. In addition, a new Eurocode has been published and is to be implemented, providing new rules for the design of composite bridges. It is therefore of interest to apply these regulations to the design carried out in this thesis.

1.2 Aim

This project aimed to develop recommendations for the preliminary design of steel-concrete composite bridges. First, the most suitable structural model for preliminary design was determined. Secondly, the model was analyzed for improvements to investigate whether it could be better aligned with a detailed modeling technique. Thirdly, workflow charts for structural modeling and cross-sectional analysis were developed. Finally, based on the yielded material quantities, the performance of the proposed method was evaluated.

1.3 Objectives

- Which structural model is most suitable for preliminary design?
- How can existing modeling approaches be improved to better represent the structural behavior?
- How much can material quantities be reduced through improved preliminary design models?
- What is a suitable workflow for preliminary design?

1.4 Method

To achieve the objectives, the project included literature studies and case studies of an existing project. Throughout the project process, meetings were held with experienced engineers and supervisors to provide feedback and guidance.

Initially, a literature study was conducted to establish a theoretical foundation. This included a review of design handbooks, new and old Eurocodes, and scientific papers. In the first step, an understanding of composite bridges, their structural behavior, and how the design process is performed was established. In the second step, a real design process for a composite bridge was studied to gain insight into current preliminary design practices. Based on the design process studied, the influence of the new Eurocode was analyzed, where any changes to the code affecting the design process were noted.

Secondly, a case study was conducted to evaluate the preliminary design methods and the underlying assumptions. In this study, different structural models were compared to identify the most suitable approach to determine the load effects. Subsequently, these were studied to evaluate whether there were opportunities for improvement. Then, a cross-section dimensioning procedure was performed to be able to compare the models based on the material quantities that they yielded.

Finally, a workflow chart was developed with the intention of assisting the designer in a preliminary design process.

1.5 Limitations

The analysis will be limited to the bridge superstructure, excluding supports and other substructures. The primary focus will be on the material quantities of the steel girders; however, the concrete slab will also be considered to a limited extent. The work will be done based on a case study and will therefore be limited to the boundary conditions and traffic type of that case, which will be presented in Section 4.1.

1.6 Use of AI

The thesis has utilized AI as a proofreader, guiding spelling and grammar throughout the report. The used generative models are ChatGPT, Gemini, and Grammarly.

2 Literature studies

In the following chapter, the literature review conducted for this thesis is presented. The chapter begins by introducing the fundamentals of composite bridges as a structural concept, including how they are manufactured. Later, different empirical methods for determining the material quantities are presented. After that, different structural modeling approaches of different complexity are reviewed. Finally, guidance regarding the choice of the number of girders in the bridge cross-section is provided.

2.1 Composite bridges

A steel-concrete composite bridge is a structural concept in which the advantages of steel and concrete are combined to create a bridge that is both lightweight and robust. The arrangement consists of steel girders and a concrete slab that is connected to the girders through shear connectors, creating a composite action between the elements. The connectors are mainly welded studs that allow the concrete deck to be part of the top flange, creating a stiff composite cross-section. By the loading of a positive bending moment, this composite cross-section results in tension in steel and compression in concrete, taking advantage of the qualities of each material (Vayas & Iliopoulos, 2015). Composite bridges are suitable for most bridge spans, with the exception of very long spans (Vayas & Iliopoulos, 2015). Steel-concrete composite bridges are commonly constructed using box girders or twin/multiple I-girders. The designer may vary both the height and thickness of the web as well as the flange dimensions to optimize the girder for the internal forces along the length of the span. However, this does not always lead to lower cost, as additional fabrication work and required bolted or welded connections can increase construction expenses. (ILES, 2014).

2.1.1 Materials

The materials considered for composite bridges in this thesis are steel and concrete. Specifically, structural steel and conventionally reinforced concrete will be used in the design and analysis.

Steel

The steel used in steel-concrete composite bridges typically consists of two primary forms: structural steel forming the main girders of the bridge and reinforcing steel bars placed in the concrete slab. Structural steels are classified according to quality and grade. The European Standard that defines the grades of structural steel is EN 10025. In this system, structural steel is designated with the capital letter S followed by a number representing the yield strength for specimens with a thickness $t \leq 16\,\mathrm{mm}$ in [MPa] (Vayas & Iliopoulos, 2015). This number is followed by one or two symbols representing the material toughness expressed by the minimum Charpy V-notch impact energy. The most common steel grade for bridges is S355 due to its favorable strength-to-cost ratio.

Reinforcing steel is used to resist tensile stresses and to control cracking of the concrete. The European standard that defines reinforcing steel is EN 10080. The most commonly used reinforcement steel is B500B, which has a characteristic yield strength of 500 MPa (Vayas & Iliopoulos, 2015). The first B indicates the reinforcement steel, and the final B is the designated ductility class of the reinforcement. These steel bars are typically ribbed to increase the bond to the surrounding concrete.

Concrete

Normal concrete is characterized by the letter C followed by two numbers representing the characteristic cylinder strength, f_{ck}, and the cube strength, $f_{ck,cube}$ at 28 days. According to SS-EN 1994-2:2005, concrete used in composite bridges should have a strength class between C20/25 and C60/75 (SIS, 2005b). In practice, the most commonly used strength class for the bridge deck is C35/45, which means a cylinder strength of 35 MPa and a cube strength of 45 MPa (Vayas & Iliopoulos, 2015). Concrete is also susceptible to long-term effects such as creep and shrinkage. These reduce the effective stiffness of the material, which therefore requires the use of an effective modulus of elasticity in the structural analysis.

Shear connectors

Shear connectors allow the steel-concrete cross-section to act as a stiff composite section by ensuring force transfer at the interface between the two materials. Without shear connectors, slip would occur at relatively low stress levels at the steel-concrete interface. There are two forms of connectors: flexible and rigid. Flexible connectors, such as headed studs, have ductile behavior that allows significant slip before failure in ULS. These are the most common on bridges, and the design provisions in SS-EN 1994-1-1:2005 are based on the assumption that such ductile connectors are used (Collings, 2013).

Rigid connectors, such as fabricated steel blocks, exhibit more brittle behavior than flexible connectors. Failure can occur either through a fracture of the weld connection between the connector and the girder or by local crushing of the concrete (Collings, 2013).

2.1.2 Number of girders

The designer has to choose whether to use a twin or multiple girder configuration. Multi-girder composite bridges are commonly used for spans up to approximately 50 m (Vayas & Iliopoulos, 2015). For longer spans, twin-girder bridges are often more cost-effective and easier to construct. However, such systems are less redundant than multi-girder structures and may therefore be more sensitive to fatigue. In addition, an even number of girders is generally preferred, as this facilitates erection by allowing girders to be paired. Although an odd number of girders can be used, additional measures are required during construction to accommodate the unpaired girder (El Sarraf et al., 2013).

Generally, twin-girder bridges require less steel than four-girder alternatives, with the greatest differences occurring at small structural widths, although this difference decreases as the width of the structure increases (Gocál & Duršová, 2012). However, the twin-girder configuration may not always be ideal. As the transverse span length increases with a reduced number of girders, the transverse reinforcement amount and concrete depth may subsequently increase the overall material consumption, compared to a multi-girder configuration. In addition to material consumption, the girder depth is an important design parameter, as many bridges are limited by a maximum structural height. The depth-to-span ratio of twin girder bridges typically ranges between L/19 and L/12, while multi-girder bridges generally range between L/21 and L/18, resulting in lower structural heights (Gocál & Duršová, 2012).

The designer must also determine the layout of the steel girders, including their spacing and location. For highway bridges, the girder spacing is typically in the range of 2-4 m (Collings, 2013). Within this range, the transverse bending moments in the concrete slab are relatively insensitive to spacing, at least for multi-girder bridge decks. For cast-in-situ slabs, the maximum girder spacing is typically limited to approximately 4.1 m, or alternatively by the ratio between the girder spacing and the slab thickness, given by FHWA (2015) in Equation 2.1.

$$\frac{S}{t_c} = 18 \tag{2.1}$$

Increasing the girder spacing generally leads to a thicker slab, higher reinforcement requirements, and higher casting costs. Consequently, the spacing and number of girders should be selected to limit the transverse span of the slab and avoid inefficient slab design.

Thus, the selection of the girder spacing and the number of girders represents a balance between structural efficiency, constructability, and cost.

2.1.3 Manufacturing

Steel girder fabrication is preferably carried out in a fabrication shop rather than on site. The advantage of this approach is that the welds can be produced using welding robots, resulting in a more consistent weld quality (Lebet & Hirt, 2013).

To reduce the amount of steel used, the girders can be optimized by varying the plate thickness depending on the load demand at a given section. However, each change in cross-section requires a weld to connect the sections, and the cost of this weld may exceed the monetary savings achieved from reducing the amount of steel. Since labor costs are relatively high in Europe and Sweden, the additional labor required for such optimization may outweigh the savings from the reduced material usage. Therefore, achieving an economical bridge design requires a careful balance between reducing material use and minimizing fabrication costs.

2.1.4 Erection

The choice of erection method is an important aspect to consider, as it defines the load history of the structure, thus influencing the evolution of stresses and deformations. These construction phases must be taken into account in the structural analysis. When concrete is poured and has not yet hardened, steel girders carry the entire weight of the bridge, the wet concrete, the formwork, and any additional loads acting on the bridge during this stage. This may represent the governing load case due to the risk of lateral torsional buckling. However, when the concrete hardens, and a composite section is formed, the top flange, which is at the highest risk of buckling, can be considered laterally stable, as per SS-EN 1994-2 6.4.1(1) (SIS, 2005b).

During erection, certain combinations of loads may occur that would not arise simultaneously during the service stage of the structure (Lebet & Hirt, 2013). However, these conditions are highly dependent on the selected erection method and construction procedure. Some commonly used erection methods are presented below.

Lifting by cranes

The structural elements can be lifted into place by cranes. This method is generally the most economical solution for small- and medium-span bridges. Heavier elements can be lifted by using the cranes in tandem, this can be especially helpful when the erection has to be performed in a limited time frame. However, this may increase the overall cost considerably (Vayas & Iliopoulos, 2015).

Launching

This method involves the use of rollers or sliders to launch the steel structure to its final position. The rollers and sliders are placed on the supports, and any temporary supports are required for longer spans. An important aspect to consider during launch is the structural stability. There is a risk of plate buckling due to bending, shear, or reaction forces at the supports, and therefore measures to prevent such instability must be investigated prior to erection (Vayas & Iliopoulos, 2015).

Shifting

This concept consists of fully constructing the steel structure on temporary supports adjacent to its final position. Once constructed, the structure is moved transversely into its permanent position using rollers. This method is often used in combination with launching because it allows for short traffic interruptions and provides good stability of the structure, as the structure remains in its final structural configuration during the movement (Vayas & Iliopoulos, 2015). However, this method may be difficult to implement in urban areas due to the limited available space.

Segmental construction

This method is also known as the cantilever method. The concept is to lift steel segments to their final elevation and weld them together while suspended in place, typically by using cranes.

Concreting sequence

The methods described above refer to the erection of the steel structure. The sequence of concreting the deck slab must also be considered. According to Vayas and Iliopoulos (2015), bridges with simply supported spans up to 25 m can be concreted in one stage, while longer single spans are cast in several stages to limit the stress in the steel girders caused by the weight of the wet concrete. Typically, the concrete is first cast in the midspan region and subsequently near the supports. In this way, the middle region, which experiences the highest stresses, already acts as a composite section when the ends are cast.

For continuous bridges, the deck slab is cast in stages in order to limit negative bending moments and thus avoid tensile stresses in the concrete.

2.2 Empirical estimation of material quantities

As mentioned previously, time is often limited during the preliminary design phase, and empirical diagrams and formulas provide a simple and efficient means of estimating steel quantities without the need to conduct a full structural analysis. However, multiple sources of such empirical estimates exist, as they depend on national design codes and the applicable regulatory framework. In addition, most bridges are subject to project-specific demands and geographical conditions, making each structure slightly different from a comparable bridge in another context. Consequently, it may be difficult to accurately predict the exact steel tonnage. However, diagrams and formulas such as those presented in the following section can provide a reasonable first approximation.

2.2.1 Empirical diagrams

Figure 2.1 presents the typical steel tonnage for steel plate girder bridges in the UK. These values are based on designs according to the Eurocodes and the UK National Annex with live loads defined by Load Model 1 (LM1). The analyzed bridge has a carriageway width of 7.3 m between curbs, corresponding to two traffic lanes, and the remaining area is subject to a uniformly distributed load (UDL) (Collings, 2013). For the purposes of this thesis, the most relevant results are those regarding highway bridges, represented by the gray diamond markers in Figure 2.1.

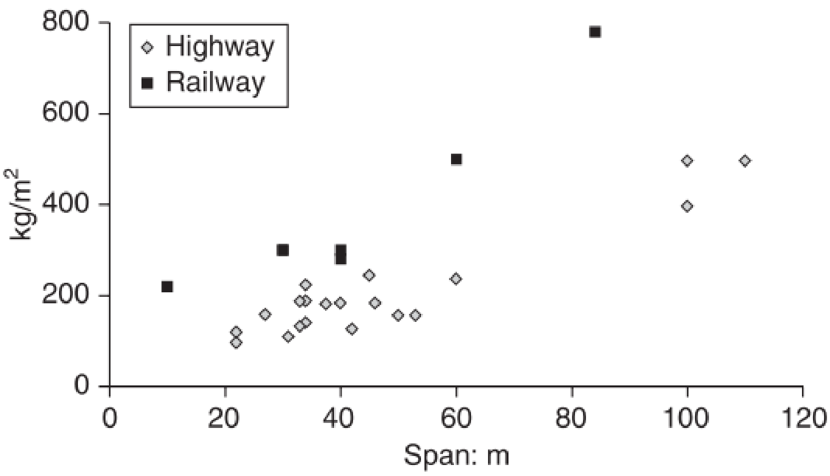

Figure 2.1: Steel weight per m^2 of deck for different spans, from Collings (2013).

As illustrated in Figure 2.1, the steel weight per square meter increases with the length of the span. This trend can be attributed to the higher bending moments and internal forces associated with longer spans, which require a higher structural capacity. Furthermore, railway bridges generally exhibit higher steel weights compared to highway bridges, reflecting the more demanding load requirements for railway traffic.

The increase in steel weight becomes more pronounced in larger spans, particularly for railway bridges, indicating a nonlinear relationship between span length and material demand. Additionally, the significant scatter observed in the mid-span range (30-60 m) highlights the influence of structural system selection, design assumptions, and site-specific conditions on steel consumption.

The graphs shown in Figure 2.2 present steel tonnage for various span-to-depth ratios and spans (Khatri et al., 2012). For each of the four graphs, the x-axis represents the variation in superstructure depth. HPS denotes High Performance Steel while MS refers to Mild Steel, corresponding to Fe 590 and Fe 410, respectively. These designations originate from the Indian standards and correspond approximately to S460 and S235-275 in the European system. D represents the total superstructure depth, including the bottom flange, web, haunch, and slab. The bridges forming the basis of these graphs were designed in accordance with the Indian Standards IS 1343:1999 and IS 2062:1999.

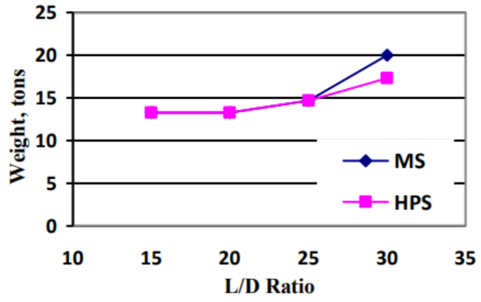

(a) Weights for 40 m span girder

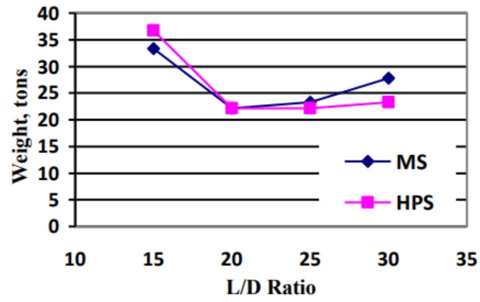

(b) Weights for 50 m span girder

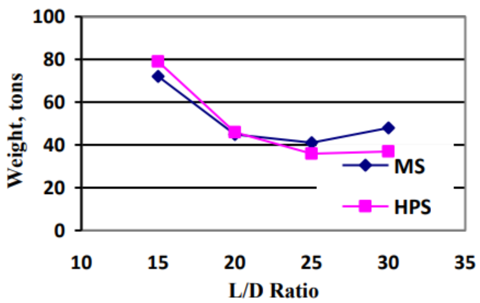

(c) Weights for 60 m span girder

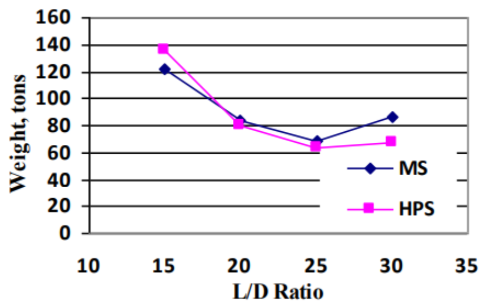

(d) Weights for 70 m span girder

Figure 2.2: Estimate of steel tonnage for different L/D-ratios and spans, from Khatri et al. (2012).

Figure 2.2 indicates an optimal range for the span-to-depth (L/D) ratio, which appears to be between 20 and 25 for all the spans considered, where the required steel tonnage is minimized. Both low and high L/D ratios result in an increase in steel weight, indicating that neither deep nor slender girders are material-efficient. The highest steel weights are generally associated with low L/D ratios.

High-performance steel (HPS) consistently results in lower steel tonnage compared to mild steel (MS), with the exception of the lowest L/D ratios. HPS appears to be particularly favorable for longer spans and non-optimal L/D ratios, where structural demands are more pronounced. Furthermore, for the shorter span (40 m), the steel weight exhibits relatively low sensitivity to variations in the L/D ratio, suggesting that other design criteria govern the structural design in this case.

The estimates of steel weight for different spans presented in Figure 2.3 show a linear relationship between steel weight and span. The data are based on bridges constructed in Japan, designed according to Japanese design standards. The applied live load used for design corresponds to a truck weight of 196 kN. The steel grades used vary, with some bridges constructed using mild steel with a yield strength of 235 MPa, while others use higher grade steels with yield strengths of 340 to 450 MPa. The data originate from annual reports published by the Japan Association of Steel Bridge Construction (JASBC), covering the years 1989-1993, which is the basis for the data presented in Figure 2.3. The graph represents steel weight for simply supported plate girder bridges. The unit of the y-axis, tf/m^2 denotes ton-force per square meter, for example, 0.2 tf/m^2 corresponds to 200 kg/m^2.

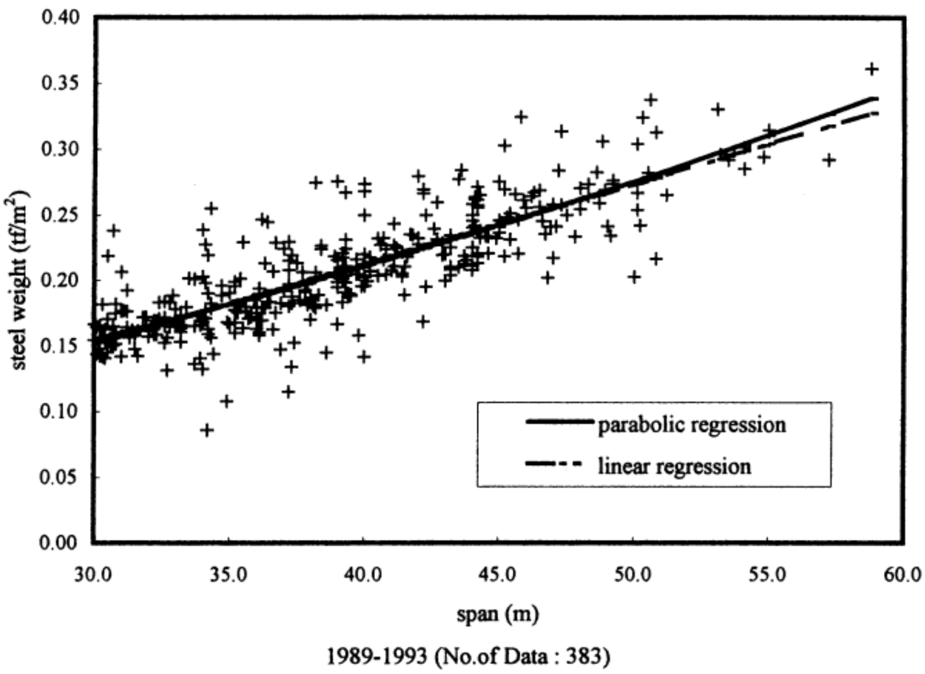

Figure 2.3: Estimate of steel tonnage for different spans, from Chen and Duan (2013).

As shown in Figure 2.3, the steel weight increases approximately linearly with span length. A limited number of outliers can be observed, which may reflect either particularly efficient or inefficient designs, as well as the influence of site-specific conditions and design assumptions.

A clear concentration of observations is present in the range of 30-45 m, while relatively few data points are available for longer spans (e.g., around 60 m). This uneven distribution affects the reliability of the regression analysis. Although both linear and parabolic regression models provide a reasonable fit within the main data range, their divergence at longer spans is likely a consequence of the limited data available in this region, reducing the accuracy of extrapolation.

2.2.2 Empirical formulas, values and tables

The simplest formula to estimate the dimensions of the bridge is a simple span/depth ratio formula. However, it is not guaranteed to be as accurate as the more thorough method to predict the steel quantities used for the bridge. Nonetheless, the methods may still prove to be valuable to the designer. Vayas and Iliopoulos (2015) describes a method to determine steel consumption as well as an estimate of the cross-section dimensions, as shown in Table 2.1.

Table 2.1: Preliminary design of a twin-girder bridge, from Vayas and Iliopoulos (2015).

Length L_{eq} [m]	For isostatic spans $L_{eq} = 1.4L$. For internal spans in continuous systems $$L_{eq} = \frac{2L_i + L_{i+1}}{3}, \quad L_i > L_{i+1}$$ End spans should be multiplied by 1.25. L_i, L_{i+1} are the two longest consecutive spans.
Steel consumption [kg/m^2]	$$G = 63+0.9\,L_{eq}^{1.2}\left(1.34 - \frac{b_c}{40}\right)+\frac{L_{eq}}{4} \quad \text{[kg/m}^2\text{]}$$
Slab reinforcement ratio	$\approx 250\,\text{kg/m}^3$
Girder height (constant depth deck) [m]	$$h_a = \max\left[\frac{L_{eq}}{28}\left(\frac{b_c}{12}\right)^{0.45},\ 0.40 + \frac{L_{eq}}{35}\right]$$
Girder height (variable depth deck) [m]	$$h_a = \frac{L_{eq}}{24} \text{ at support, } h_a = \frac{L_{eq}}{36} \text{ at midspan}$$
Slab thickness [m]	$$h_c = \frac{b_c - a}{26} + 0.13 \text{ at main girders}$$ $$h_c = \frac{a}{50} + 0.12 \text{ at deck center}$$
Main girder c-c distance [m]	$$a \approx 0.55b_c$$
Bottom flange width [m]	$$b_{fu} = \left(0.25 + \frac{b_c}{40} + \frac{L_{eq}}{125}\right)\cdot\left(0.92 + \frac{b_c}{150}\right)$$
Top flange width [m]	$$b_{fo} = b_{fu} - 0.1 \text{ for a two lane deck}$$ $$b_{fo} = b_{fu} - 0.2 \text{ for a four lane deck}$$

For the preliminary design of the concrete slab, the thickness should, according to Lebet and Hirt (2013), not be less than 240 mm, including the edges of the cantilever. However, Collings (2013) suggests that a minimum slab thickness of 200 mm is enough to ensure adequate concrete cover for the reinforcement. In addition, Collings (2013) provides recommended span/depth ratios for steel girders and concrete slab, as presented in Table 2.2 with geometries according to Figure 2.4.

Table 2.2: Span-depth ratios for structural elements of the bridge, from Collings (2013).

Structural element	Span/depth ratio
Steel girders	18-22
Concrete slab spanning between girders	10-25
Concrete slab cantilevers	5-10

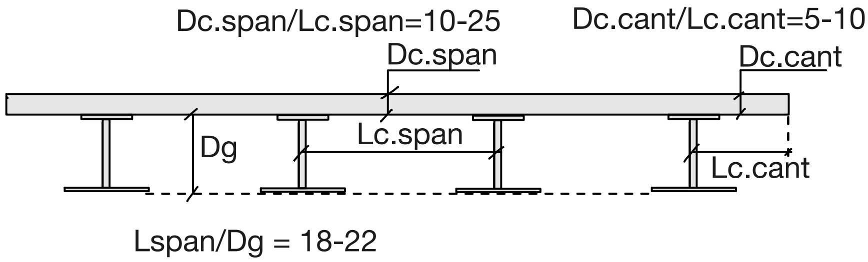

Figure 2.4: Visualization of the structural elements, explaining Table 2.2.

According to El Sarraf et al. (2013), the thickness of the concrete slab can be assumed to be 250 mm during the initial design stage, with a reinforcement layout consisting of $\phi = 20$ mm bars with a top-bottom c-c of 150 mm. ILES (2014) provides a thickness range for the slab of 240-260 mm, with a similar reinforcement layout comprising $\phi = 20$ mm bars with a top-bottom layer spacing of 150 mm.

According to Lebet and Hirt (2013), the longitudinal reinforcement in the concrete slab within a span section is generally about $0.75\% - 1\%$ of the concrete area, whereas the tension reinforcement over an intermediate support can reach to $1\% - 2\%$ of the concrete area.

2.3 Estimating material quantities using structural analysis

To gain a more detailed understanding of the required material quantities, a structural analysis may be performed. Such analyses can be conducted at different levels of detail, where greater detail generally provides a more accurate representation of the structure, but requires more computational power, consequently making it more time-consuming. This section aims to present suitable methods applicable to the preliminary design process, their implementation, and their respective pros and cons.

2.3.1 2D Beam models

One of the simplest ways of analyzing the global behavior of a bridge is using beam models, either through analytical beam theory or, more rigorously, by using FEM with beam elements (Vayas & Iliopoulos, 2015). A beam model analysis can be conducted either in 2D or 3D, where the former is described in the following section, while the latter is described in Section 2.3.2.

The main advantage of a 2D beam model is that it is generally time-efficient due to its low computational cost. Additionally, the results obtained are relatively easy to interpret since sectional forces can be obtained directly as an output, which is convenient when designing according to Eurocode. On the other hand, a disadvantage is that it does not represent the full 3D behavior, meaning that it does not cover the response of elements other than the main beams, such as cross girders and bracings, in one analysis (Vayas & Iliopoulos, 2015). Instead, this method requires the designer to perform multiple analyses to capture the results needed for different parts of the structural system. Furthermore, another disadvantage is that the transverse load distribution has to be determined by a separate model.

To represent a bridge behavior by the use of a beam element, one of the girders in the longitudinal direction is typically analyzed, see Figure 2.5.

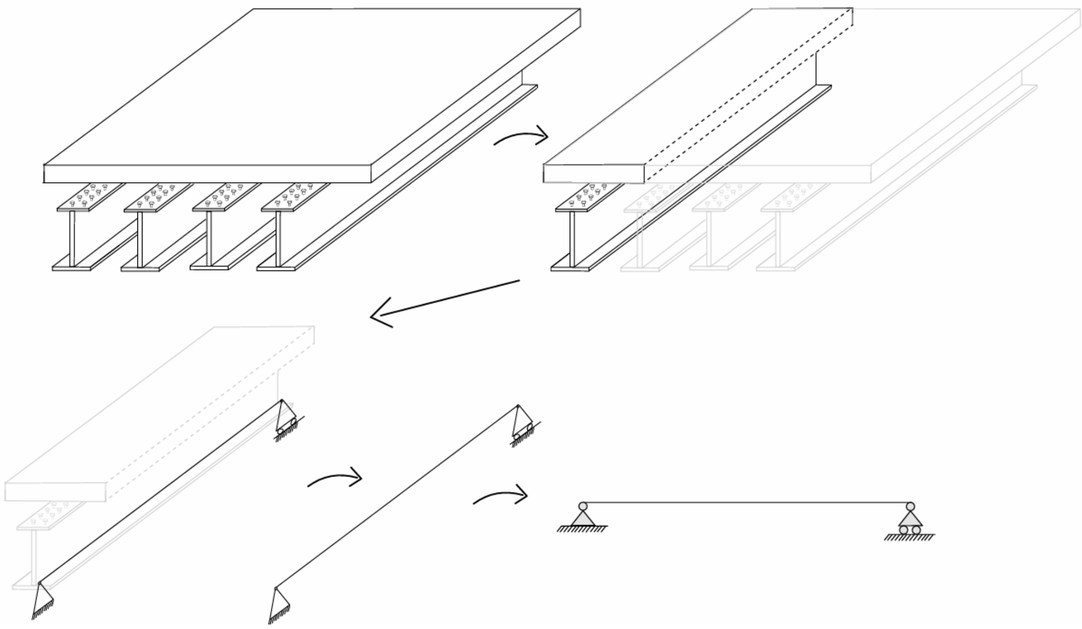

Figure 2.5: Graphical explanation of how to analyze the bridge using 2D beam models.

However, since the model accounts only for the longitudinal direction, the bridge behavior in the transverse direction requires an additional model to describe the load distribution between the beams, which in practice can be done by considering a load distribution factor (LDF). This factor describes the fraction of the total applied load that acts on a specific girder, and is considered in the longitudinal model by scaling its load effects, see Figure 2.6.

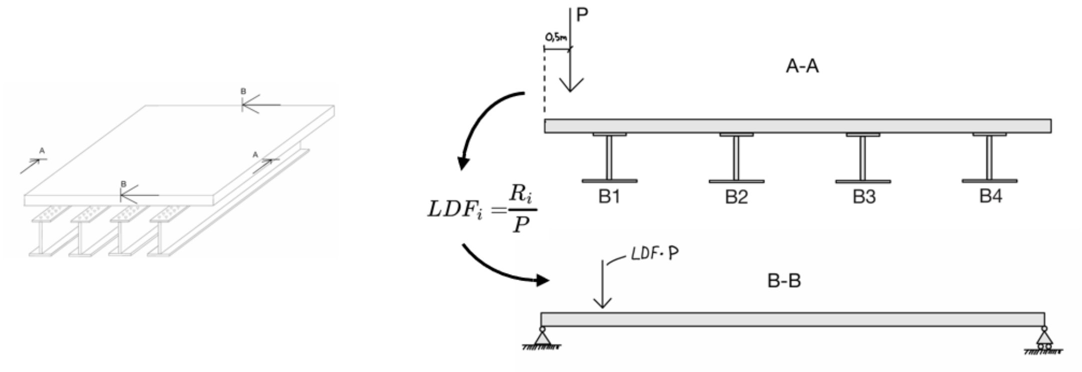

Figure 2.6: The LDF factors is describing the load distribution in the transverse direction and implemented by scaling the load effects in the longitudinal beam model.

The LDF is found as the reaction force in a specific girder in the transverse model, and putting it into relation to the load that is applied in the longitudinal model, yielding the following expression:

$$LDF = \frac{Reaction\ force\ in\ transverse\ model}{Load\ applied\ in\ longitudinal\ model} \tag{2.2}$$

The LDF can be determined by several different methods, where the simplest case is that of twin girder bridges. That is because the system is statically determinate and the distribution of forces is obtained solely from equilibrium equations. However, it gets more complicated in a multiple girder configuration since it is statically indeterminate. Then, other methods are needed which will be presented further down in this section.

2.3.1.1 Twin girder systems - statically determinate

The load distribution for a statically determinate system is solved solely from moment and force equilibrium. An example of how to find the reaction force for a point load F in this case is shown in Figure 2.7.

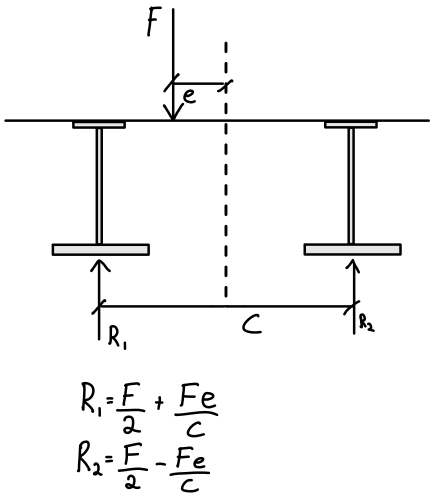

Figure 2.7: Calculation of reaction forces in a statically determinate cross-section to use for calculation of the LDF.

2.3.1.2 Multiple girder systems - statically indeterminate

Composite bridges consisting of a system with multiple girders will be statically indeterminate in their transverse direction. Consequently, the load distribution cannot be solved solely through equilibrium, which necessitates the use of alternative methods. In the following sections, relevant methods to use for determining the LDFs of a multi-girder bridge will be presented and explained.

Lever rule

A straightforward approach to determining the LDF of a multiple-girder system is based on the lever rule. This method assumes hinges in the bridge deck over the girders, meaning that the deck is seen as simply supported over the girders (Ligocki Pedro, 2017). Due to this assumption, the deck becomes statically determinate, and the reaction forces in the girders under a specific loading configuration can be solved solely from static equilibrium, and the methods presented in Section 2.3.1.1 can be utilized. In Figure 2.8, this assumption is visualized.

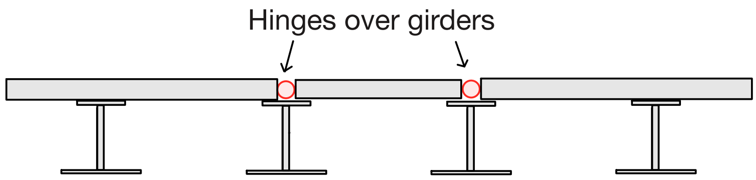

Figure 2.8: Visualization of the lever rule.

Courbon's method

Courbon's method is one of the easiest models to apply, and it generally provides conservative results, making it a suitable method to use in preliminary design (Vayas & Iliopoulos, 2015). The method assumes that, because the transverse stiffness of the deck is substantially higher than the longitudinal stiffness of the beams, the deck will deform while maintaining its geometry, implying that it is treated as rigid. It also assumes that the girders are either flexible in torsion or connected to the slab by means of hinges, and the girders have the same length and can be represented by the cross-section stiffness, EI. This also means that for curved and skewed bridges, the beams are not of the same length, and the method is therefore not applicable in those cases. According to Mohan et al. (2022), the method requires that the span to width ratio should be at least 2 but less than 4.

The results from the method are a transverse influence line that can be used to calculate the reaction force in one of the girders and subsequently the LDF. Vayas and Iliopoulos (2015) gives Equation 2.3 to calculate the transverse influence line ordinates, η_i. The expressions are based on the eccentricity of the load, e, the position of the girder in relation to the girders center of gravity, x_i, and the stiffness of the girders $(EI)_i$. The different distances are specified in Figure 2.9.

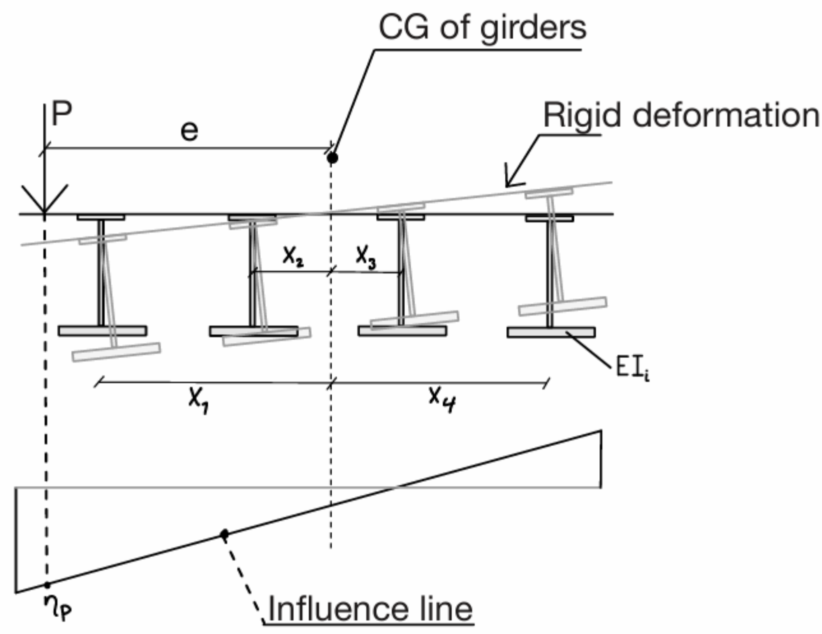

Figure 2.9: Overview of Courbon's method showing the definition of distances, deformed shape, and influence line.

$$\eta_i = \frac{(EI)_i}{\sum(EI)_i} + \frac{(EI)_i \cdot x_i}{\sum[(EI)_i \cdot x_i^2]} \cdot e \tag{2.3}$$

In the case of equal stiffness, $(EI)_i$, in all girders Equation 2.3 can be simplified to:

$$\eta_i = \frac{1}{n} + \frac{x_i}{\sum x_i^2} e \tag{2.4}$$

Where n is the total number of girders.

While this method defines the reaction for a single load, actual traffic models consist of multiple loads. In such cases, the total reaction P_{long} from multiple point loads, P_i, can be calculated by summing the product from multiplying the loads with their corresponding influence line ordinate, $\eta_{p,i}$, determined from Equation 2.3 or Equation 2.4, which yields the following expression given in Equation 2.5.

$$P_{long} = \sum_i (P_i \cdot \eta_{p,i}) \tag{2.5}$$

For loads distributed in the transverse direction, the reaction, q_{long}, should, according to Vayas and Iliopoulos (2015), be calculated by multiplying the applied load in the transverse direction, ($q_{sur,i}$, with the transverse distribution length, $L_{q,i}$, and the mean of the ordinates at both ends of the transverse loads ($\eta_{q1,i}$ and $\eta_{q2,i}$), see Figure 2.10 and Equation 2.6.

$$q_{long} = \sum_i \left(q_{sur,i} \cdot \frac{\eta_{q1,i} + \eta_{q2,i}}{2} \cdot L_{q,i} \right) \tag{2.6}$$

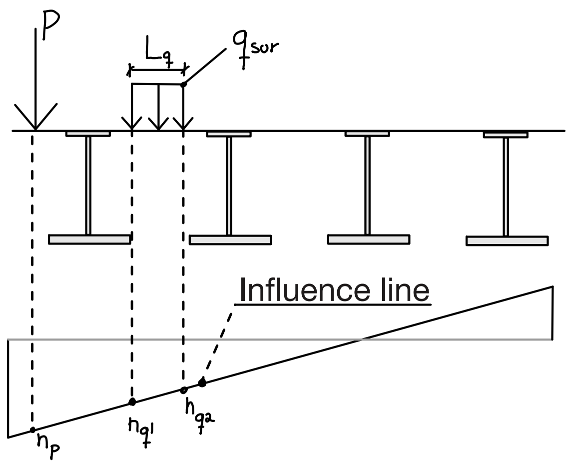

Figure 2.10: Handling of distributed loads according to Courbon's method, redrawn from Vayas and Iliopoulos (2015).

Then, the LDF factor is found by comparing the reaction forces as calculated above with the forces applied in the actual model according to Equation 2.2.

Fauchart method

The Fauchart method can be utilized according to Parra Benítez et al. (2022) in the case of simply supported bridges with multiple girders with constant moment of inertia and without intermediate diaphragms. The method accounts for the transverse flexibility of the deck, which may be a more realistic approach than Courbon's method, which assumes a rigid deck. The method utilizes vertical and rotational springs to represent the composite girders supporting the deck, and their stiffness is calculated according to Equations 2.7 and 2.8.

$$k_v = \left(\frac{\pi}{l}\right)^4 EI_i \tag{2.7}$$

$$k_t = \left(\frac{\pi}{l}\right)^2 GI_t \tag{2.8}$$

Where l is the span length in meters and k_v and k_t are the vertical and rotational stiffness of the springs, respectively. I_i and I_t represent the moment of inertia and the torsional constant of the effective composite cross-section, respectively. E and G are the girder's elastic and shear modulus, respectively. According to Ferreira et al. (2016), the expressions are derived from the differential equation for the elastic line and the differential equation for torsion, using a Fourier sine series to transform these differential equations into the algebraic equations presented above.

The springs are then used in the structural model shown in Figure 2.11.

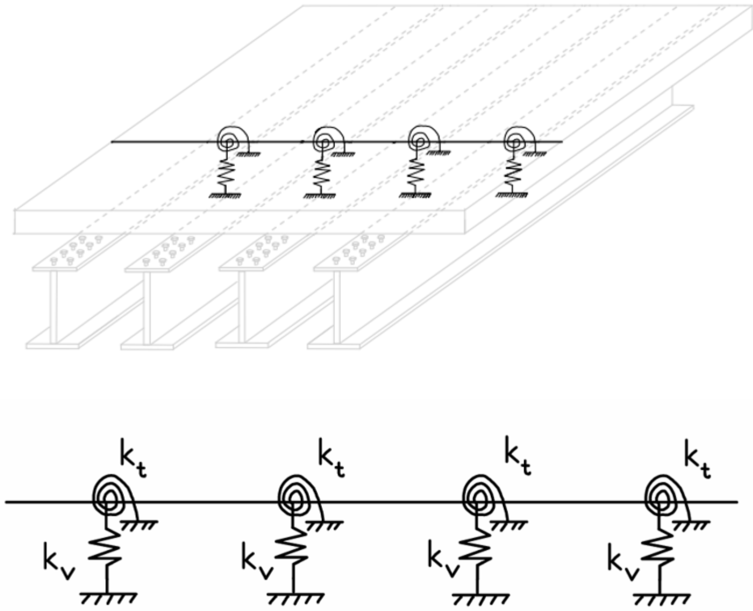

Figure 2.11: Fauchart model.

Henry's method

Another way of determining the LDF is by the use of Henry's method (Yuprasert et al., 2024). This method assumes that all girders share the same load effects, but takes into account the probability of multiple load presences. The method gives the following expression to calculate the LDF:

$$LDF = 1.09 \cdot \frac{W_{roadway}}{3.05} \cdot IF \cdot \left(\frac{2}{n}\right) \tag{2.9}$$

Where $W_{roadway}$ is the width of the roadway, n is the number of girders. IF is the intensity factor which is determined according to Table 2.3.

Table 2.3: Intensity factor, IF, in Henry's method (Yuprasert et al., 2024).

Number of lanes	2	3	> 4
Intensity factor, IF	100%	90%	75%

Transverse beam model with spring supports

Another way of describing the transverse behavior is shown in Figure 2.12 where the girders are modeled as springs. These are in turn supporting a beam element which represents the concrete slab.

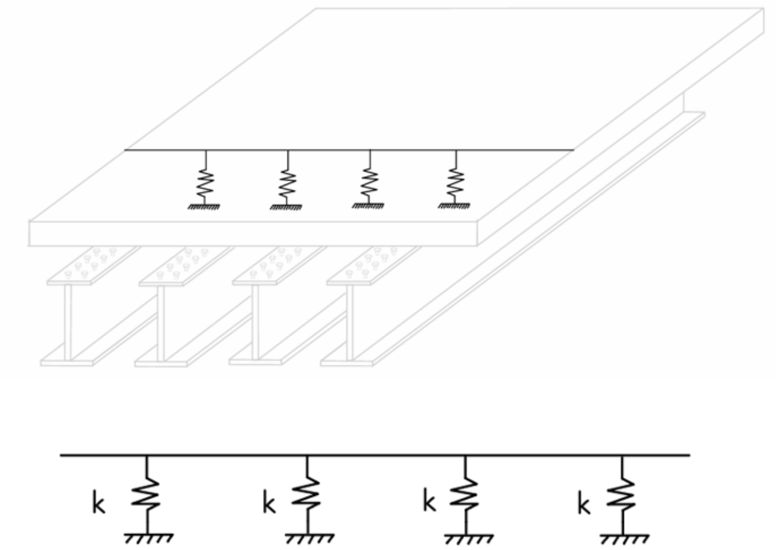

Figure 2.12: Transverse beam model with vertical springs representing the girders supporting the concrete slab.

The spring stiffness is intended to represent the stiffnesses of the girders, which will be proportional to their deflection in the longitudinal direction, see Figure 2.13.

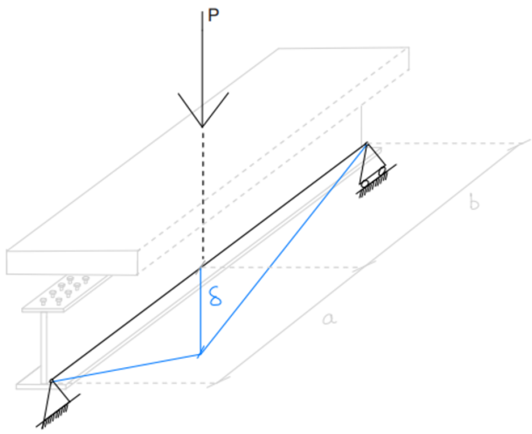

Figure 2.13: The spring stiffnesses of the transversal model supported by springs are based on the deflection of the beam under a point load.

The value of the spring stiffness k in any longitudinal position of the bridge is calculated from the deflection of a unit point load, P:

$$k = \frac{P}{\delta} \tag{2.10}$$

$$\delta = \frac{Pa^2b^2}{3EIL} \tag{2.11}$$

Where a is the distance from the left support to the section where the load is applied (the longitudinal position where one wants to calculate the stiffness of the beams) and

$b = L - a$. The LDF of a girder is then found by calculating the reaction force in its equivalent spring and comparing it with the load that is applied in the longitudinal 2D model according to Equation 2.2.

The load distribution will vary along the longitudinal axis since it depends on the spring stiffness of the supports, which is governed by the deflection, which in turn varies with the longitudinal position. This makes the choice of longitudinal position for calculating the LDF crucial, as the designer must be aware that it will significantly influence the results. For example, if one were to analyze the bending moment, it typically reaches its maximum at mid-span. At this location, the deflection is also at its largest, resulting in the lowest spring stiffness and, consequently, the highest load distribution. Therefore, it is important to verify whether the increased load sharing at mid-span actually results in less critical load effects compared to other sections, even if the bending moment itself is largest there.

2.3.2 3D beam model - grillage model

One way to more accurately model the bridge behavior in 3D without the need for an LDF approach is by the use of a grillage model. This model is according to Vayas and Iliopoulos (2015) built up as a grid of beams, where the longitudinal and transverse beams represent the bridge behavior in longitudinal and transverse direction, respectively, see Figure 2.14 below. The model is easy to apply and interpret, it is also computationally light, and its accuracy has been proven for a wide range of bridges (Patel & Patel, 2023).

The model is built up by placing longitudinal beam elements at the position of the steel girders with properties that represent the effective composite section of the I-girders and the concrete slab, including area, moment of inertia, and torsional constants (Vayas et al., 2010). The effective properties of the cross section consider the effects of shear lag as per SS-EN 1994-2 5.4.1.2 (SIS, 2005b). The properties are then calculated on the basis of equivalent steel cross-section by the use of modular ratios. To model any cantilever edges of a bridge, O'Brien and Keogh (1999) proposes the use of longitudinal "dummy" beams that are assigned a low stiffness of 0.5% of the other members spanning in the same direction.

The transverse elements can, according to El Sarraf et al. (2013), be placed with a c-c distance of the designer's choice but should not exceed 1/8 of the total span length modeled. Vayas and Iliopoulos (2015) proposes choosing a c-c distance equal to the distance between axle loads, such as 1.2 m for LM1. This choice results in a dense arrangement of the transverse elements, which can be advantageous. The sectional properties of these should represent those of the concrete deck, where each transverse element should represent its proportion of the deck. This results in their sectional constants being proportional to the choice of c-c distance between the transverse elements. To represent the behavior of any diaphragm beams in the transverse direction, elements should be placed there with the properties of those (O'Brien & Keogh, 1999).

According to Vayas and Iliopoulos (2015), the torsional rigidity of the slab can be neglected, as it has little effect on the final results. However, Jaeger and Bakht (1982) propose that the transverse and longitudinal elements can be assigned a torsional rigidity calculated according to Equations 2.12 and 2.13, respectively.

$$J_y = \frac{E_c}{G_c} \cdot \frac{L_x t_c^3}{12} \tag{2.12}$$

$$J_x = J_y + \frac{L_y t_c^3}{6} \tag{2.13}$$

L_x = transverse element spacing $[m]$
L_y = longitudinal element spacing $[m]$
t_c = slab thickness $[m]$
E_c = modulus of elasticity for concrete $[GPa]$
G_c = shear modulus for concrete $[GPa]$

In Figure 2.14, a general representation of the grillage model is shown with its different types of element and their associated cross sections.

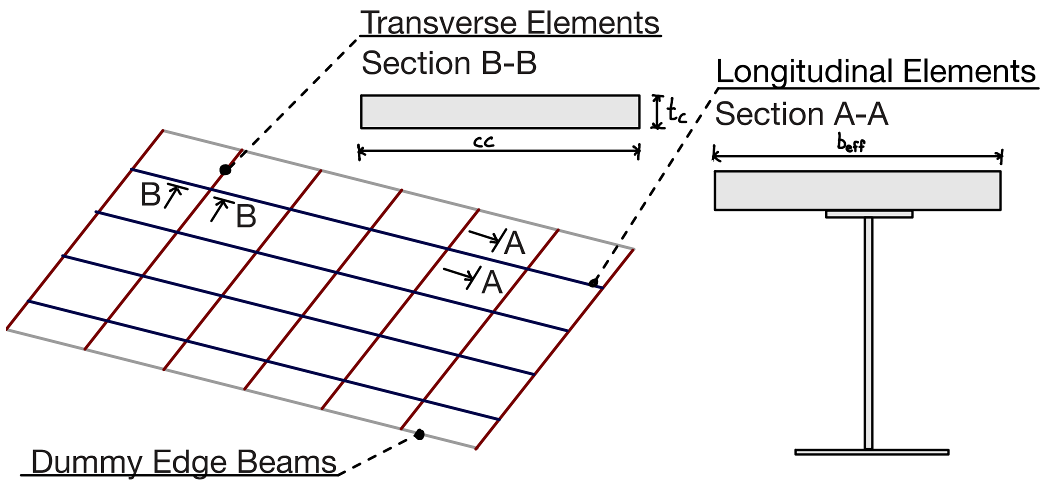

Figure 2.14: The grillage representation of the bridge with the different types of elements and their associated cross-section.

To capture the effect of the different stages of the construction, several models need to be conducted with different sectional properties. For the construction stage, the concrete is excluded from the sectional properties and is instead added as a load on the steel beams. The sectional properties will also change whether one looks at the short- or long-term response, since the effects of creep and shrinkage, as well as the change of material properties in the long term.

However, research has shown that the use of this type of analysis can have a great benefit of not overestimating the load effects of live loads compared to Courbon's method (Patel & Patel, 2023). What they found was that Courbon's method tends to overestimate the bending moments in individual girders due to live loads, making it conservative for that load case. However, the same source found that, for distributed loads such as self-weight, Courbon's method produced results very similar to those obtained from the grillage model.

2.3.3 3D equivalent truss model

Another way to model the behavior of the bridge to capture the load distribution in three dimensions is presented by Vayas and Iliopoulos (2015). This model is built by creating equivalent trusses that will represent the behavior of the steel and composite cross sections. The procedure for creating the equivalent truss is as follows:

- The cross-section of the flanges in the truss will be modeled by beam elements in a T-shape. The cross-section is composed of 1/3 of the height of the web together with the flange of the steel girder. The center of gravity of the truss flanges should be placed in the center of gravity of the aforementioned T-sections in the original cross-section.
- The diagonals of the truss are composed of a cross-section that has the same properties as the remaining 1/3 of the web ($h_{diagonal} = 1/3 \cdot h_w,\ t_{diagonal} = t_w$).
- The vertical posts of the truss are modeled with a spacing of $s = 0.05 \cdot L_{span}$ and with a cross-sectional area, $A_{post} = s \cdot t_w$.
- The concrete slab is taken into account by adding an additional beam element to the top flange of the truss with an offset, C_c, equal to the distance between the centroids of the upper T-section in the C_{fo} and the bottom T-section, C_{fu}

According to Vayas et al. (2010), this model has the benefit that it is not complicated, yet not time-consuming. They also claim that it predicts 3D effects better than the grillage model mentioned in Section 2.3.2. Another advantage of the model is that the load distribution in three dimensions is given by one model, and one does not have to make several models in different directions as for the beam models in Section 2.3.1.

2.3.4 Shell model

A detailed approach to model a steel-concrete composite bridge is to use a model with shell and beam elements. In this approach, the concrete slab and web of the I-girder are modeled using shell elements, while the flanges of the steel girders are represented by beam elements. To simulate the composite action between the slab and the girders, full interaction can be assumed by imposing no releases between the shell and beam elements. If haunches are included in the slab design, volume elements may be preferable as they provide more accurate results (Vayas & Iliopoulos, 2015).

When stiffeners are included, they should be modeled using beam elements (Vayas & Iliopoulos, 2015). Based on the internal forces obtained in the stiffeners, their significance for overall structural behavior can be assessed.

The shell model has the main advantage that it can capture complex 3D effects more precisely than the previously mentioned methods. However, these types of models also have some drawbacks. In particular, a large amount of computational calculations is required, leading to long analysis times, and there are multiple potential sources of error. For example, the choice of element type, element shape, and mesh size can significantly influence the accuracy of the results (Vayas et al., 2010). In addition, the modeling of the shell model may be time-consuming as well. However, the shell model is capable of considering buckling of the steel girders if such an analysis is performed.

3 Verification of cross sections

The design and analysis of a composite section is an iterative procedure where the structure's different stages during its lifetime need to be considered. Typically, a composite bridge will be constructed in an order where the steel girders are placed first, then the concrete is cast upon them. This means that the structure will get completely different behavior in the construction phase compared to the long-term. When the concrete is not yet hardened, all of its weight, along with the weight of the formwork and the steel girders, will be carried by the steel cross-section. However, when the concrete is hardened, the steel and the concrete will act together to carry loads in the long-term perspective, such as the traffic loads. In the following section, the different stages will be covered, and what checks need to be done to verify the structural capacity.

3.1 Relevant design codes

Civil engineering design is often guided by various design codes. The European guidelines are called the Eurocodes, which consist of multiple parts, EN 1990 to EN 1999. However, not all of these are relevant for composite bridges or this thesis. The relevant ones are shown in Figure 3.1 and Table 3.1. In addition, multiple national parameters are published in national annexes that vary from country to country. The Swedish implementation of the Eurocodes is published by the Swedish Standards Institute (SIS) and is the one that will be utilized in this thesis. These Eurocodes are denoted as SS-EN 199X. The Swedish national annexes regarding road and railway structures are published by Transportstyrelsen, referred to as TSFS (Transportstyrelsen, 2018). All national choices relevant to this thesis are presented in TSFS.

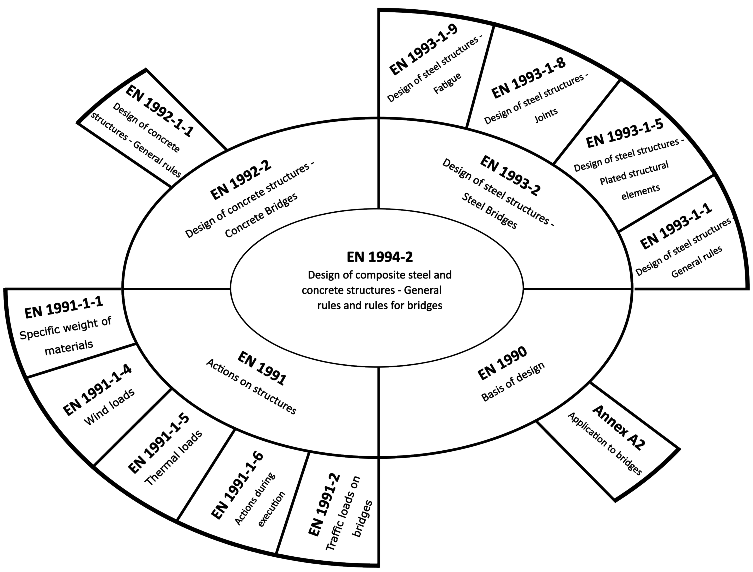

Figure 3.1: Relevant Eurocodes for composite bridges.

To note is that a second generation of Eurocodes is to be implemented in a few years, and while not all of them are officially released yet, the ones that are will be used for this thesis. The Eurocodes and corresponding versions that will be utilized in this thesis and their source are shown in Table 3.1, having been identified as the most relevant for the preliminary design phase.

Table 3.1: Versions used for each Eurocode and their corresponding source.

Code	Version	Source
SS-EN 1990:2023	NEW	SIS (2023a)
SS-EN 1991-1-1:2025	NEW	SIS (2025a)
SS-EN 1991-1-4:2026	NEW	SIS (2026)
SS-EN 1991-1-5:2025	NEW	SIS (2025b)
SS-EN 1991-1-6:2005	OLD	SIS (2005c)
SS-EN 1991-2:2024	NEW	SIS (2024a)
SS-EN 1992-1-1:2023	NEW	SIS (2023b)
SS-EN 1993-1-1:2022	NEW	SIS (2022)
SS-EN 1993-1-5:2024	NEW	SIS (2024b)
SS-EN 1993-1-9:2025	NEW	SIS (2025c)
SS-EN 1993-2:2006	OLD	SIS (2006)
SS-EN 1994-1-1:2005	OLD	SIS (2005a)
SS-EN 1994-2:2005	OLD	SIS (2005b)

The Eurocodes are not the only design codes that apply to composite bridges in Sweden, as Trafikverket has its own codes as well, called TRVINFRA (Trafikverket, 2025). These codes expand on the Eurocodes with specific demands or requirements pertaining to Swedish regulations. However, these codes and the National Annex, TSFS, have not yet been updated to align with the second generation of Eurocodes, and any national choice is not accurate. For this thesis, the current versions of TSFS and TRVINFRA will be used for the necessary choices.

3.2 Cross-sectional properties

The basis of the cross-sectional analysis of a composite section will be covered in the following sections. The analysis is split into different stages, which require different sets of cross-sectional properties, where the first set is determined for the steel section. The second is determined by including the concrete, where the contributing part of the concrete is determined with respect to shear lag according to SS-EN 1994-2:2005 5.4.1.2. To account for the different stiffnesses of concrete and steel, the concrete is transferred into an equivalent steel section by the use of the long-term modular ratio n_L, which is determined according to SS-EN 1994-1-1:2005 eq. 5.6.

3.3 Design of the concrete slab

The slab should, by experience, be designed with a sufficient concrete thickness, t_c, so that it can resist shear forces in the transverse direction without the need for shear reinforcement. This is due to insufficient space to anchor the stirrups. SS-EN 1992-1-1:2023 6.5.2, together with TSFS Table 12.1, provides the minimum concrete cover thickness. The shear capacity for a concrete member without shear reinforcement is provided by SS-EN 1992-1-1:2023 eq. 8.27. To account for the shear force distribution in the slab, Pacoste et al. (2012) provides recommendations on how to consider this in the design of the slab.

3.4 Construction stage

The construction stage is split into two stages. The first, denoted as G1.1, covers the concreting phase, and the second stage, G1.2, follows when the formwork is removed.

Stage G1.1 - concreting phase

The first stage is typically denoted stage G1.1, and covers the concreting phase. This means that the steel girders will carry the loads from the self-weight of the steel girders, the wet concrete, the construction loads, and the formwork. In addition, this stage must be checked for lateral torsional (LT) buckling since the steel girders are not braced when the concrete is not hardened. The stress distribution in this stage, $\sigma_{steel.G1.1}(z)$, is seen in Figure 3.2, which depends on the bending moment from the aforementioned loads and the moment of inertia of the steel girder alone, $I_{y.steel}$.

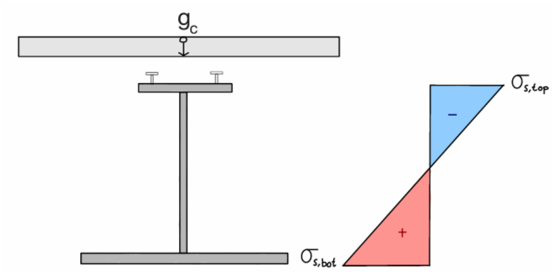

Figure 3.2: Stress distribution in the steel cross-section during casting of concrete.

To determine whether the steel girder is sufficient to carry the loads in G1.1, it should be verified in bending, see SS-EN 1993-1-1:2022 8.2.5. The resistance to LT buckling is assessed by the simplified procedure in SS-EN 1993-1-1:2022 8.3.2.4, which verifies that the flange, together with an equivalent part of the web, is sufficiently stiff to withstand the compressive stresses without buckling.

Stage G1.2 - formwork removal

The next stage is denoted G1.2 and covers the case when the concrete has hardened, and the formwork and construction loads are removed. This creates another stress distribution, $\sigma_{G1.2}(z)$, seen in Figure 3.3, which depends on the negative bending moment (for a simply supported bridge) from the load removal as well as the long-term moment of inertia of the composite section, $I_{y.L}$. The concrete now participates in the load carrying, carrying compressive stresses. Due to the difference in stiffness in the materials, there is a discontinuity between the steel and concrete stresses.

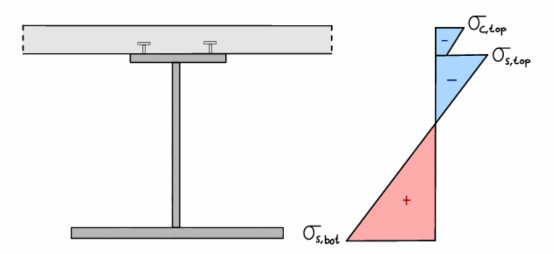

Figure 3.3: Stress distribution in the composite cross-section.

In this stage, stresses are present in both the concrete and the steel. The stresses in the concrete are found by dividing the stresses in the equivalent steel cross-section by the long-term sectional modulus, as seen in Equation 3.1.

$$\sigma_c(z) = \frac{\sigma_{steel}(z)}{n_L} \tag{3.1}$$

3.5 Pavement application

The third stage is G2 and covers the case when the construction is finished and the pavement is applied. This yields a stress distribution, $\sigma_{G2}(z)$, with a similar shape to what was seen in Figure 3.3, that depends on the loads from the pavement and the long-term moment of inertia of the composite section, $I_{y.L}$. The stresses in the concrete are calculated as before by Equation 3.1.

3.6 Ultimate limit state

The next stage that should be checked is the ultimate limit state, ULS. In this case, the stresses from the previous stages will still be present but with an additional contribution in the equivalent steel section from the traffic loads, $\sigma_{traffic}(z)$. This extra contribution will be governed by the bending moment from the traffic and the long-term moment of inertia of the composite section, $I_{y.L}$. The concrete stresses are obtained in the same way as before, according to Equation 3.1.

The total stress, $\sigma_{tot}(z)$, to check the section for is obtained by superimposing the stress distributions from all stages together with ULS load combination factors, producing a distribution shape similar to that seen in Figure 3.3. The stress is calculated as shown in Equation 3.2 for the steel stresses and for the concrete in Equation 3.3.

$$\sigma_{tot.a}(z) = \gamma_G \cdot \sigma_{a.G1.1}(z) + \gamma_{G.fav.} \cdot \sigma_{a.G1.2}(z) + \gamma_{G.pave.} \cdot \sigma_{a.G2}(z) + \gamma_Q \cdot \sigma_{a.traffic}(z) \tag{3.2}$$

$$\sigma_{tot.c}(z) = \gamma_{G.fav.} \cdot \sigma_{c.G1.2}(z) + \gamma_{G.pave.} \cdot \sigma_{c.G2}(z) + \gamma_Q \cdot \sigma_{c.traffic}(z) \tag{3.3}$$

These stresses should then be verified against the bending capacity of the composite cross-section according to SS-EN 1994-1-1 6.2.1.5 (2).

The shear capacity, according to SS-EN 1994-2 6.2.2.3, should be taken as the capacity of the steel girder alone, neglecting the capacity of the concrete slab. The risk of shear buckling should be evaluated by SS-EN 1993-1-1:2022 eq. 8.27. If there is no risk of shear buckling, the capacity is calculated by SS-EN 1993-1-1:2022 8.2.6, and if there is a risk, it is calculated by SS-EN 1993-1-5:2024 7.2.

3.7 Fatigue limit state

The capacity in the fatigue limit state, FLS, should be verified. SS-EN 1993-2:2006 9.5.2 presents a λ-coefficient method, which is a simplified approach where the fatigue damage caused by a stress spectrum is considered by an equivalent stress range, $\Delta\sigma_E$ (Al-Emrani & Aygül, 2014). The method includes the use of a damage equivalence factor, λ, which is defined in Equation 3.4.

$$\lambda = \lambda_1 \cdot \lambda_2 \cdot \lambda_3 \cdot \lambda_4 \tag{3.4}$$

Where λ_1 is a factor considering the span of the bridge determined by SS-EN 1993-2:2006 9.5.2 (2). λ_2 is determined by SS-EN 1993-2:2006 9.5.2 (3) and considers the traffic volume, where the gross weight of each lorry should, according to TRVINFRA-00227 6.0 Tab. 7.2-7, be set as $Q_{m1} = 445$ kN. λ_3 considers the design life of the bridge and is determined by SS-EN 1993-2:2006 9.5.2 (5). λ_4 can, according to TSFS 2018:57 3§ 14, be set as $\lambda_4 = 1$, to account for traffic in other lanes.

According to SS-EN 1993-2:2006 9.2.2, FLM 3 should be used as the fatigue load model when analyzing fatigue using the λ-coefficient method. Each relevant fatigue-loaded detail is then verified using SS-EN 1993-2:2006 eq 9.7 and 9.8 with relevant detail categories defined in SS-EN 1993-1-9:2025 tab. 10.1-10.12.

3.8 Workflow chart for cross-section verification

In Figure 3.4, a flowchart for the design and analysis of a cross-section is shown. The chart refers to an additional flowchart for the modeling procedure, which will be presented in further detail in Section 4.8 below.

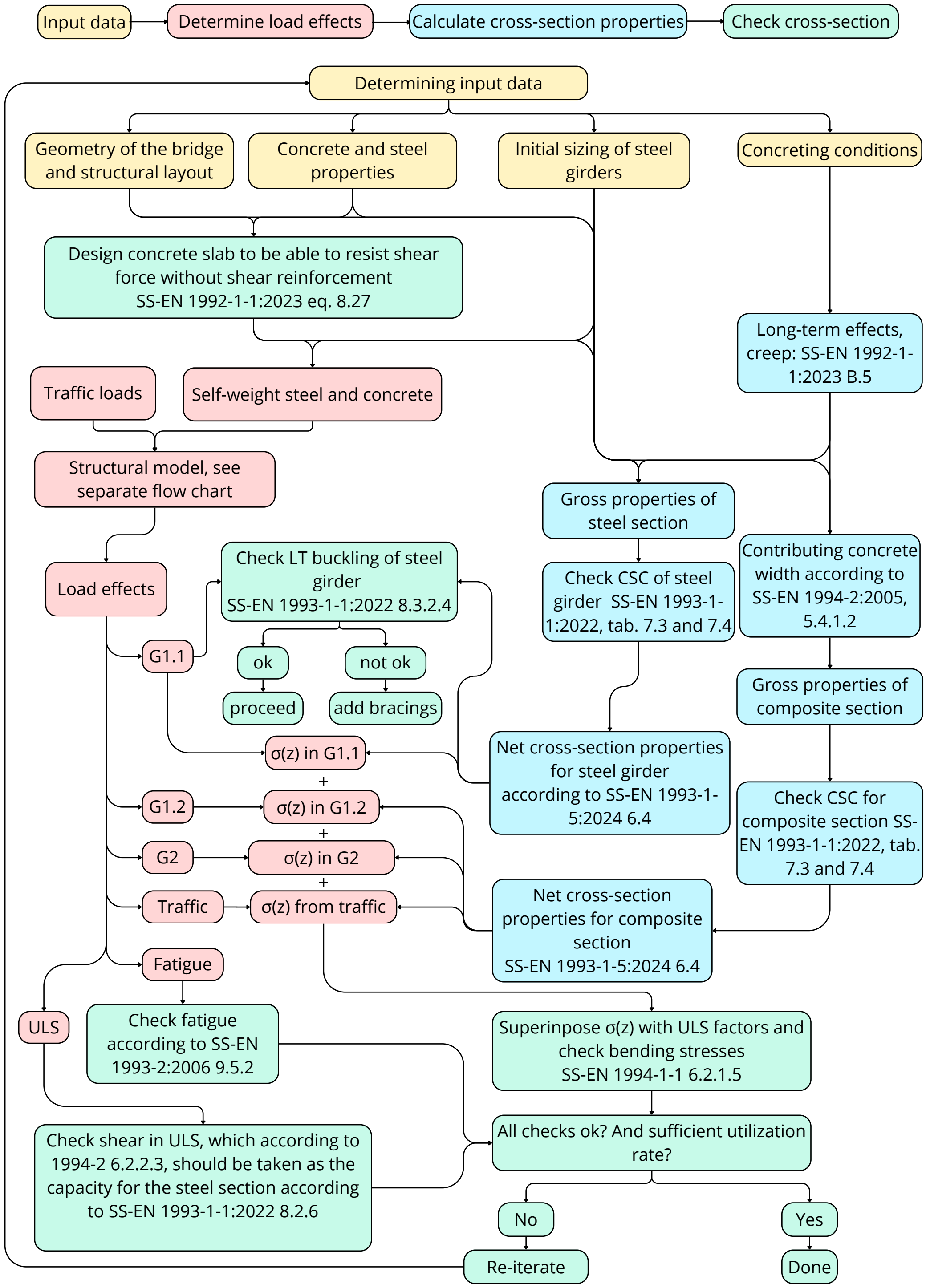

Figure 3.4: Flowchart for cross-section design and analysis.

4 Case study

In this chapter, a case study will be performed with the aim of evaluating the methods presented in previous chapters to find a suitable method to use in preliminary design. The method, results, and discussion to accomplish this will all be covered in this chapter.

4.1 Case description

The case study is based on a real procurement project for a road bridge in Akalla, just north of Stockholm. The client was Trafikverket, which provided the tender documents that were used as the basis for the study. These are viewed in Figure 4.1.

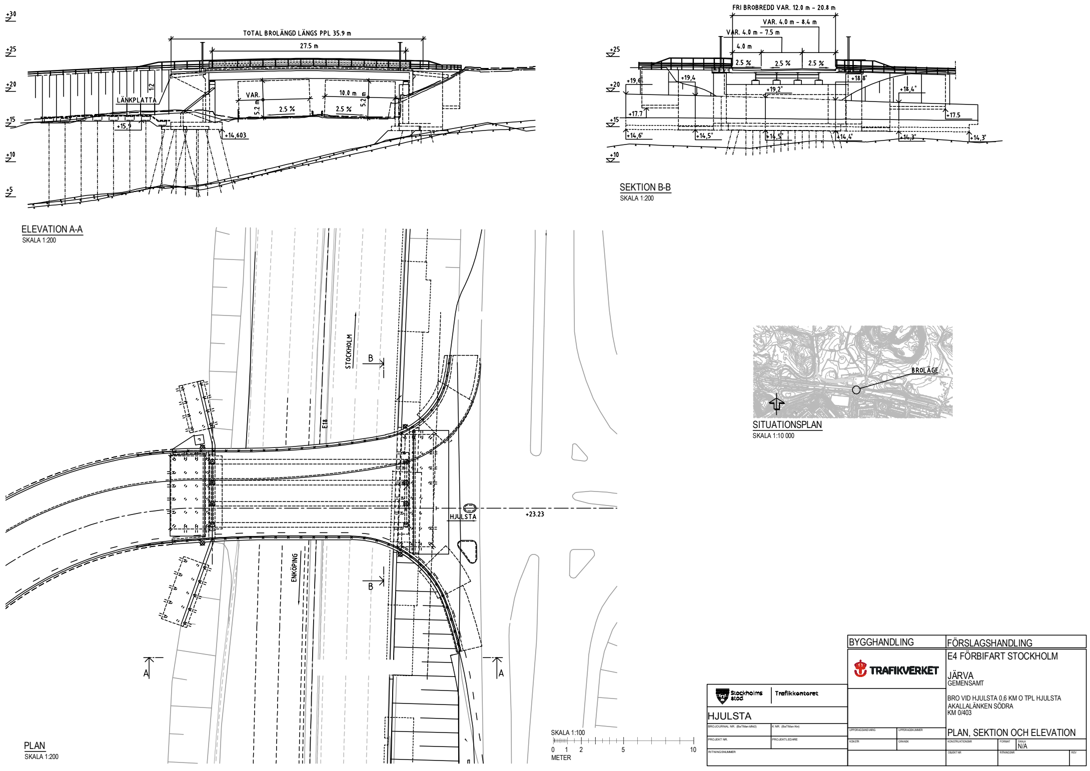

Figure 4.1: Tender documents for the road bridge in Akalla.

To simplify the analysis, several assumptions were introduced. The geometry of the bridge was idealized as non-skewed with a constant width of 12 m. In addition, the carriageway was assumed to consist solely of traffic lanes, without walkways, simplifying load application. The bridge was assumed to be simply supported with a span length of 27 m, and the construction height was limited to 1330 mm.

The design life was assumed to be 120 years, and the surrounding relative humidity was taken as $RH = 80\%$. Furthermore, it was assumed that the girders were lifted in place with the concrete slab subsequently cast on top of them. A further simplification was made by neglecting the verification of the girders during lifting.

The geometry of the bridge is shown in Figures 4.2 and 4.3.

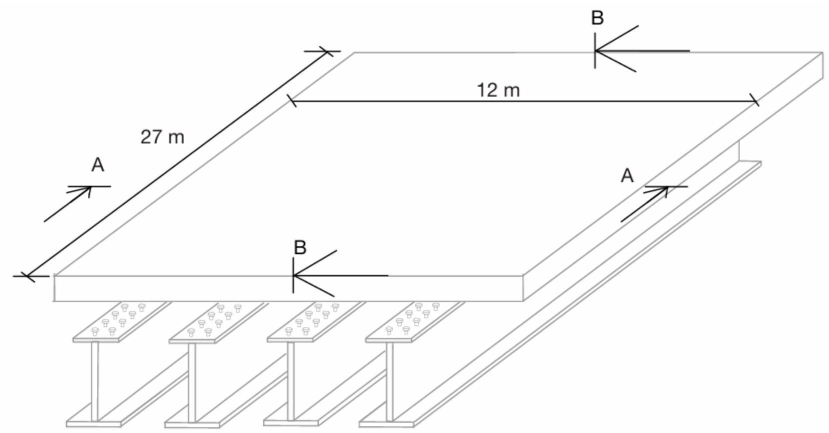

Figure 4.2: Simplified geometry of case study, 3D view.

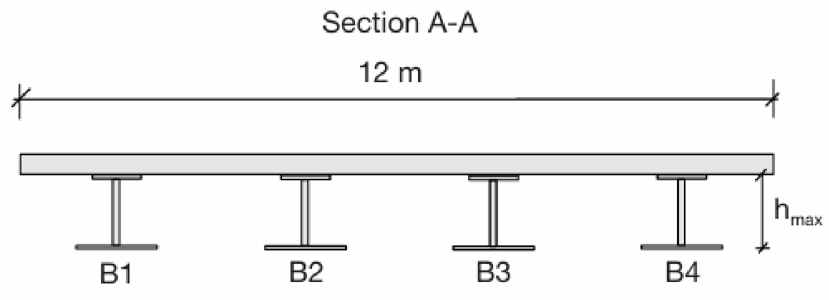

Figure 4.3: Simplified geometry of case study, section view.

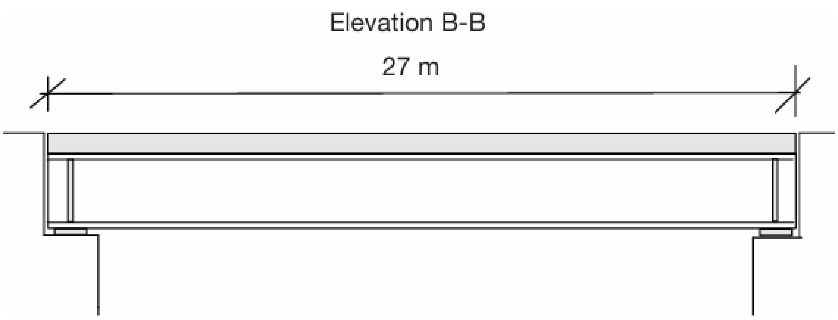

Figure 4.4: Simplified geometry of case study, elevation view.

4.2 Method of analysis

In this section, the method of analysis for the case study is described. The analysis aimed to evaluate the different modeling approaches presented in Section 2.3, where an initial selection of models was made in Section 4.3 based on the relevance for preliminary design.

The evaluation of the models was then done based on how they distribute the LDFs for each beam compared to the shell model, which acted as a reference since that is considered the most exact modeling approach. The LDFs were calculated by the load case presented in Figure 4.5, where a point load, P, is moved along a line positioned 0.5 m from the cantilever edge. This represents the most outer position for a tandem load as defined in Figure 6.2 of SS-EN 1991-2:2024.

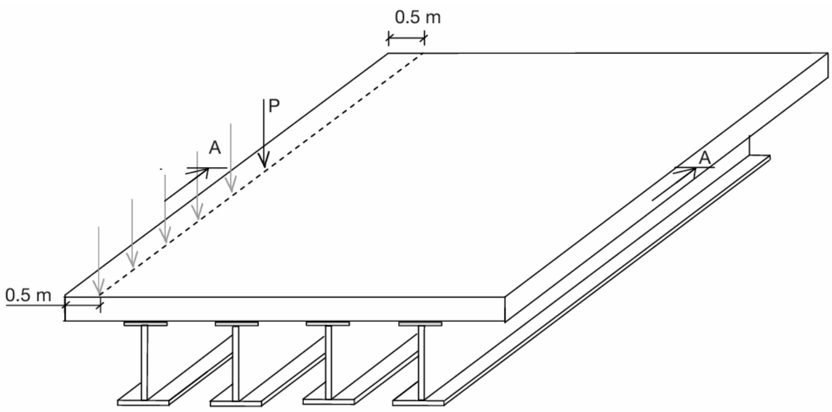

Figure 4.5: Loading line positioned at $y = 0.5$ m from the edge of the bridge, where a point load P is moved along to calculate the LDF at different longitudinal sections.

The models were constructed and analyzed through the program Brigade/Plus, and subsequently, LDFs were calculated and plotted for each position of the load, P, along the span of the bridge. This was first done for the shell model in Section 4.4. Thereafter, the LDFs were determined for the grillage model and compared with the shell model in Section 4.5. This comparison was repeated for the beam models by determining the LDFs based on Courbon's method, Fauchart's method, and the transverse spring model method in Section 4.6.1, 4.6.2, 4.6.3, respectively.

Based on these results, along with the advantages and limitations of the different modeling approaches, Section 4.7 presents an evaluation and discussion of their suitability for preliminary design. The selected model is subsequently evaluated and modified in Section 4.8 by adjusting its properties to improve its agreement with the shell model.

Structural analysis using bridge load models was conducted in Section 4.9 to evaluate how the non-updated (original), the updated beam model, and the shell model differ in terms of load effects. The results from the original and updated beam models were then used in Section 4.10 for cross-section designs. The resulting material quantities were then used in an evaluation between the two models.

Finally, Section 4.11 compares the material quantities obtained from empirical methods against those determined with the structural analysis.

To do an initial comparison of the different models, an arbitrary cross-section according to Figure 4.6 was defined, with dimensions given in Table 4.1 and material properties listed in Table 4.2.

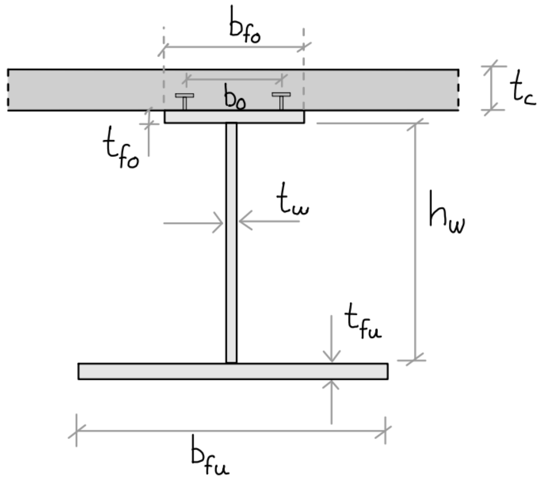

Figure 4.6: Reference cross section used to compare the different modeling approaches.

Table 4.1: Dimensions for reference cross-section.

Part	Parameter	Value
Concrete slab	t_c	230 mm
Over flange	b_{fo} t_{fo}	370 mm 25 mm
Web	h_w t_w	1025 mm 17 mm
Under flange	b_{fu} t_{fu}	650 mm 50 mm

Table 4.2: Material properties for the reference cross section used when comparing the different modeling approaches.

Property	Concrete C35/45	Steel S355
E	34 GPa	210 GPa

4.3 Modeling approaches

The models described in the literature study all have their unique areas of application; however, some are more suitable than others for the case study conducted in this thesis. The first selected model is the shell model, which is regarded as the most accurate model and therefore serves as a reference model for comparisons and evaluation. The second model is the grillage model, which offers an interesting way to represent the slab behavior. In addition, beam models are included in the study. These models require a load distribution factor (LDF), for which there are multiple approaches to calculate. The approaches investigated are Courbon's method, Fauchart's method, and the transverse beam model with spring supports. Preliminary comparisons indicate that these approaches provide LDFs that are reasonably consistent with the shell model, and they will therefore be examined further in Section 4.6.

However, not all models identified in the literature were considered suitable for this case study. The models excluded from further consideration are discussed below.

The first to be excluded is the lever rule since this approach assumes that the slab is simply supported rather than acting continuously over the girders. Consequently, it is considered an overly simplified representation of the structural behavior and is therefore unlikely to provide accurate results.

Henry's method for determining the LDF was also excluded. Preliminary calculations indicated that this method would produce overly conservative results. Through the application of Equation 2.9 and the parameters given in Table 2.3 with $W_{roadway} = 12\,m$, four traffic lanes, and four girders, the resulting LDF is:

$$LDF = 1.09 \cdot \frac{12m}{3.05} \cdot 0.75 \cdot \frac{2}{4} = 1.6 \tag{4.1}$$

This load distribution factor (LDF) is significantly larger than the corresponding LDFs obtained using the other methods presented above. As a result, the method would lead to substantially more conservative results and was therefore excluded from the case study.

The final model excluded from the study is the 3D equivalent truss model. Although the method may provide accurate results, it was excluded due to its implementation complexity compared to the other investigated methods. Since one of the objectives is to evaluate which methods are suitable for preliminary design, the use of the 3D equivalent truss model could not be justified.

4.4 Shell model

The general implementation of the shell model is carried out as described in Section 2.3.4. Since both the modeling and the analysis are highly time-consuming and require several hours to complete, the shell model is not suitable for preliminary design. Instead, it is used as a reference model for evaluating the other load distribution methods.

The shell model was constructed using shell elements for the web and slab. The girder webs and slab were constructed separately and later merged into one instance. The beams representing the top and bottom flanges were placed at the top and respective bottom of the web and coupled using rigid connections. The bridge is as described in Section 4.1, simply supported, and the boundary conditions reflect that with degrees of freedom as seen in Figure 4.7. Along with the movement locked in the vertical direction for all beams, one side has the longitudinal direction locked, and one beam has the transverse direction locked on both ends.

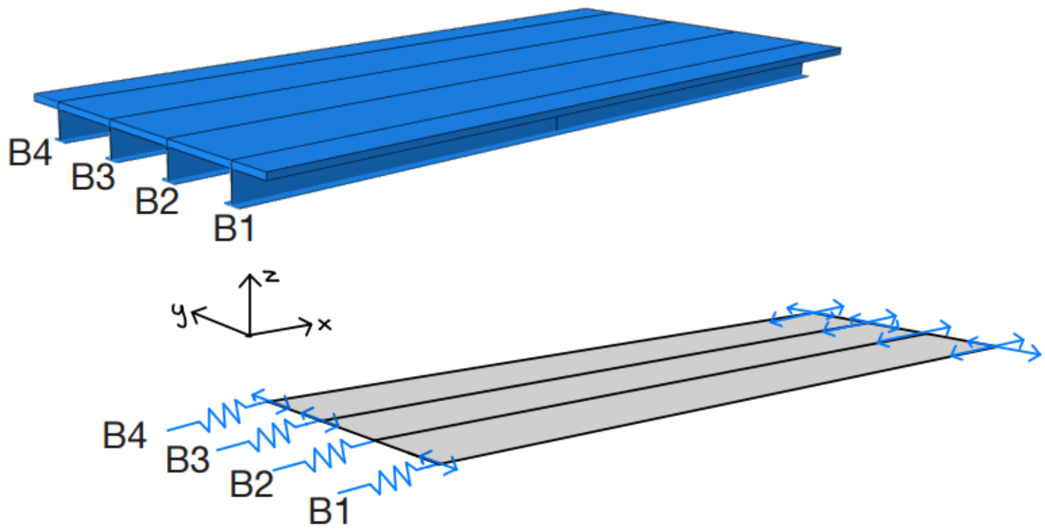

Figure 4.7: Degrees of freedom for beams B1 to B4, blue arrows indicate where the structure is allowed to move. The springs at the left support indicate a partial restraint in the x-direction.

The boundary conditions are set to ensure that the bridge is simply supported. The rotations were left unconstrained to allow bending behavior consistent with a simply supported system. The constraints are applied to the longitudinal elements, specifically the steel girders. At one end, the vertical translations in the upward z-direction are restricted. During analysis, it became clear that fully restricting movement in the longitudinal translation in the x-direction results in restraint moments at the supports. As a result, springs with a stiffness of $k = 1 \cdot 10^6$ N/m were implemented to allow some movement in order to remove the support moments, as they should be 0 in a simply supported system. In addition, one of the middle girders is restrained in the transverse y-direction to restrict horizontal movement. At the other end, the vertical translation in the z-direction is restricted, and the same girder as previously mentioned is also horizontally restrained in the transverse y-direction. A schematic view of the boundary conditions is presented in Figure 4.7.

For analysis and comparison purposes, a simplified load case was analyzed, consisting of a point load of $P = 100$ kN applied 0.5 m from the cantilever edge of the concrete slab, as shown in Figure 4.5. In addition, self-weight, shrinkage, and temperature loads have been analyzed to verify the model and to determine whether these effects can be neglected in the other structural models.

The self-weight is calculated based on the material densities specified in the model definition and is applied as a gravity load using a gravitational acceleration of $g = 9.81$ m/s^2.

Free body cuts are made to integrate the stresses into sectional forces. These are made on each of the four girders, including 50% of the slab between them. The cuts are made in increments of 0.5 m. However, while the number of cuts can easily be increased, the increased number results in significantly longer computational times. More cuts will increase the accuracy of the graph, but not change any actual values at the cuts. If only the maximum moment of the girder is of interest, one cut in the middle of the beam would suffice, as the maximum moment will be in the middle of a simply supported girder.

The shrinkage of the concrete is modeled as an equivalent temperature load, defined by Vayas et al. (2010) as:

$$\Delta T = \frac{\epsilon_{cs}}{\alpha_T} \tag{4.2}$$

where

$$\begin{aligned} \epsilon_{cs} &= \text{shrinkage strain in the concrete [-]} \\ \alpha_T &= \text{expansion coefficient of the concrete [1/°C]} \\ \Delta T &= \text{temperature difference [°C]} \end{aligned}$$

This temperature change is applied as a negative temperature load to represent the contraction caused by shrinkage. The resulting restraining forces on the steel girders can then be evaluated. These are analyzed to determine whether the effects of shrinkage can be neglected in the other models or not. The resulting bending moment from this shrinkage is shown in Figure 4.8.

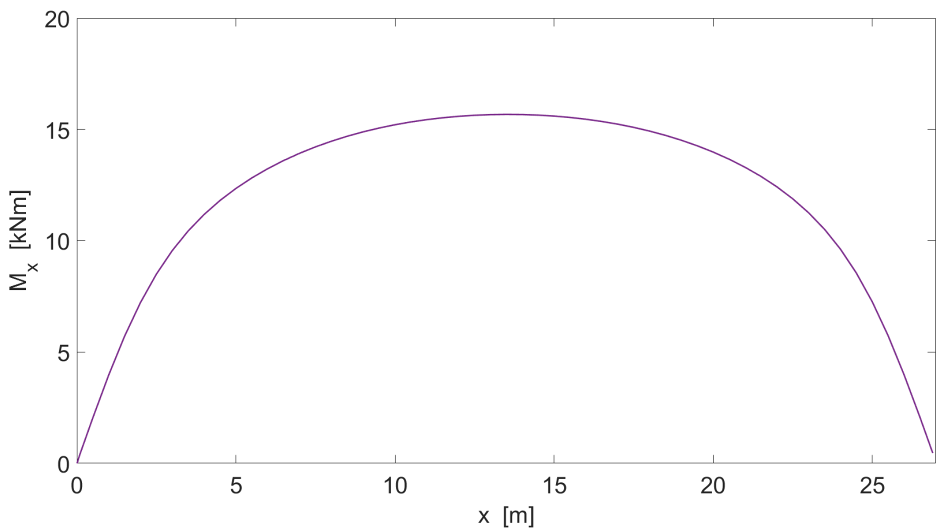

Figure 4.8: Bending moment caused by the shrinkage of the concrete slab.

The maximum bending moment caused by shrinkage is 16 kNm. This relatively small restraint moment is reasonable, as the bridge is simply supported and therefore has limited restraints that prevent the shrinkage of the concrete slab. Similarly, temperature loads cause a bending moment of approximately 20 kNm, the low bending moment is due to the aforementioned fact that the bridge is simply supported.

For comparison, the maximum bending moment at the same location caused by self-weight is 7829 kNm, as shown in Table 4.3. Thus, the moment caused by shrinkage and temperature loads corresponds to approximately 0.2% of the self-weight moment, and an even smaller percentage when traffic loads are also considered. Consequently, the effects of shrinkage and temperature loads are neglected in the remaining structural models analyzed in this thesis.

To determine the load distribution factors (LDFs) for the girders in the shell model, the moment distribution for each girder was extracted and used together with elementary beam cases to calculate the LDF. This procedure is explained in more detail in Figure A.1 in Appendix A.

Since the bridge is simply supported, the bending moment at the supports is zero, resulting in an LDF of zero for all girders at this location. As a result, the support section has been excluded from the graph. The resulting LDF distribution between the support section (x = 1 m) and the mid-span section (x = 13.5 m) for the shell model is presented in Figure 4.9. Due to the bridge being simply supported, it becomes symmetric around the mid-span, which is why this and the upcoming plots of LDFs are shown only up to the symmetry line.

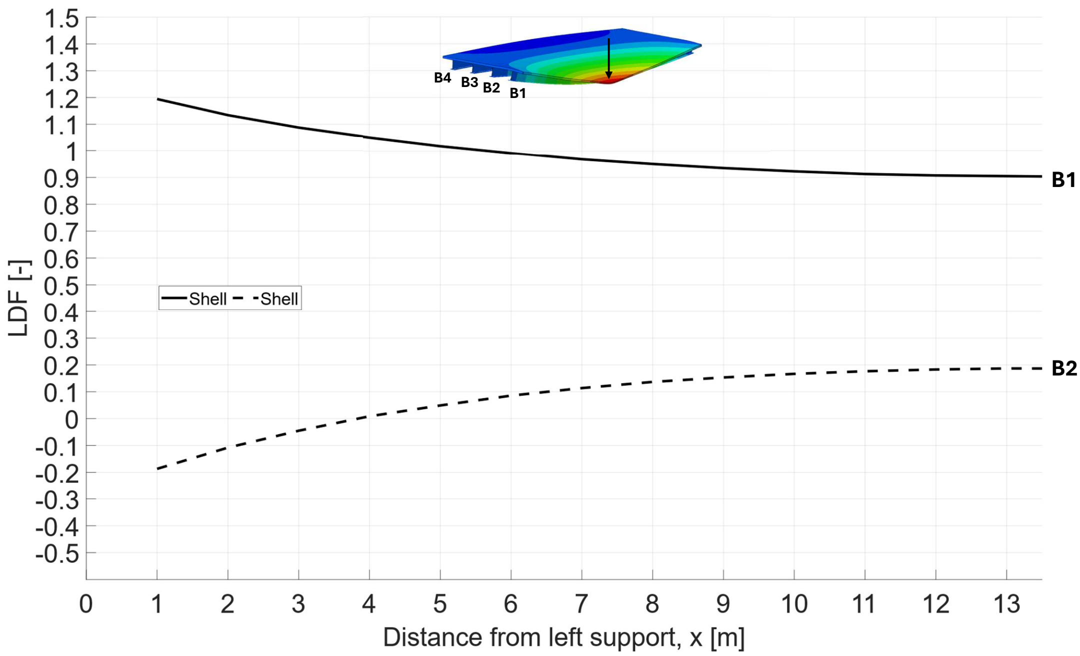

Figure 4.9: Load distribution factor (LDF) based on the bending moment for the shell model.

It can be seen in the figure that as the point load moves towards the support, the structural response becomes stiffer due to the proximity of the support. Consequently, Beam 1 carries a larger portion of the load, while the remaining beams begin to deform upward, resulting in negative bending moments in those girders. Although Beam 1 continues to be the main load-carrying girder throughout the span, the contribution of Beam 2 increases slightly as the load approaches the support.

To verify the shell model, a simple analysis of the self-weight was performed. A hand calculation of the self-weight of the bridge, presented in Appendix B, was compared with the self-weight applied to the entire bridge in Brigade/Plus. The comparison considered both the maximum bending moment and the shear force, and the results are shown in Table 4.3. The results indicate a good agreement between the two methods, confirming that the model provides a reliable representation of the structural behavior.

Table 4.3: Results for the verification of the shell model.

	Brigade/Plus	Hand calculation	Difference
M [kNm]	7829	7827	0.03 %
V [kN]	1148	1159	0.99 %

4.5 Grillage model

The implementation of the grillage model followed the procedures presented in Section 2.3.2, where the details are specified in this section. Brigade/Plus was used to construct and analyze the model.

Varying the number of transverse elements demonstrated that a higher density of those elements yields more accurate results. Because transverse elements connect to longitudinal girders at discrete nodes, increasing their number allows for a more continuous load distribution, enabling the model to better simulate true slab behavior. The initial model contained 9 transverse elements based on El Sarraf et al. (2013), with a spacing of $\frac{L_{span}}{8}$. However, the final model was based on Vayas and Iliopoulos (2015) recommendation to use the same spacing as for the tandem spacing of Load Model 1 (LM1), $cc_{trans} = 1.2$ m, which resulted in $\frac{27m}{1.2m} = 22.5 \simeq 23$ transverse elements.

The torsional rigidity of the transverse elements was initially set to zero according to (Vayas & Iliopoulos, 2015), but it turned out that the approach given by Jaeger and Bakht (1982) in Equation 2.12 provided results closer to the shell model.

The un-rendered geometry of the grillage model is presented in Figure 4.10, where one sees the arrangement of the different members. The longitudinal and the horizontal members share the same nodes, but to account for their eccentricities relative to each other, they are assigned the center of gravity of the composite section and the slab, respectively. To create nodes for the load application, dummy beams were modeled with a very low stiffness of 0.5% of the longitudinal elements according to O'Brien and Keogh (1999), but it was discovered that it was better to make them weaker, with a stiffness of $0.05‰$ of the longitudinal elements. This was due to the fact that the dummy beams seemed to distribute too much load when they were assigned the initial stiffness. Also, according to O'Brien and Keogh (1999), the cantilever edges were modeled with dummy beams as well.

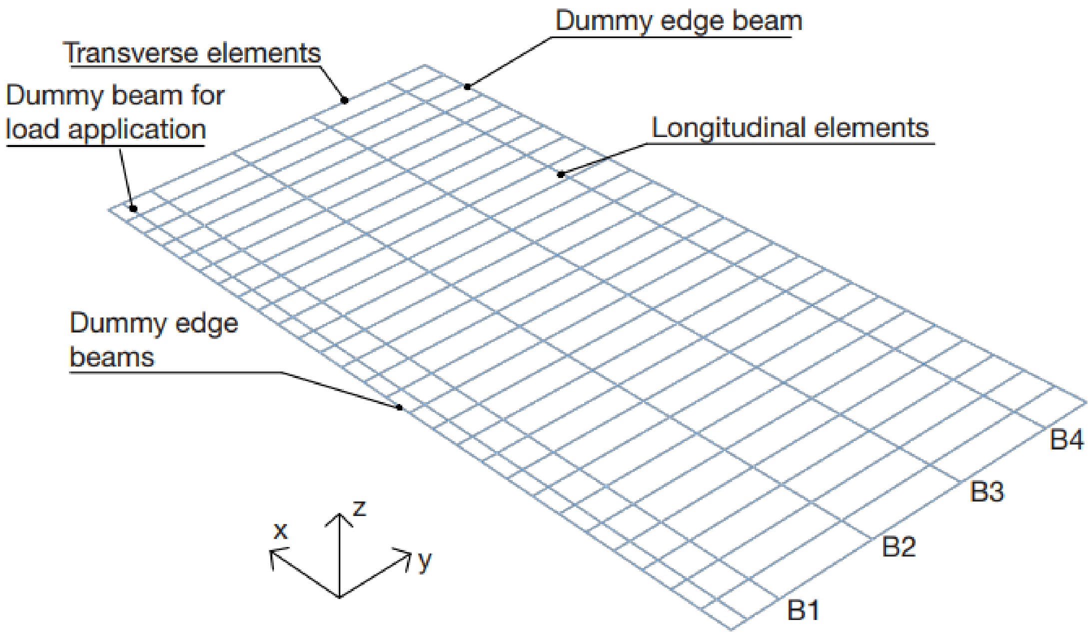

Figure 4.10: Un-rendered geometry of the grillage model, showing the longitudinal and transverse members as well as the dummy beams.

In Figure 4.11, the rendered grillage model is shown, where one can see the relative stiffness of each member.

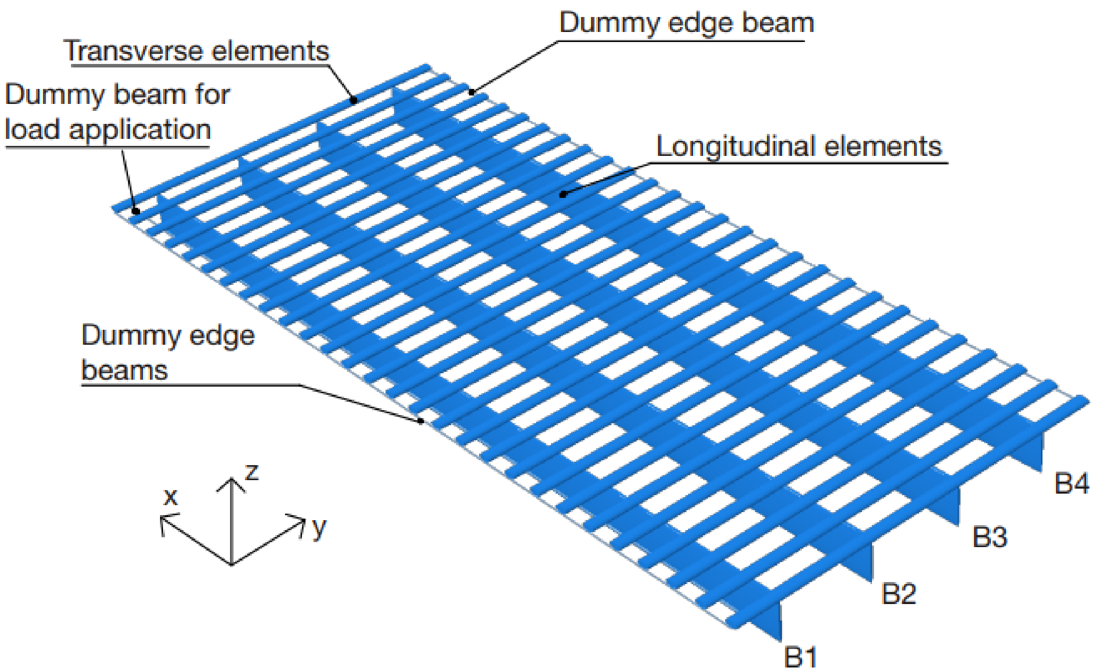

Figure 4.11: Rendered grillage geometry, showing the relative stiffness for the longitudinal and transverse members as well as the dummy beams.

The boundary conditions are close to the same as for the shell model described in Section 4.4 and can be viewed in Figure 4.7 above. Similar to the shell model, springs had to be added in the longitudinal (x) direction to address support bending moments. However, for the grillage model, these had to be added for the transverse (y) direction in both supports for beam 2 (B2) as well. The springs were assigned a stiffness of $k = 1 \cdot 10^6$ N/m in both directions.

To determine the LDF of the grillage elements, the moment distribution in each girder was extracted and used together with elementary beam cases to calculate the LDF. This procedure is further explained in Figure A.1 in Appendix A.

The resulting LDF distribution from the supports section ($x = 1$ m) to the mid-span section ($x = 13.5$ m) for the grillage model compared to the shell model for beam 1 (B1) and beam 2 (B2), is shown in Figure 4.12.

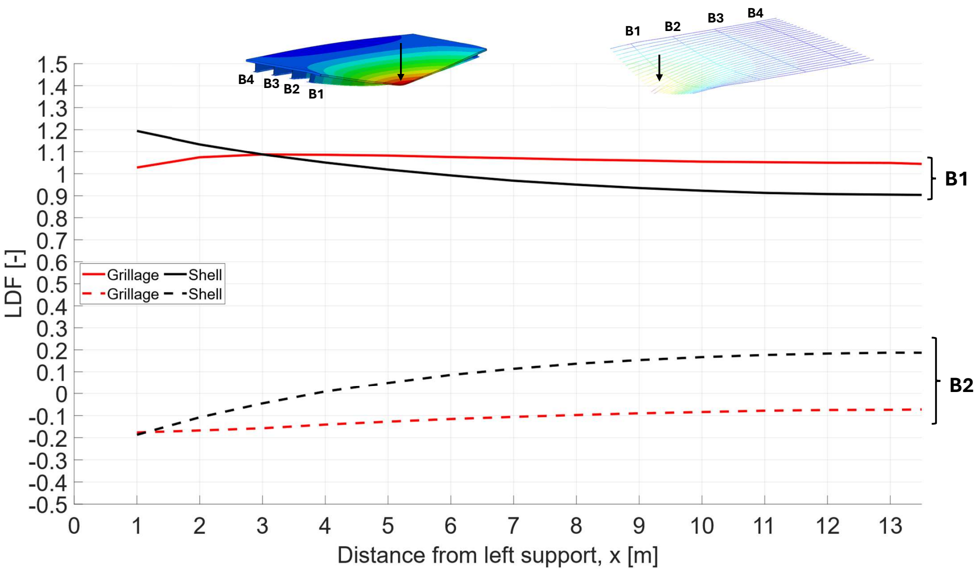

Figure 4.12: LDF for beams B1 and B2 in different longitudinal sections (x) for the grillage and the shell model, plotted for half of the span.

From the results above, one can see that the grillage model generally provides conservative results, except near the supports. The reason for the conservatism may be explained by the flow of forces in the model. Since the model is built up by a grid of beam elements, which connect through discrete nodes, the force has to flow through the elements via the nodes to transfer between the elements. This means that when the forces spread transversely, it has to flow through a transverse element and be applied to the next longitudinal in a discrete node, creating a concentrated load application on that girder. The fewer transverse elements that are used, the more concentrated this load will be, thus creating higher load effects in that girder. Also, this flow of forces prevents the load from spreading continuously at inclined angles, as it must spread through a discrete transverse element before reaching the longitudinal ones. Meaning that the load spreading will be in a stepwise shape. In contrast, the shell model can capture load spreading in all directions, leading to greater load distribution and thus lowering the LDFs.

Figure 4.13 shows the deformation shapes for both models under the loading in the midspan.

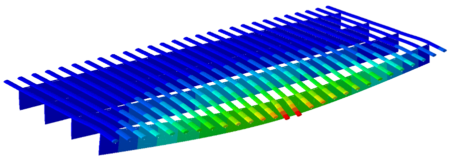

(a) Deformation shape for the grillage model

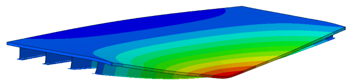

(b) Deformation shape for the shell model

Figure 4.13: Deformation shapes from the shell and the grillage model for a load placed in midspan.

The figure demonstrates that the deformation shapes of both models differ, with the grillage model capturing more of an uplift in B2 compared to the shell model. This is due to a weak behavior of the slab, which makes it transfer a small amount of load to the other girders as well as a large deformation under the load, causing it to uplift over B2. This insufficient stiffness may be due to several reasons, including how the connections between the elements are defined, the stiffness of the transverse elements themselves, and insufficient load spreading, as previously discussed.

One apparent difference between the shell model and the grillage model is the connections between the longitudinal and the transverse elements. Whereas the modeling with shells makes the girders and the slab have a composite action in both directions, the approach of beam elements does not allow for the same composite actions between the elements themselves. Even though the longitudinal elements are assigned the stiffness of the composite section, there is nothing that defines that the transversal elements should work together with the longitudinal ones. This creates more of an approach where the slab is put on top of girders of composite action, rather than the slab being cast with the girders, which makes the slab and the girders work as a whole, as the shell model can describe. This lack of stiffness representation is likely to cause some of the differences that we see between the approaches in terms of the lack of load spreading and uplift in B2.

4.6 2D beam models

The implementation of the beam models consisted of two parts: determining the transverse load distribution by determining the LDF and then applying that to a longitudinal beam model. As described in the literature studies of Section 2.3.1, several different methods could determine the LDF, and those that were included in this case study were the Fauchart method, Courbon's method, and the beam model with vertical spring supports.

The loading case presented in Figure 4.5 yields the transverse model in Figure 4.14, which will serve as the basis for the upcoming models.

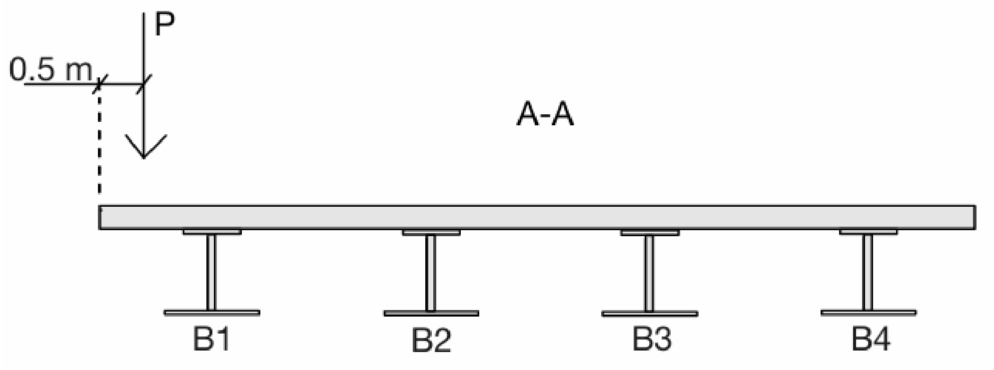

Figure 4.14: The LDFs are calculated from each modeling approach by moving a point load P along a longitudinal line positioned at $y = 0.5$ m.

4.6.1 LDF determined by Courbons method

Courbon's method was implemented using Equation 2.4 to determine the LDF for beams B1 to B4 under the loading of P. The girders were assumed to have equal stiffness, which was considered constant throughout the span. The calculations of the LDFs using this method are presented in Appendix C. Furthermore, the resulting LDFs calculated using Courbon's method compared to those determined by the shell model for beam 1 (B1) and beam 2 (B2) are shown in Figure 4.15.

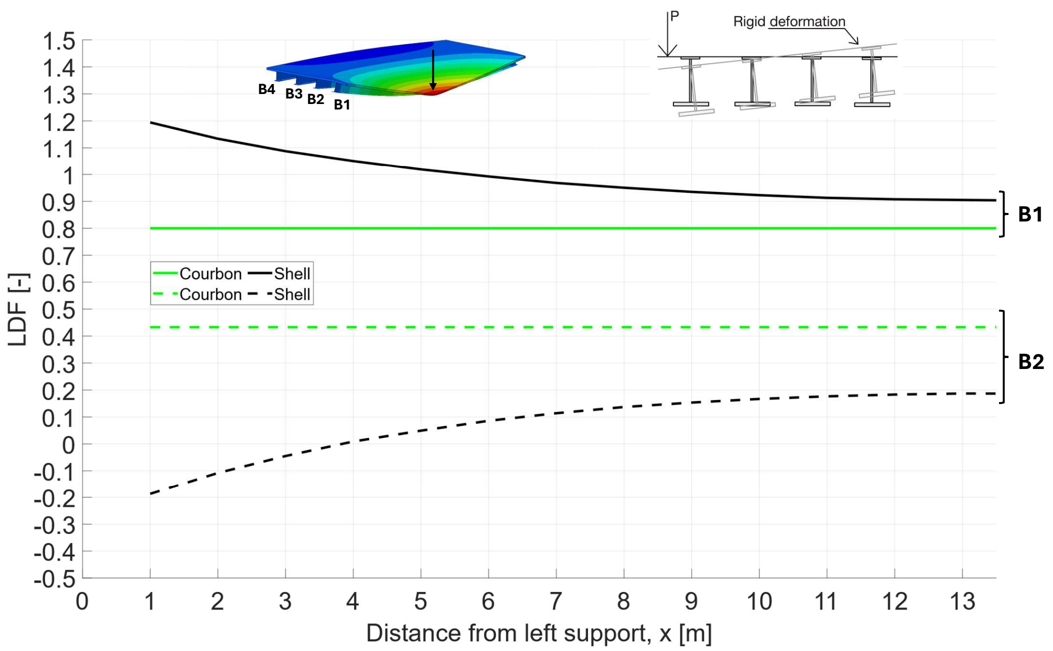

Figure 4.15: LDF for beams B1 and B2 in different longitudinal sections (x) for Courbon's method and shell model, plotted for half of the span.

From the results, one can see that Courbon's method produces unconservative results for beam 1 (B1), leading to an underestimation of the load effects under this loading case for that beam. This difference is greatest near the supports but gradually decreases towards the midspan. Furthermore, the LDF is overestimated for B2.

This can be explained by the fact that Courbon's method assumes a rigid deformation, resulting in a more even load distribution between the girders. However, the deformation in this case is non-rigid, as illustrated in the deformation figure from the shell model. Especially for this case study, where the lack of transverse beams connecting the girders causes more non-rigid deformation behavior. A non-rigid deformation will reduce the slab's ability to distribute the loads, and more load will reach B1. Since the shell model can capture these non-rigid deformations, it will yield a higher LDF for B1. Therefore, one can see that for this case, the structural system is too flexible in its transverse direction to be considered rigid, and the main assumption behind Courbon's method is therefore not fulfilled, which makes it unsuitable. Instead, this method may be more applicable in cases where transverse beams connect the girders, making the transverse deformation more rigid, thus fulfilling the assumption behind the method.

Furthermore, one can see that the difference between the models is greatest close to the supports, whereas it decreases toward midspan. This can be explained by the relative stiffness of the components. At midspan, the girders are flexible, which forces the slab to distribute loads more evenly between the girders, resulting in a more rigid-like deformation that yields results that align with Courbon's method. On the other hand, at the supports, the deformation approaches zero, and the stiffness of the girders is effectively infinite. However, the slab's stiffness is not infinite and will therefore undergo a non-rigid deformation, which will affect the load distribution. This effect is clearly seen in Figure 4.16, where the deformation shapes for the load placed at the support and the midspan are presented. This figure illustrates that the deformation at the support is less rigid than at midspan, which also explains why Courbon's method better predicts the LDF at this location.

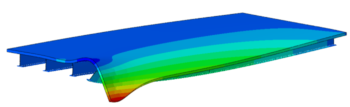

(a) Deformation shape for a load placed close to the support.

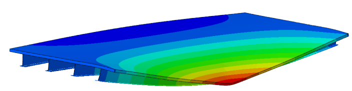

(b) Deformation shape for a load placed in mid-span.

Figure 4.16: Deformation shapes from the shell model for a load placed at the support and at the mid-span.

4.6.2 LDF determined by Fauchart's method

The Fauchart method was implemented by utilizing Equation 2.7 and Equation 2.8 to calculate the stiffnesses of the vertical and rotational springs, respectively. Where the parameters in the formulas were taken as those of the composite section. The stiffnesses were then implemented in a transverse beam model in Brigade/Plus by the structural model seen in Figure 4.17.

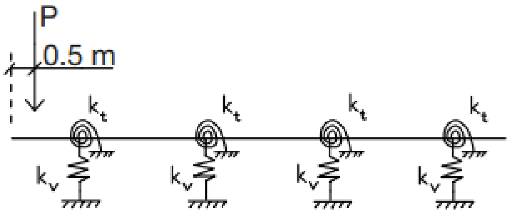

Figure 4.17: Structural model for the implementation of the Fauchart method.

From the analysis, the reaction forces in the vertical springs were extracted, and the LDF was subsequently calculated. The resulting LDF for beams 1 (B1) and beam 2 (B2) compared to those from the shell model is seen in Figure 4.18.

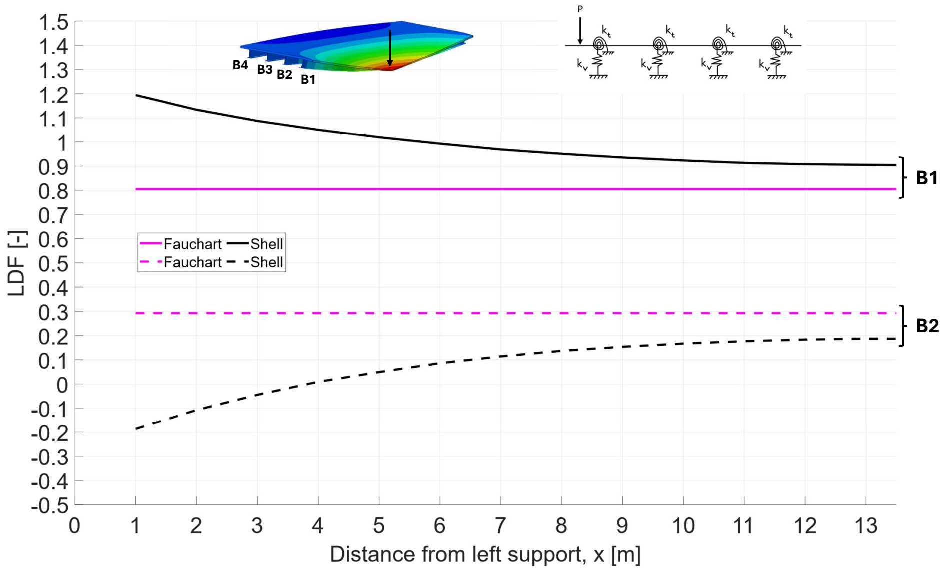

Figure 4.18: LDF for beams B1 and B2 in different longitudinal sections (x) for Fauchart's method and shell model, plotted for half of the span.

From the figure above, it can be seen that the LDF for B1 is underestimated compared to the shell model, which will lead to unconservative results. Similarly to Courbon's method, it seems to distribute the load more towards beams B2-B4. One can also see that it provides a better estimation closer to mid-span, whereas the estimation becomes worse towards the end section.

One source of error with this modeling approach is the consideration of the rotational springs and how that is transferred into an LDF. In the results presented above, the LDF has been calculated by extracting the reaction force in the vertical springs. However, it can be questioned if that really represents the true structural behavior or if the reaction force in the rotation spring has to be considered as well. Then the question arises about how the inclusion of the rotational reaction should be implemented practically. In this thesis, this topic has been left open and not investigated further, which leaves room for further studies.

4.6.3 LDF determined by the transverse beam model with vertical spring supports

The transverse model uses a beam equivalent to a 1 m wide strip of the concrete slab, resting on four vertical springs representing the four girders supporting the slab. To determine the load distribution factor (LDF), a point load is applied 0.5 m from the edge of the slab cantilever and 1 m from the first spring support, as described in Section 4.6. The deflection of the girder is dependent on the longitudinal position (x), as the girder exhibits a stiffer behavior close to the supports than in the midspan. Consequently, the stiffness of the vertical spring supports for each cut is calculated based on the deflection of the girder at that longitudinal position, shown in Figure 4.19.

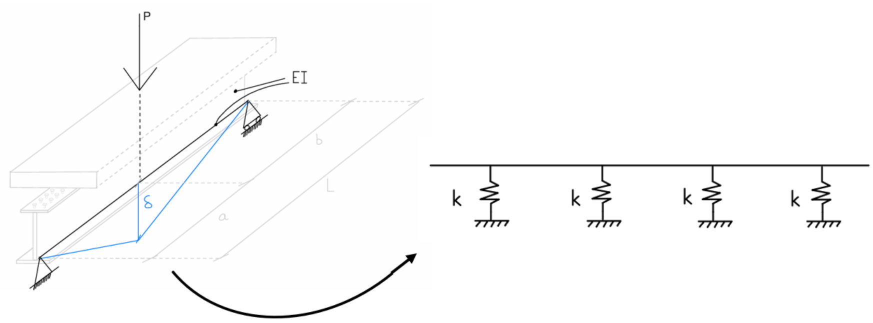

Figure 4.19: How the spring stiffness is calculated for each cut.

As the point load is moved along the x-axis towards the support, new spring stiffnesses are calculated for each cut. Consequently, the spring stiffness is assumed constant for all four girders at a given cut along the x-axis.

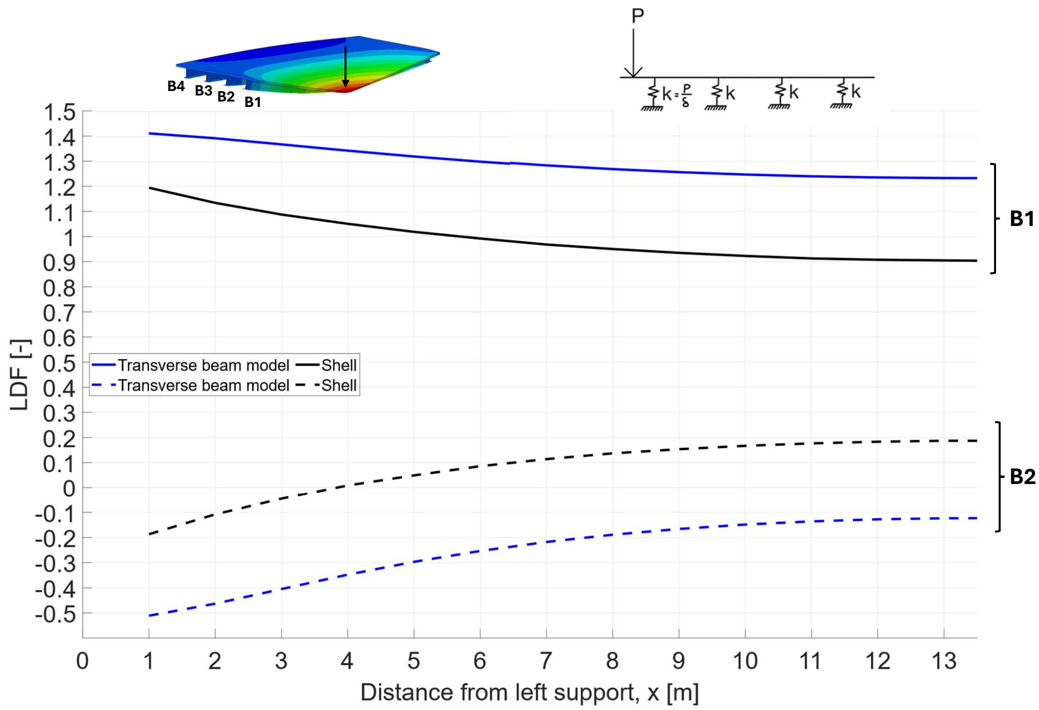

Figure 4.20: Comparison of LDF between the transversal beam model and the shell model.

The results presented in Figure 4.20 show that the transverse beam model produces conservative results for beams 1 (B1) and 2 (B2). The discrepancy is greatest at mid-span; however, it remains approximately constant throughout the span. One possible explanation for the difference between models is that the load distribution, or "smearing" of the load through the concrete slab, is not accounted for. Furthermore, the assumption that all girders have equal stiffness is not entirely accurate, as their deflections vary with load position, the load distribution through the slab, and other structural effects. Especially since the girders exhibit stiffer behavior the farther they are from the load, meaning that, since stiffness attracts load, more load should go to beams 3 and 4.

In addition, beam 2 has a negative LDF, which means that the girder is bending upward, experiencing an uplift for all cuts. However, the shell model displays a similar behavior, but only in the cuts close to the supports, and as the load moves towards the mid-span, the girder begins to bend downward, as one would expect. The difference in behavior may be due to the assumption of the 1 m strip width, as the load will most likely spread out more towards the girders further away, leading to a stiffer slab strip.

4.7 Determining the most suitable modeling approach

The load distribution factor (LDF) for Beam 1 (B1) and Beam 2 (B2) for all previously introduced models is shown in Figures 4.21 and 4.22, respectively. In the graphs, it can be seen that the transverse beam model is conservative for all sections, with approximately 30% higher LDF values than the shell model.

In Figure 4.21, it can also be seen that both Fauchart and Courbon's methods underestimate the load carried by B1, while also having the drawback of being constant for all sections, meaning no variation is seen compared to the other models, where the load distribution varies depending on which section is analyzed. However, it is reasonable to consider a variation, as the girders have a stiffer behavior closer to the supports than in the mid-span.

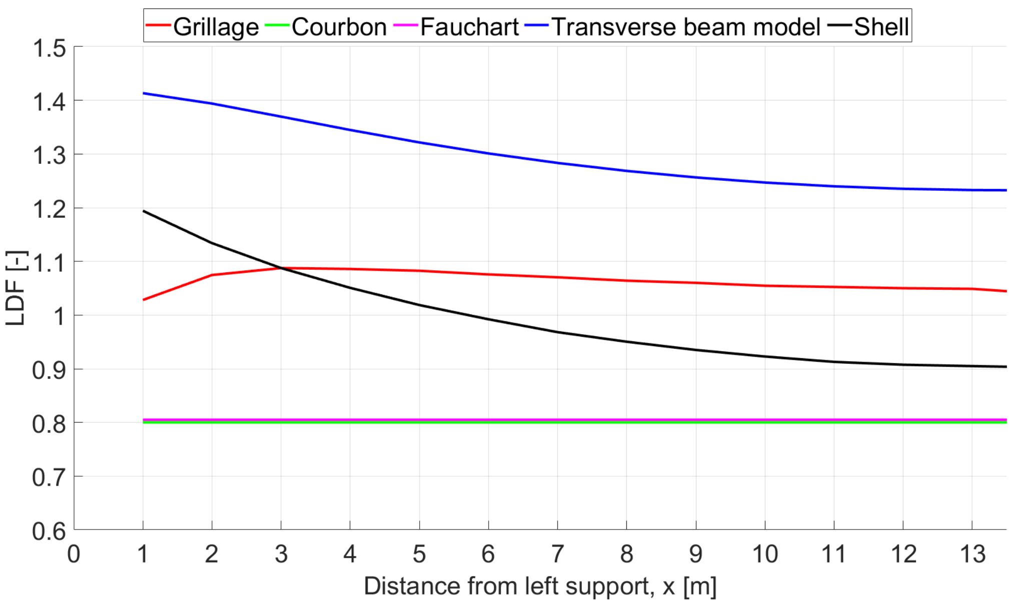

Figure 4.21: Load distribution factor (LDF) for Beam 1 in all models.

In contrast, Fauchart's and Courbon's methods overestimate the load carried by B2. The transverse beam model also overestimates the load, but follows the same overall trend as the shell model. The grillage model also gives conservative results for both beams in all sections except those close to the support. However, this model is complex to construct and not practical to use, and is therefore excluded from further consideration.

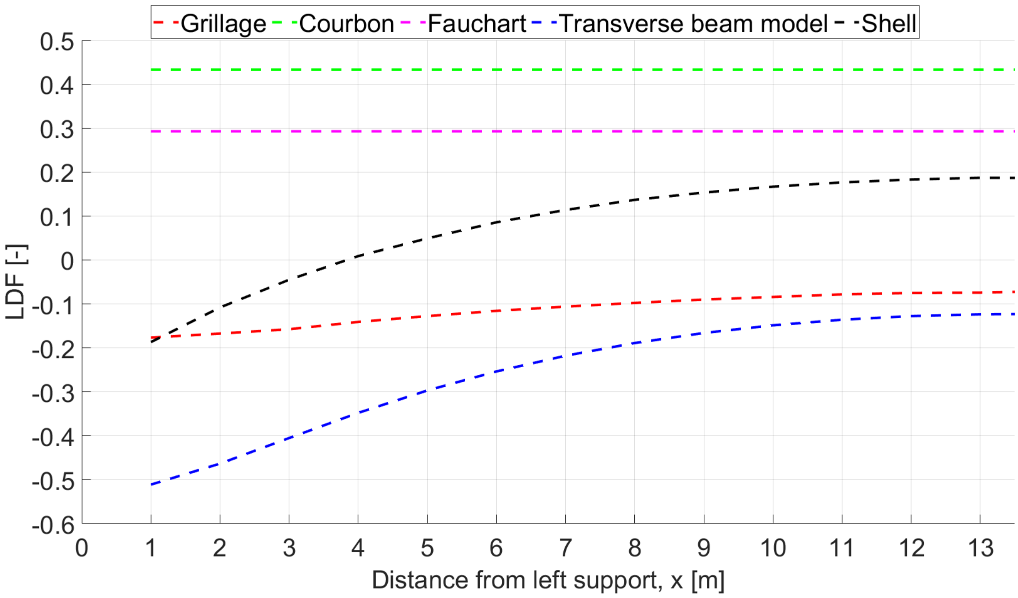

Figure 4.22: Load distribution factor (LDF) for Beam 2 in all models.

As mentioned in Section 4.4, the model is very time-consuming, where the analysis time often takes more than 12 hours to complete. In addition, the building of the model is time-consuming as it is complex with many aspects to consider in order to make the model representative of the structure. As a result of these factors, the shell is solely used as a reference model throughout the thesis.

The most suitable modeling approach was determined as the transverse beam model. The model is both conservative for all sections and simple to adjust and interpret, while at the same time being very quick to analyze, only taking up to 5 min for an analysis. As viewed in Figures 4.21 and 4.22, the transverse beam model consistently overestimates the load in both beams compared to the shell model.

The observed difference of approximately 30% can be attributed to the fact that all springs that represent the beams are assigned the same stiffness. Although the spring stiffness is calculated based on beam deflection, Figure 4.16 shows that each beam experiences a different level of deflection. Consequently, the springs representing the beams should be assigned different stiffness values, as the response becomes more flexible the closer a beam is to the applied load. Furthermore, the transverse beam model does not account for the load spreading through the slab. Consequently, beams located further from the applied load should be subjected to a distributed load rather than a concentrated point load. In addition, as the load spreads, more of the slab width contributes to carry the load, and this wider width should be considered in the slab strip used in the model.

Consequently, the transverse beam model was identified as the most suitable modeling approach. However, further improvements are possible, and these are explained in Section 4.8.

4.8 Updated beam model

In this section, the proposed modeling approach has been updated with the aim of providing more accurate results. To understand how the model performs over the whole bridge, two load cases with a point load, $P = 100$ kN, were defined. The first load case is the same as previously described in Sections 4.2 and 4.6, where the point load is placed 0.5 m from the edge of the slab cantilever, as viewed in Figure 4.5. In the second case, the point load P is placed on the transverse symmetry line of the slab, as viewed in Figure 4.23. With this second load case, an understanding of how the load is distributed from the middle of the slab will be established.

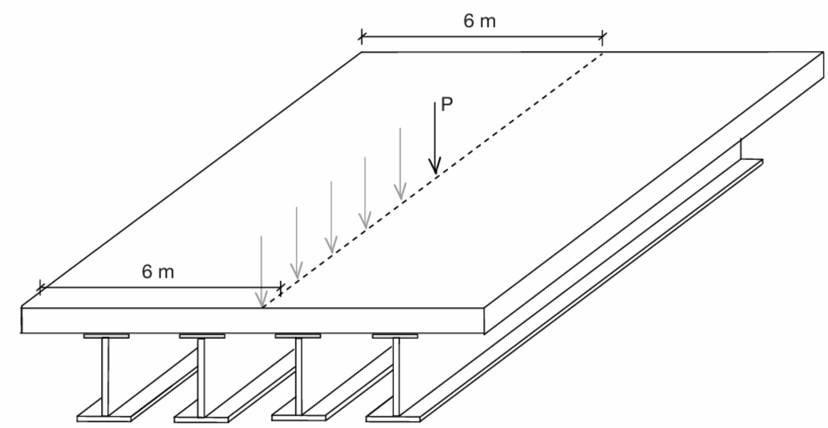

Figure 4.23: Loading line positioned at $y = 6$ m (transverse symmetry line of the bridge), where a point load P is moved along to calculate the LDF at different longitudinal sections.

The transverse model with vertical springs has been updated using the results obtained from the analysis of the shell model. To improve the transverse model, the shear force distribution in the slab and the reaction force in each girder have been analyzed to determine how much the load is smeared across the slab, and using that width to calculate both the deflection on that girder and the width for the considered strip of the concrete slab. To calculate the deflection and consequently the spring stiffness, the smeared load is approximated as a uniformly distributed load throughout that width, as viewed in Figure 4.24.

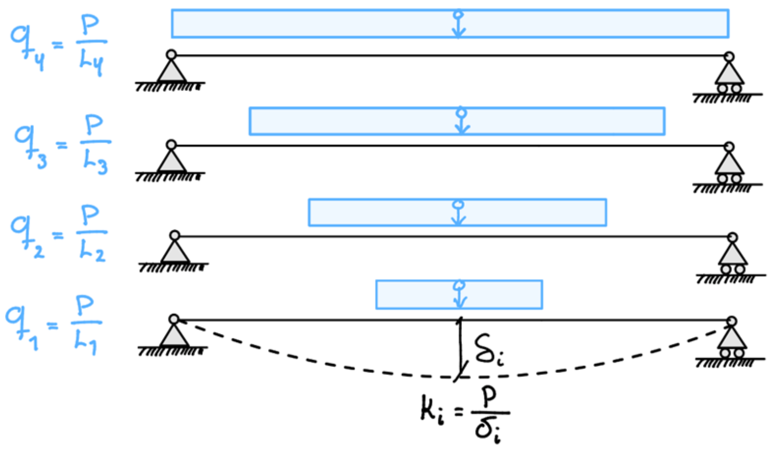

Figure 4.24: Calculation of deflection from smeared loads.

The effective width is determined using different load-spreading angles that aim to capture the load distribution behavior within the slab. Some load-spreading angles were investigated, and they are seen together with the black curves representing the reaction forces, in Figures 4.25 and 4.26. The reaction force in each girder is calculated as the difference between the slab shear force in a section immediately before the girder and that in a section immediately after the girder. Therefore, this difference represents the portion of the applied load that is transferred to each girder through the slab. For sections located near the support, the load-spreading is limited by the slab boundaries. Since the load cannot spread beyond the slab edges, the effective width increases only on one side of the load.

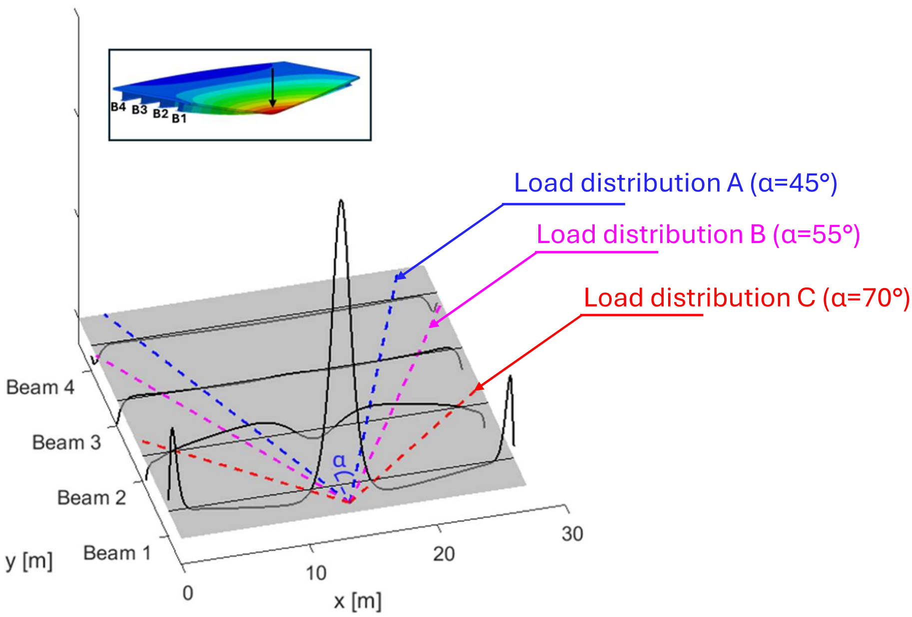

Figure 4.25: Reaction force in each girder with a point load applied on the slab cantilever edge in mid-span, with the estimated distribution angles plotted.

In the figure, it is clear that the reaction force in the girder is strongly concentrated close to the point load. This is seen as the peak over girder 1, since that is closest to the load, which means that the load has not spread. The peak is getting smaller for the other girders, meaning that the load has been distributed.

For the load case where the point load is applied on the edge of the slab cantilever, as in Figure 4.25 and Appendix D, three load distribution angles were considered: $45°$, $55°$, and $70°$. The $45°$ angle represents the conventional assumption commonly used for shear distribution in concrete. The $55°$ angle corresponds to an approximately even distribution from the load application point to the ends of Beam 4, as the load appears to be completely spread over the length of that girder, as seen in the reaction force in Figure 4.25. While the $70°$ angle was selected to match the zero-points of the reaction force diagram for Beam 2.

In particular, the $70°$ distribution was chosen to provide the most accurate representation possible of the load distribution for Beams 1 and 2. Since other load cases are expected to govern Beams 3 and 4, the focus for this load case has primarily been on Beams 1 and 2.

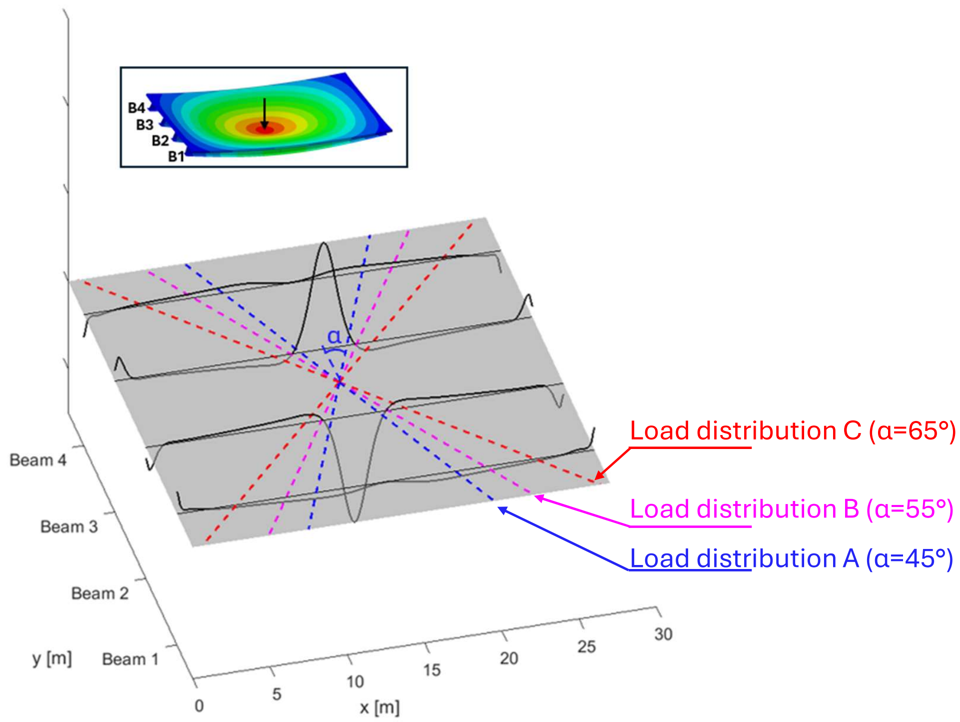

Figure 4.26: Reaction force in each girder with a point load applied in the middle of the slab in mid-span, with the estimated distribution angles plotted.

For the load case where the point load is applied in the center of the slab, shown in Figure 4.26 and Appendix D, three load distribution angles were considered: $45°$, $55°$, and $65°$. The $45°$ angle represents the conventional assumption commonly used for shear distribution in concrete. The $55°$ angle was selected to match the zero-points of the reaction force diagram for Beams 2 and 3, while the $65°$ angle corresponds to an approximately even distribution from the load application point to the corners of the slab, and to approximately match the zero-points of Beams 1 and 4.

At first, only the spring stiffness was changed based on the distribution angles for each load case while keeping the same 1 m strip width to represent the concrete slab. The updated models are shown in Figure 4.27.

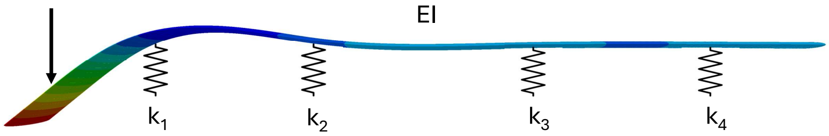

(a) Load applied at the edge of the slab cantilever, where $k_1 < k_2 < k_3 < k_4$.

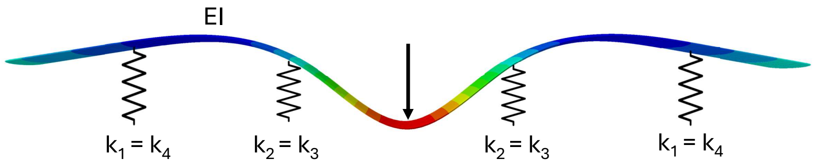

(b) Load applied in the center of the slab, where $k_2 = k_3 < k_1 = k_4$.

Figure 4.27: Updated transverse beam model with varying spring stiffness and constant strip width of 1 m, resulting in a constant stiffness EI.

As seen in Figure 4.27, the deflection is largest under and close to the load, resulting in weaker springs. Furthermore, an uplift between springs 1 and 2 can be viewed in Figure 4.27a and on both sides of the load in Figure 4.27b. New LDFs are calculated with these updated models, and the results are shown in Figures 4.28 and 4.29.

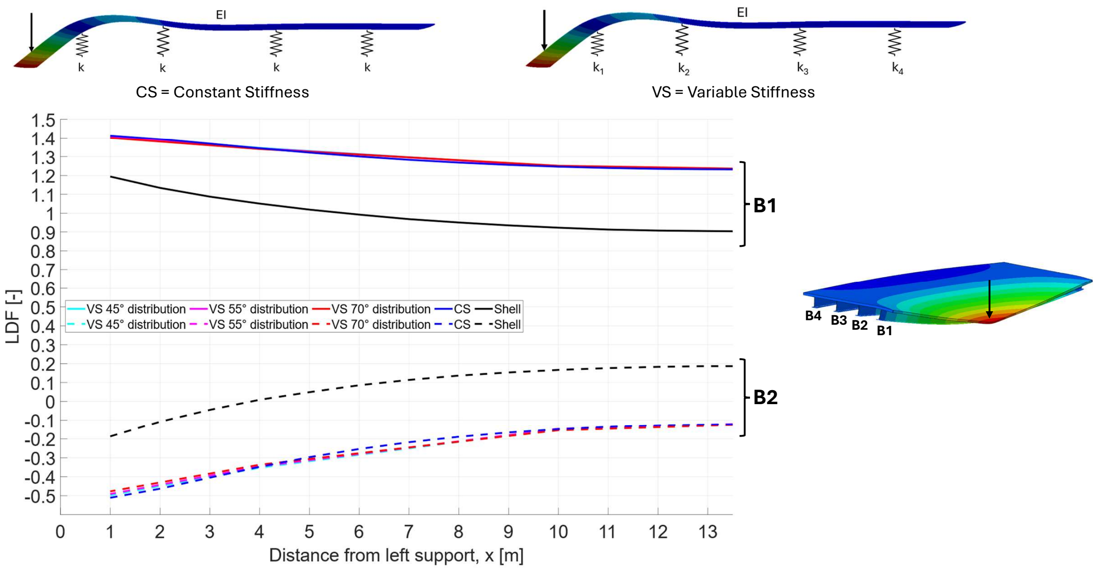

Figure 4.28: LDF results from only changing the spring stiffness of each vertical spring with the load applied on the slab edge.

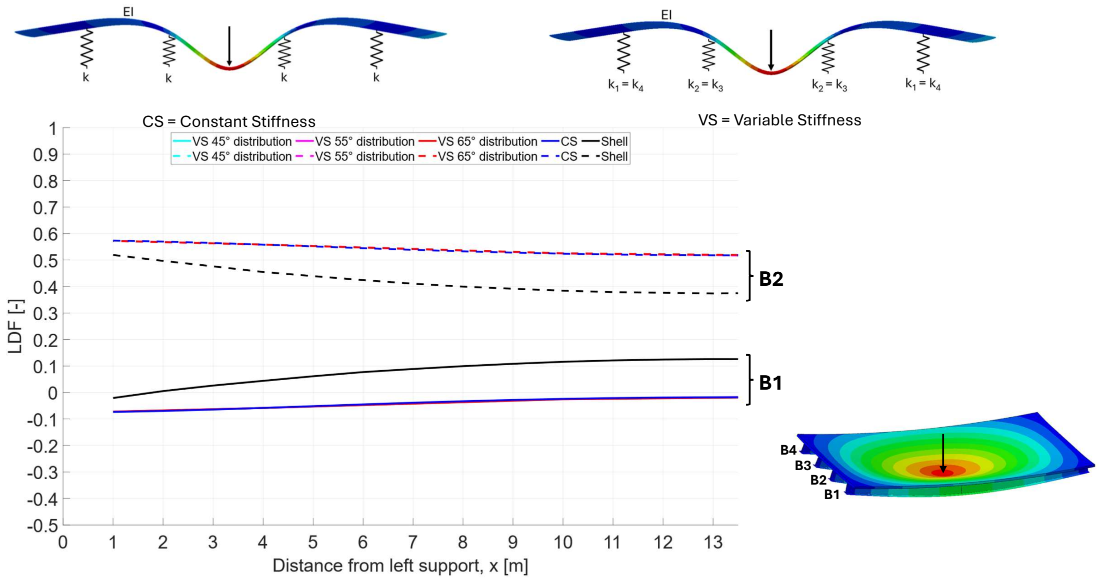

Figure 4.29: LDF results from only changing the spring stiffness of each vertical spring with the load applied in the middle of the slab.

The results in Figures 4.28 and 4.29 do not show any particular improvement when changing the spring stiffness for each beam, depending on the shear distribution width. This is due to the fact that the model does not consider the increased stiffness of the slab, since more of the width can be considered as the load spreads.

To further improve the models, different strip widths are applied to the spans between the vertical springs based on the load-spreads. These models are viewed in Figure 4.30, and an overall stiffer response can be observed compared to Figure 4.27.

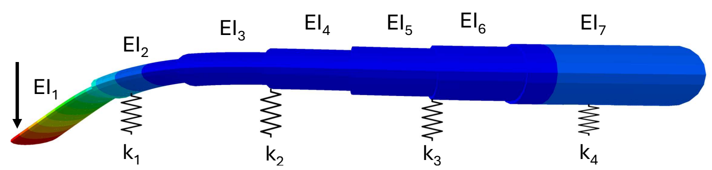

(a) Load applied at the edge of the slab cantilever, where $k_1 < k_2 < k_3 < k_4$ and $EI_1 < EI_2 < ... < EI_7$.

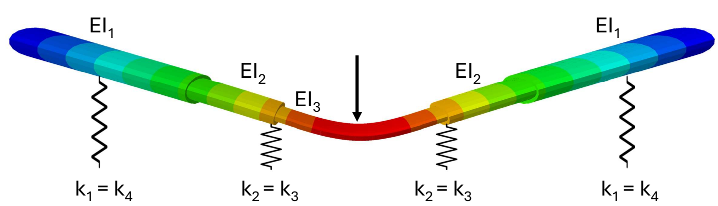

(b) Load applied in the center of the slab, where $k_2 = k_3 < k_1 = k_4$ and $EI_3 < EI_2 < EI_1$.

Figure 4.30: Updated transverse beam model with varying spring stiffness and varying strip width.

As viewed in Figure 4.30, the stiffness of the slab strip is increased in segments. The strip is the weakest under the point load, with the stiffness increasing further away from the load. Consequently, new analyses with these improved models are conducted, and the results of the load distribution factor (LDF) are shown in Figures 4.31 and 4.32.

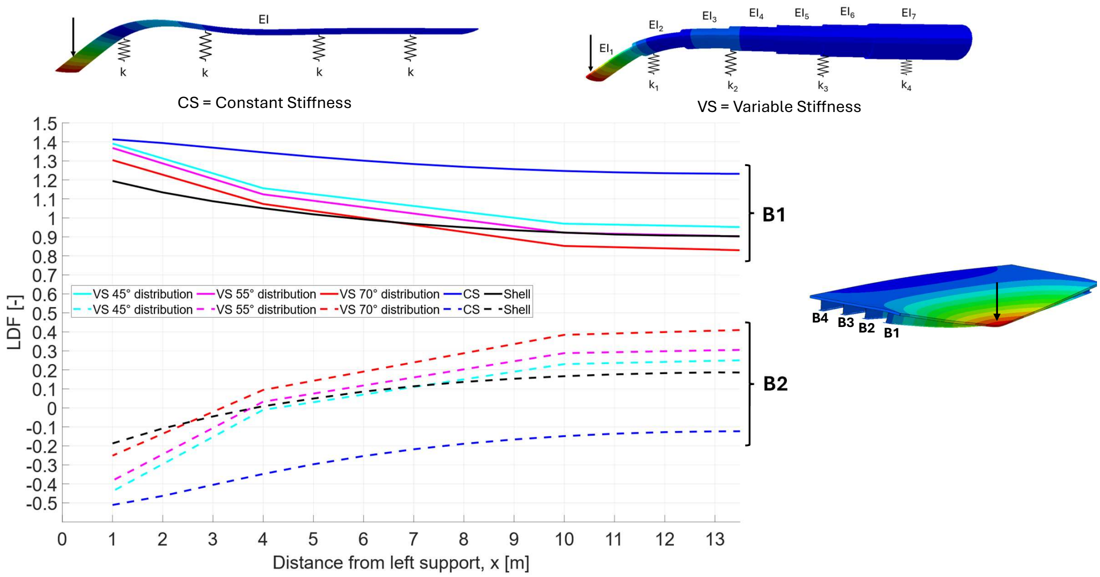

Figure 4.31: LDF for the improved iterations of the transversal spring model VS the shell model with the load applied on the slab edge.

The change in strip width has a large effect on the LDF, with the greatest improvement observed at the mid-span. This can be explained by the rationale behind the selected spreading angles, as discussed previously. Notably, these angles were chosen based on the distribution obtained when the load is applied in the mid-span, as shown in Figure 4.25.

At the mid-span, the angle of $55°$ provides the most accurate results for Beam 1 (B1), while the $45°$ angle is the most accurate for Beam 2 (B2). In addition, all investigated angles yield conservative results, which is desired, as the load effects will not be underestimated. As a result, the angle of $55°$ is chosen as B1 is the most critical for this load application; thus, a high accuracy for that beam is desired. Similarly, the second load case will be governing for B2, as viewed in Figure 4.32.

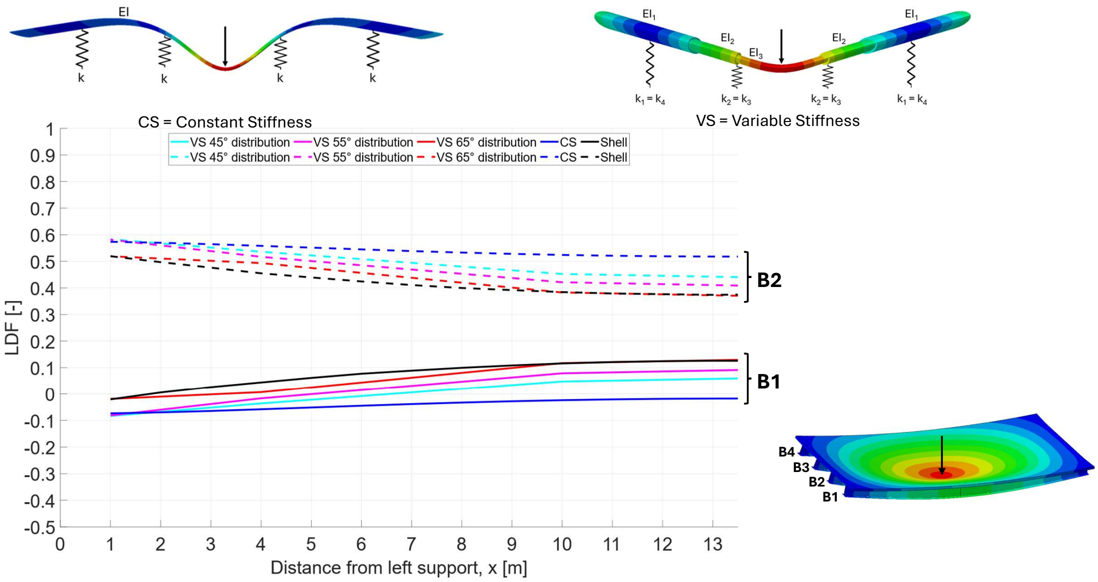

Figure 4.32: LDF for the improved iterations of the transversal spring model VS the shell model with the load applied in the middle of the slab.

As expected, Beam 2 carries a larger proportion of the load when a point load is applied near the center of the deck than when the load is applied at the cantilever edge. The results indicate that a load spreading angle of 65° is in the best agreement with the shell model for Beam 1 and Beam 2. Particularly in the mid-span and the support sections, which are the most critical sections for the bending moment and shear force, respectively.

Based on the results presented in Figures 4.31 and 4.32, a workflow has been developed to determine the load distribution factors (LDFs) and load effects. The workflow illustrates a procedure that designers can utilize in a preliminary design to determine LDFs for bridges subjected to concentrated point loads and distributed loads. The complete workflow is presented in Figure 4.33.

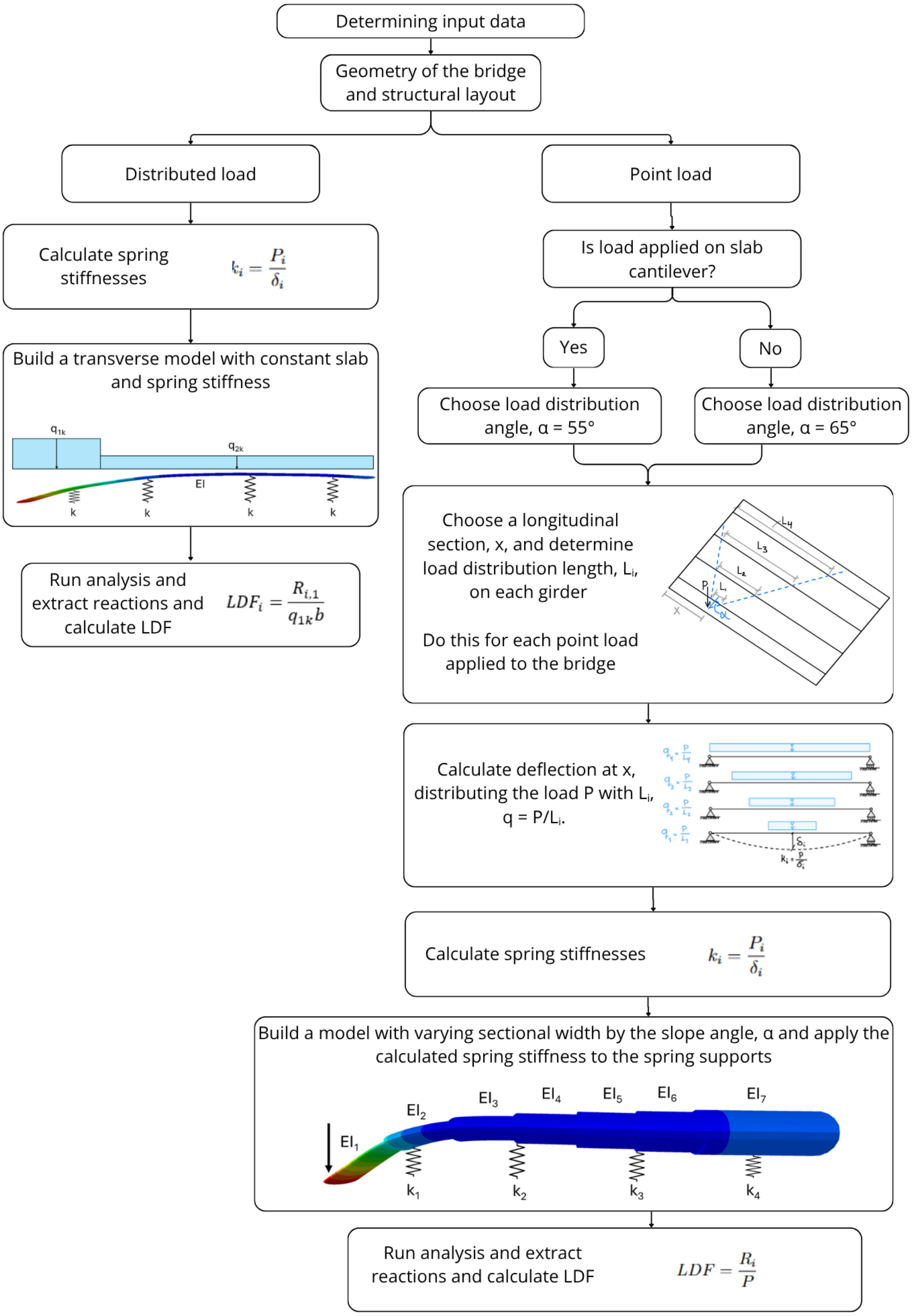

Figure 4.33: Workflow-chart for a proposed approach to the determination of the load distribution factor.

In the remainder of this thesis, the model with varying stiffnesses is referred to as "the updated transverse beam model", whereas the original model with constant stiffnesses and a slab strip width of 1 m is referred to as the "original transverse beam model".

4.9 Full structural analysis with the selected modeling approach

The next step was to implement the recommended modeling approach in a full structural analysis of the bridge. In this thesis, the load effects were calculated at mid-span to find the maximum bending moment, and at the supports to find the maximum shear force. As explained in Chapter 3, the cross-sectional design involves the calculation of stresses in different stages. Therefore, the load effects need to be determined for each stage. The different load cases and what loads are considered are seen in Table 4.4.

Table 4.4: Description of load cases and stages for which the load effects are calculated.

Loadcase/Stages	Description	Loads
G1_1	Construction, concreting	Self-weight of wet concrete, steel girders and formwork as well as construction loads.
G1_2	Formwork removal	Upward load from the self-weight of the formwork, the difference between wet and hardened concrete, and construction loads.
G2	Pavement application	Self-weight of pavement.
TR_Char	Traffic loads	LM1, LM2, and Transportstyrelsen classification vehicles.
TR_FAT	Fatigue loads	FLM 3.

The loads considered included permanent-, traffic-, and fatigue loads, with a focus on vertical loads, thus neglecting horizontal actions, such as braking loads. Shrinkage and temperature loads were also excluded from the analysis, which was shown to be a reasonable simplification in Section 4.4.

The traffic loads are the Load Model 1 (LM1) and Load Model 2 (LM2) according to SS-EN 1991-2:2024 6.3.2 and 6.3.3, as well as the classification of vehicles from Transportstyrelsen given in TSFS, Chapter 11 (Transportstyrelsen, 2018). Fatigue loads are considered using the Fatigue Load Model 3 (FLM 3) provided in SS-EN 1991-2:2024 6.6.7.

Permanent loads included the self-weight of the structural elements themselves, along with the pavement. In addition to these, an approximate load of 0.5 kN/m^2 was applied for the formwork, and 0.75 kN/m^2 was added to account for construction loads, according to SS-EN 1991-1-6:2005 tab 4.1. The self-weight of the concrete was increased by 1 kN/m^3 in the concreting stage (G1.1), as wet concrete is slightly heavier, according to SS-EN 1991-1-6:2002 4.11.2.

To evaluate the performance of the updated model compared to the original beam model with constant stiffness and the shell model, structural analyses were conducted using all three models. The implementation of the original model followed the procedure described in Section 4.6.3, where a transverse beam model is constructed with constant spring and beam stiffness. Whereas the analysis with the shell model followed the same procedure as explained in Section 4.4, incorporating additional traffic surfaces to allow Brigade/Plus to apply traffic loads.

To find the LDF using the updated beam model with varying stiffnesses, the following procedure was applied. The highest load effects occur in one of the outer girders when the tandem loads are positioned as far out on the cantilever as possible. For LM1, this load placement is illustrated in Figure 4.34.

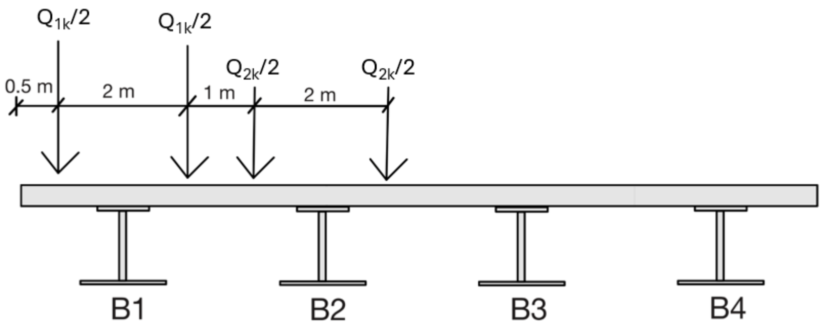

Figure 4.34: Placement of LM1 axle loads that yield the highest load effects in any girder of the bridge, which will be in the outer girder, B1.

Subsequently, two different models were constructed based on the load-spreading from the center of the wheel loads in each lane. A graphical explanation of this is viewed in Figure 4.35.

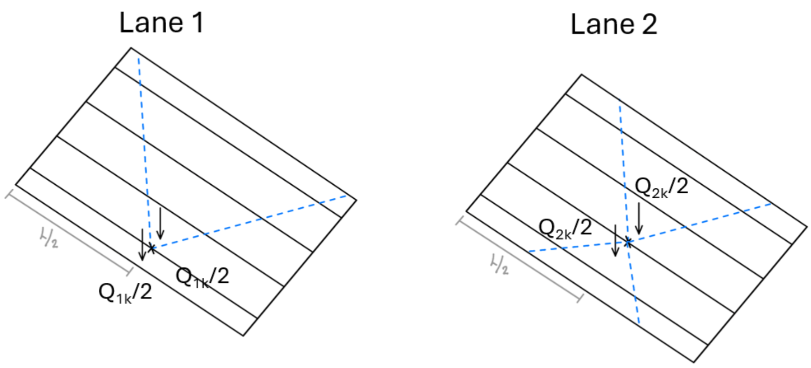

Figure 4.35: The principle that was used to build the transverse models to find the LDF in the full structural analysis of the case.

By using the proposed modeling method presented in Section 4.8, these two models presented in Figure 4.36 were constructed. Since the transverse tandem configuration of LM1 and Transportstyrelsen classification vehicles is the same, the same models could be used for both of the load cases.

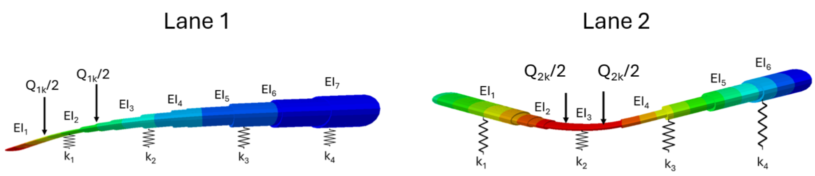

Figure 4.36: Models to find the LDF of tandem loads in the full structural analysis of the case.

The models shown above were constructed for the mid-span section to determine the maximum bending moment. Conversely, the maximum shear force occurs at the support section, requiring the models to be reconstructed for that specific location. Regarding the load distribution at the supports, it was defined using the recommended distribution angles, but constrained to not extend beyond the bridge boundaries, as illustrated in Figure 4.37.

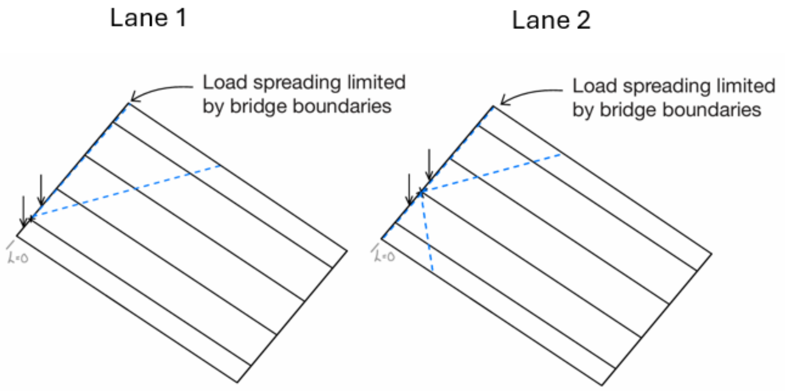

Figure 4.37: The load distribution that was accounted for when constructing the models for the support sections ($x = 0$ m), illustrating that the distribution is limited by the bridge boundaries.

As shown in Figure 4.37 above, the load spreading is asymmetrical, as it only extends to one side. However, this asymmetry was not considered in the development of the models, which were instead based solely on the increasing stiffness.

The LDF from the tandem loads was calculated by summing the reaction forces in beam 1, from the models in lanes 1 and 2, and dividing this sum by the applied load in the longitudinal 2D beam model, as explained in Section 2.3.1.

For the self-weight and the distributed loads of LM1 and Transportstyrelsen classification vehicles, the LDF was obtained using the original transverse beam model with constant stiffnesses. This is because the maximum load effects from the distributed loads occur when they are applied across the entire bridge, meaning no effects from load spreading need to be considered. Therefore, the original model with constant stiffnesses performs equally well as the updated model with varying stiffnesses for those loading cases. The highest load effect in the outer girder due to the distributed loads in LM1 is obtained from the following configuration, where the highest intensity is placed in lane 1, see Figure 4.38.

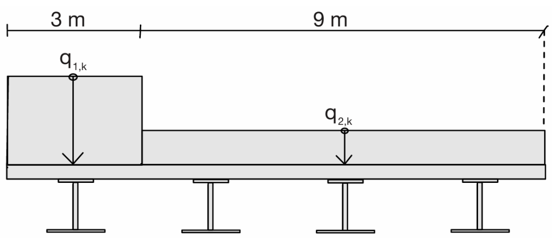

Figure 4.38: Placement of the distributed LM1 loads that yields the highest load in Beam 1.

However, the self-weights and the distributed loads from the Transportstyrelsen classification vehicles have a constant intensity, meaning there is no specific load placement to consider. The model used to calculate the LDF from the distributed loads was established in accordance with Section 4.6.3, and is seen in Figure 4.39. The figure illustrates that the model has equal stiffness for the spring supports, as well as a constant slab stiffness.

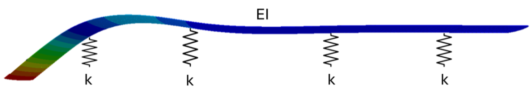

Figure 4.39: The model with constant stiffnesses was used for the determination of LDF from the distributed loads.

Subsequently, a 2D longitudinal beam model analysis was conducted using the LDFs calculated according to the above. The resulting bending moments for the characteristic traffic loads and the fatigue loads from the original model with constant stiffnesses, the updated model with variable stiffnesses, and the shell model are presented in Figure 4.40.

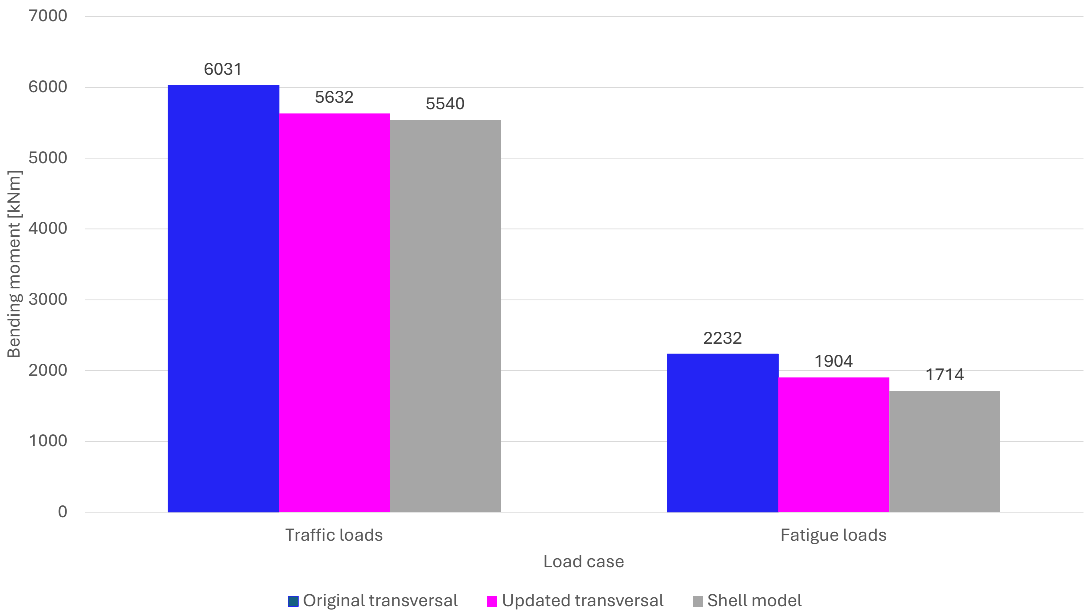

Figure 4.40: Resulting bending moment at mid-span for the outer girder using the original model with constant stiffness, the updated model with varying stiffness, and the shell model.

The diagram illustrates a clear benefit of using the updated model, as the bending moments from the characteristic traffic loads decreased from 6031 kNm to 5632 kNm, representing a reduction of 6.6%. Furthermore, the results of the updated model closely align with those of the shell model, which yielded 5540 kNm. This represents a difference of 1.6%, compared to the 8.9% difference between the shell and the original model. The same applies to the fatigue loads, where the updated model yielded an improvement of 14.7%. Additionally, the difference between the updated model and the shell model for the fatigue loads was 11.1%, compared to 30.2% for the original model.

The resulting maximum shear force at the support section from the characteristic traffic loads and the fatigue loads for the original model, the updated model, and the shell model are presented in Figure 4.41.

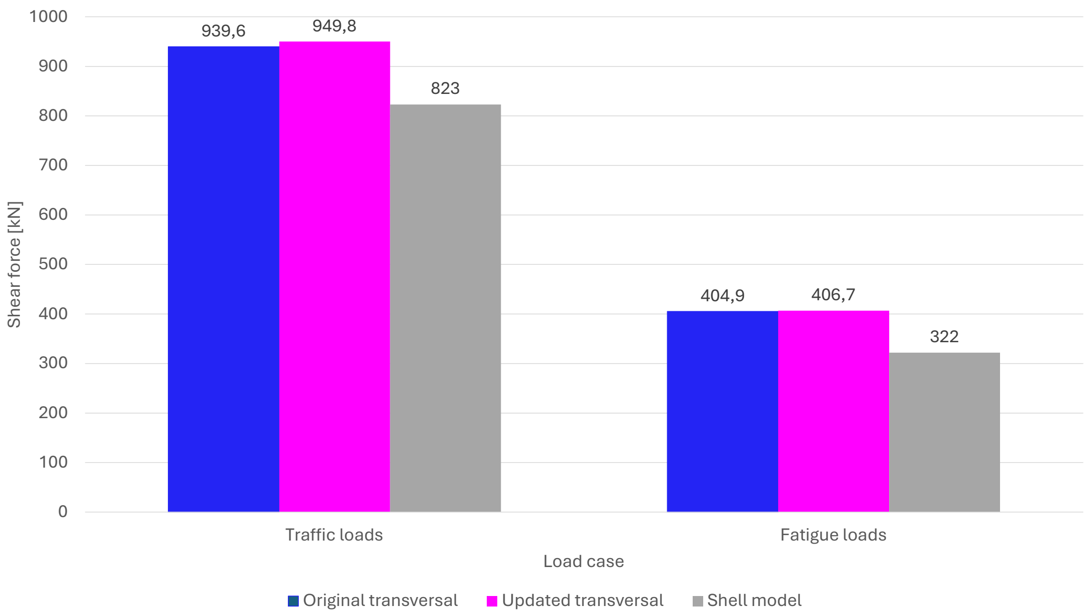

Figure 4.41: Resulting shear force at support for the outer girder using the original model with constant stiffness, the updated model with varying stiffness, and the shell model.

The results indicate that the shear forces are slightly overestimated when using the updated model compared to the original model. The updated model overestimates the shear force caused by traffic loads by 15.4% compared to the shell model, whereas the original overestimates it by 14.2%, meaning that the updated model overestimates the shear force by an additional 1.1% compared to the original model. Regarding the shear forces from the fatigue loads, it can be seen that the updated model predicts a 0.44% higher shear force than the original model. Compared to the shell model, the updated model yields a 26.3% higher shear force, whereas the original model yields an increase of 25.7%.

The reason for this is a combination of the stiffness distribution in the beam element and the stiffnesses of the springs. Close to the support, the deflection will reach zero, leading to an infinitely large stiffness of the springs. A beam supported by stiff supports will spread less load between the supports than if it had soft supports. The shell model, on the other hand, has the ability to include the deformation of the web itself, meaning that the supports have some flexibility and the stiffness will not be as high as for the beam model. Therefore, the load will spread more for the shell model than the beam model, which is one of the explanations for the difference in shear force close to the supports between the models. It is worth noting that, in this case, web stiffeners at the supports were not included, which allows for this deformation of the web. In practice, however, stiffeners are generally included, which would decrease the deformation of the web and thus increase the LDF in B1.

However, as previously shown in Figure 4.28, the stiffness of the springs did not have much effect on the load distribution; it is likely that the difference may originate from the stiffness distribution of the slab. This means that the load spreading angles that were used are not perfect for the construction of a model to predict the shear force at the supports. The explanation for this is one of the following scenarios. The first being the model used for calculating the LDF for lane 1 has insufficient stiffness increase away from the load, meaning that the load is not spread enough from Beam 1 towards Beams 2-4. The second is that the stiffness distribution for the model to calculate the LDF for the loads in lane 2 is too stiff towards Beam 1, meaning that the slab will distribute too much load to that beam.

However, the effects of overestimating the shear force slightly at the supports are believed to be small for the dimensions of the cross-section compared to the benefit of accurately predicting the bending moment in mid-span. To more accurately predict the shear force at the supports, it might be suitable to build models with a stiffness distribution other than that this thesis has suggested using. However, that would lead to additional computational and modeling work with different angles of stiffness distribution for different sections along the bridge. By that, some of the convenience by means of simplicity of using the suggested method is removed. It is also beneficial that the model overestimates the shear force compared to the shell model, which makes it conservative and safe to use. Therefore, the decision was made that it is more convenient to only use the provided angles, with the loss of slightly overestimating the shear force at the supports, as the shear force rarely governs the design.

Worth pointing out again is that the distributed loads do not depend on the load distribution in the slab, since they are already distributed over the whole bridge in this case. Therefore, they are not covered in this comparison above since the concept of load distribution that has been covered in this thesis will not affect the results of these types of loads. However, they are included in calculating the total load effects to use in the cross-section design.

In Table 4.5 below, the resulting load effects in each stage (see Table 4.4) from the structural analysis are presented, where the maximum bending moment in midspan and the maximum shear force at supports are seen.

Table 4.5: Resulting load effects in each stage from the structural analysis based on the original model and the updated model.

Max bending moment [kNm]		
Stage	Original model	Updated model
G1_1	2441	2441
G1_2	-421	-421
G2	1243	1243
TR_Char	6031	5632
TR_UTM	2232	1904

Max shear force [kN]		
Stage	Original model	Updated model
G1_1	360	397
G1_2	-62	-63
G2	184	185
TR_Char	940	950
TR_FAT	405	407

The table shows that the load effects due to the distributed loads remain constant between the updated and the original model. This is because they are distributed across the entire bridge, meaning that load spreading will not affect these particular load responses. Consequently, the updated model yields no different load effects in these cases. The benefits of the updated model are once again for the traffic loads and the fatigue loads, where one can see a clear reduction of bending moment, which often governs the design. The shear force is, however, slightly increased with the use of the updated model.

To obtain the shear forces for the design of the slab, the original transverse beam model seen in Figure 4.39 was used. The loads that were considered were LM1, LM2, Transportstyrelsen classification vehicles, and the self-weight of the concrete and the pavement. Since the load effects of the slab in the transverse is not of great interest for the scope of this thesis, they are not presented here but can be further viewed in Appendix E.

4.10 Cross-section analysis and evaluation of material quantities

To evaluate the influence of changes in load effects from the model improvement, a cross-section dimensioning was performed for both the original and the updated model. The checks were performed according to Chapter 3, with load effects obtained as explained in Section 4.9. In this analysis, the bridge is assumed to have a constant cross-section, and only the worst load effects are considered for the most loaded girder, i.e., bending moment in mid-span and shear at support section for the outer girders.

The slab was designed to be able to resist the shear without the need for shear reinforcement. Based on this, a required thickness of the slab, t_c, was determined and kept constant for all cross-sections throughout the analysis. C35/45 was chosen as the class of the concrete, with XD1 as the governing exposure class. The longitudinal reinforcement area was assumed to be 1% of the concrete cross-sectional area with a rebar diameter of $\phi = 20$ mm. The lower bound of the upper sieve size was assumed to be $D_{lower} = 32$ mm.

With the loads obtained from the structural analysis as explained in Section 4.9, the resulting concrete thickness was determined as $t_c = 230$ mm, which yields a total concrete tonnage of 186.3 tonne for the whole bridge. The design and analysis of the slab are further presented in Appendix E.

For the design of the composite section, the total height of the cross-section was restrained by the maximum construction height of 1330 mm. The stud's diameter was set to $\phi_{studs} = 22$ mm, with a c/c equal to $b_0 = 335$ mm. A minimum width of the top flange is obtained by the requirement from SS-EN 1994-2:2005 6.6.5.6 (2) that the distance between the edge of the flange and the edge of the stud should be at least $e_D = 25$ mm.

In the LT-buckling analysis in stage G1.1, the girders were set to have bracings at mid-span as well as at supports. To be able to use the resulting material quantities as the cost reduction measure, the steel quality was held constant as S355, since a higher steel grade is generally more expensive and would need weighting factors to consider that.

The fatigue assessment was carried out by checking the regions together with their corresponding detail categories as presented in Figure 4.42. The detail categories are as follows:

- A: web to flange weld
- B: butt weld in flange connection
- C: stresses in the top flange around studs
- D: shear stresses in web

It was assumed that each detail was located such that it experiences the worst load effects, i.e., mid-span for normal stresses due to bending and at supports for shear stresses. It was assumed that the butt welds were ground flushed and that the welds were performed in a workshop, meaning that no cope holes are needed.

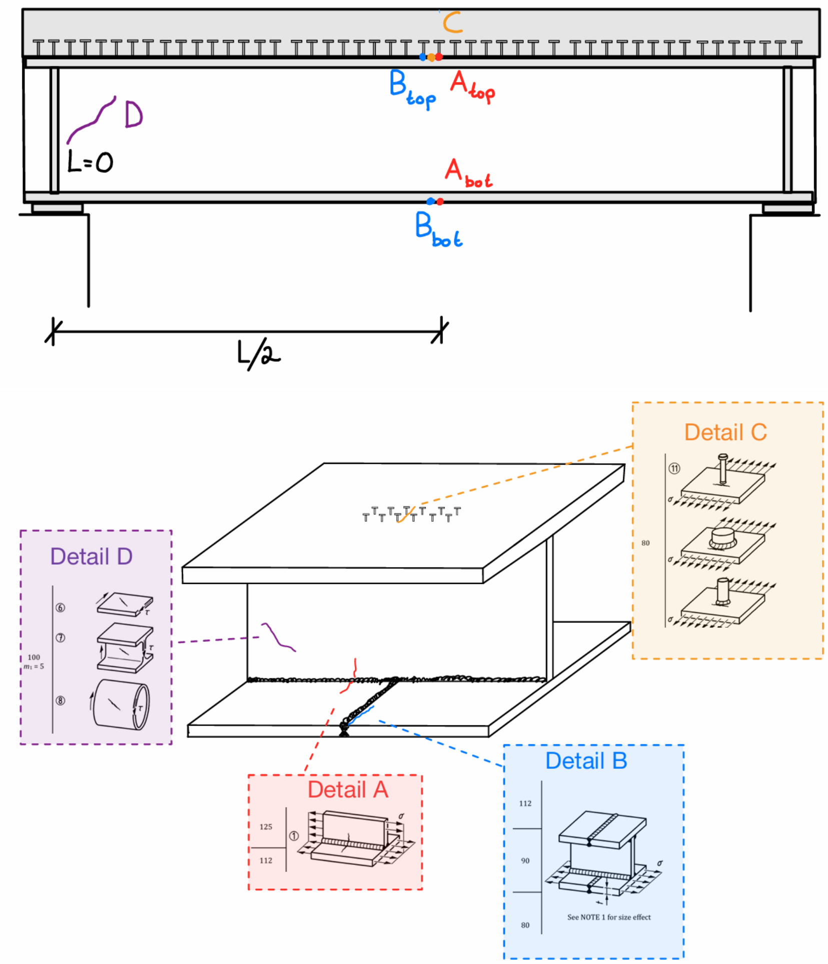

Figure 4.42: Checked fatigue regions with corresponding detail categories according to SS-EN 1993-1-9:2025 10.

The cross sections were designed with respect to the different stages during the structure's lifetime. As described in the case description in Section 4.1, the erection method was chosen as lifting. This means that there will be a load case for the girders from this lifting. However, that has been neglected in this thesis.

The checks were done as explained in Chapter 3 for the cross-section with the highest load effects, and since it is a simply supported bridge, they are at mid-span for bending moments and at the support for shear force. The goals for the designs were to reach utilization rates as close to 100% as possible. The design was carried out by using the following procedure:

1. The flange widths were varied in increments of 5 mm and adjusted iteratively until the utilization ratios were as close as possible to 100%.
2. The flange thicknesses were rounded up to the nearest integer such that the flanges were in CSC 3 for the chosen flange widths.
3. The web height was set equal to the remaining available construction height $h_w = h_{max} - t_c - t_{fo} - t_{fu}$.
4. The web thickness, t_w, was chosen such that the web provided sufficient shear resistance.

It was observed that fatigue frequently governed the design for this particular case. Consequently, the models were also evaluated under different traffic intensities in the fatigue analysis. This was achieved by varying the traffic categories according to SS-EN 1991-2:2024 tab. 6.7, which specifies different values of the annual number of lorries, N_{obs}. Traffic categories 2, 3, and 4 were considered the most relevant to include in the analysis of this case.

The detailed design procedure is presented in Appendix F for a representative cross-section based on the load effects obtained from the original beam model and $N_{OBS} = 0.5 \cdot 10^6$ corresponding to traffic category 2. This procedure illustrates the complete design process and calculation procedure.

The remaining cross-sections were analyzed using the same calculation sheet and design methodology. For each analysis, the relevant input parameters in terms of different traffic categories (N_{OBS}), and the different load effects obtained from the original and updated beam models, were updated. A total of six cross-sections were analyzed. Three analyses were performed using load effects from the original beam model for traffic categories 2, 3, and 4, respectively. The remaining three analyses were carried out using load effects from the updated beam model for the same traffic categories.

The calculated utilization rates, together with their definitions and the stages at which they are checked, are presented in Table 4.6. ULS refers to the ultimate limit state and is based on the combined load effects from the stages G1.1, G1.2, G2, and Tra_Char. FLS refers to the fatigue limit state and is based on the load effects from the Tra_FAT stage.

Table 4.6: Description of utilization rate parameters and corresponding design stages.

Parameter	Description	Stage
Construction Stage (G1.1)		
$\eta_{b,G1.1,\mathrm{top}}$	Check of bending stresses in top flange	G1.1
$\eta_{b,G1.1,\mathrm{bot}}$	Check of bending stresses in bottom flange	G1.1
$\eta_{b,G1.1,\mathrm{LT}}$	Check of LT buckling	G1.1
ULS		
$\eta_{b,\mathrm{concrete}}$	Check of bending stresses in concrete slab	ULS
$\eta_{b,\mathrm{steel,top}}$	Check of bending stresses in top flange	ULS
$\eta_{b,\mathrm{steel,bot}}$	Check of bending stresses in bottom flange	ULS
$\eta_{v,\mathrm{web,steel}}$	Check of shear capacity in steel girder web	ULS
Fatigue		
$\eta_{b,\mathrm{FAT,A,top}}$	Fatigue normal stress at fillet weld between top flange and web	FLS
$\eta_{b,\mathrm{FAT,A,bot}}$	Fatigue normal stress at fillet weld between bottom flange and web	FLS
$\eta_{b,\mathrm{FAT,B,top}}$	Fatigue normal stress at butt weld connecting top flange	FLS
$\eta_{b,\mathrm{FAT,B,bot}}$	Fatigue normal stress at butt weld connecting bottom flange	FLS
$\eta_{b,\mathrm{FAT,C}}$	Fatigue normal stresses at top flange around studs	FLS
$\eta_{b,\mathrm{FAT,D}}$	Fatigue shear stresses in web	FLS

The resulting dimensions of the cross-section using the original and updated model for different traffic categories (N_{obs}), the utilization ratios for each check, and the resulting steel tonnage are seen in Table 4.7. The governing checks in the top and bottom flanges are marked in red for each case.

Table 4.7: Resulting cross-section dimensions, steel tonnage, and utilization ratios for the original and updated model using different N_{obs}. The governing utilization ratios are marked in red.

	$\mathrm{N_{obs}} = 0.5 \cdot 10^6$		$\mathrm{N_{obs}} = 0.125 \cdot 10^6$		$\mathrm{N_{obs}} = 0.05 \cdot 10^6$	
Parameter	**Original**	**Updated**	**Original**	**Updated**	**Original**	**Updated**
Cross-section dimensions [mm]						
b_{fo}	655	540	550	530	540	525
t_{fo}	29	24	24	23	24	23
h_w	1023	1032	1032	1038	1037	1039
t_w	14	14	14	14	14	14
b_{fu}	1100	995	995	900	885	860
t_{fu}	48	44	44	39	39	38
Steel tonnage [tonne]	73.0	60.4	60.6	52.4	52.6	50.3
Improvement	–	-17.3%	–	-13.4%	–	-4.3%
Utilization rates [%]						
Construction stage						
$\eta_{b,G1.1,\mathrm{top}}$	44.2%	57.4%	56.7%	58.6%	56.0%	58.6%
$\eta_{b,G1.1,\mathrm{bot}}$	20.6%	24.1%	24.1%	27.6%	27.8%	29.1%
$\eta_{b,G1.1,\mathrm{LT}}$	53.9%	84.5%	82.0%	93.4%	88.1%	96.5%
ULS						
$\eta_{b,\mathrm{concrete}}$	46.3%	47.9%	50.6%	49.8%	52.5%	50.4%
$\eta_{b,\mathrm{steel,top}}$	84.3%	98.4%	99.97%	99.7%	99%	99.6%
$\eta_{b,\mathrm{steel,bot}}$	71.5%	80.2%	83.6%	93.1%	98.4%	98.7%
$\eta_{v,\mathrm{web,steel}}$	91.6%	91.3%	90.7%	90.8%	90.1%	90.6%
Fatigue						
$\eta_{b,\mathrm{FAT,A,top}}$	80.5%	81.3%	82.6%	85.9%	85.1%	76.1%
$\eta_{b,\mathrm{FAT,A,bot}}$	67.0%	62.4%	63.2%	54.0%	51.9%	44.8%
$\eta_{b,\mathrm{FAT,B,top}}$	73.3%	65.2%	66.0%	56.1%	54.6%	46.7%
$\eta_{b,\mathrm{FAT,B,bot}}$	99.6%	97.8%	99.5%	99.6%	98.7%	87.6%
$\eta_{b,\mathrm{FAT,C}}$	99.7%	92.0%	93.2%	79.9%	77.1%	66.4%
$\eta_{b,\mathrm{FAT,D}}$	78.8%	81.6%	70.3%	70.0%	57.6%	58.1%

From the results presented in the table above, it is observed that the fatigue limit state (FLS) governs the design in at least one verification for all cross-sections except for the case corresponding to the updated model and the lowest traffic category, $N_{obs} = 0.05 \cdot 10^6$.

Furthermore, the butt weld in the bottom flange is identified as the critical detail category, $\eta_{b,\mathrm{FAT,B,bot}}$. For the top flange, the governing check is, in most of the cases, in ULS ($\eta_{b,\mathrm{steel,top}}$), indicating that an increase in the steel quality for the top flange could improve the overall capacity of the sections.

The bottom flange generally exhibits relatively low utilization ratios in ULS ($\eta_{b,\text{steel,bot}}$), suggesting a potential for reducing the steel quality in the bottom flanges to lower material costs. However, since FLS governs the design of the bottom flange in these cases ($\eta_{b,\text{FAT,B,bot}}$), the dimensions cannot be reduced, as it would lead to increased stress ranges.

In addition, since the welded connection in the flange was the governing detail category ($\eta_{b,\text{FAT,B,bot}}$), it may be beneficial to relocate the weld away from the critical section at mid-span towards the supports, where stress ranges are lower. This could potentially reduce fatigue demand and allow for a more efficient design, thus reducing the material quantities.

Since the concrete dimensions were kept constant for all cross-sections, the comparison of material quantities between the different models is based solely on steel consumption. The resulting steel tonnage for the original and updated models for the different traffic categories is shown in Figure 4.43.

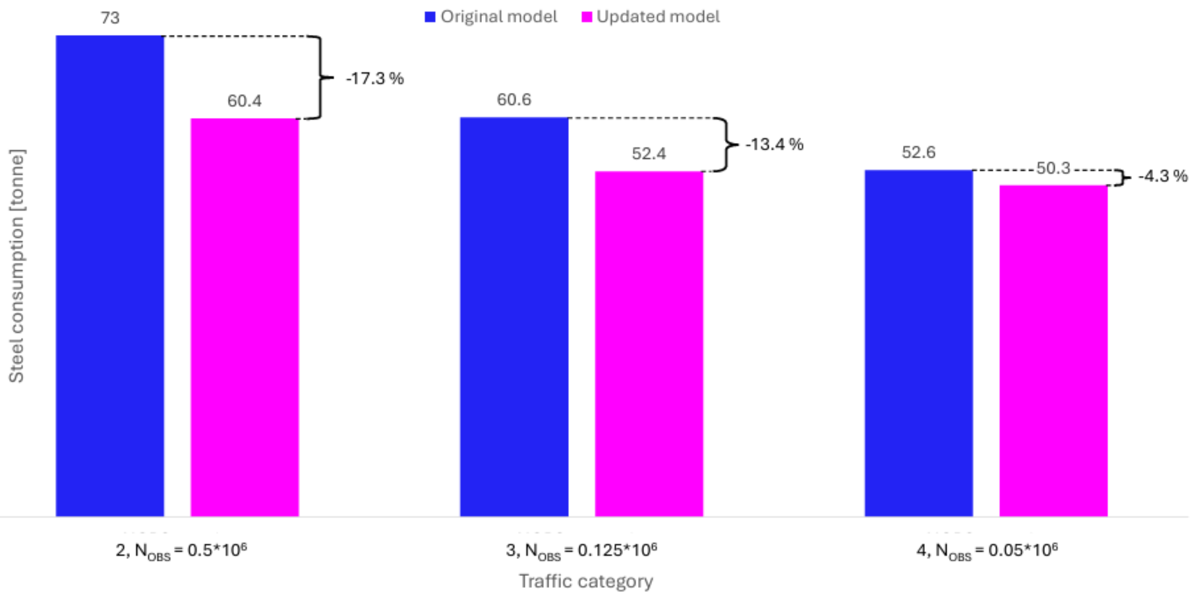

Figure 4.43: Comparison of steel tonnage between the original transverse beam model (constant stiffnesses) and the updated model (varying stiffnesses), using different traffic categories for fatigue loading.

As shown in Figure 4.43, steel tonnage can be reduced by up to 17.3% when using the updated model instead of the original model for a bridge subjected to traffic category 2, i.e., heavy fatigue loading. However, this difference decreases for bridges subjected to lighter fatigue loading, although an overall reduction in material consumption is still observed.

The reason why the greatest benefit is seen under heavy fatigue loading is evident in Table 4.7, where, for bridges with heavy fatigue loads, the fatigue limit state (FLS) governs the design. In contrast, for lighter fatigue loading, the ultimate limit state (ULS) is generally governing.

The main reason why the updated model has a more significant impact on fatigue loading is that this type of loading only considers tandem vehicle loads, which, as previously explained, are the only loads that the updated model captures more accurately than the original one. In contrast, a significant portion of ULS loads consists of distributed loads. As a result, the updated model has a limited impact in these cases, which ultimately makes its application less advantageous in cases where ULS governs the design.

When ULS governs the design, it is possible, unlike in FLS, to use plastic analysis and optimizations of steel qualities to improve the resistance of the cross-section. These aspects have been neglected in this thesis, but provide an opportunity for further improvement.

4.11 Comparison with empirical methods

In Figure 4.44, the steel quantities predicted by various empirical formulas presented in Section 2.2 are compared with those obtained using the transverse beam model, with the results presented in Section 4.10. Detailed calculations and graph readings are provided in Appendix G.

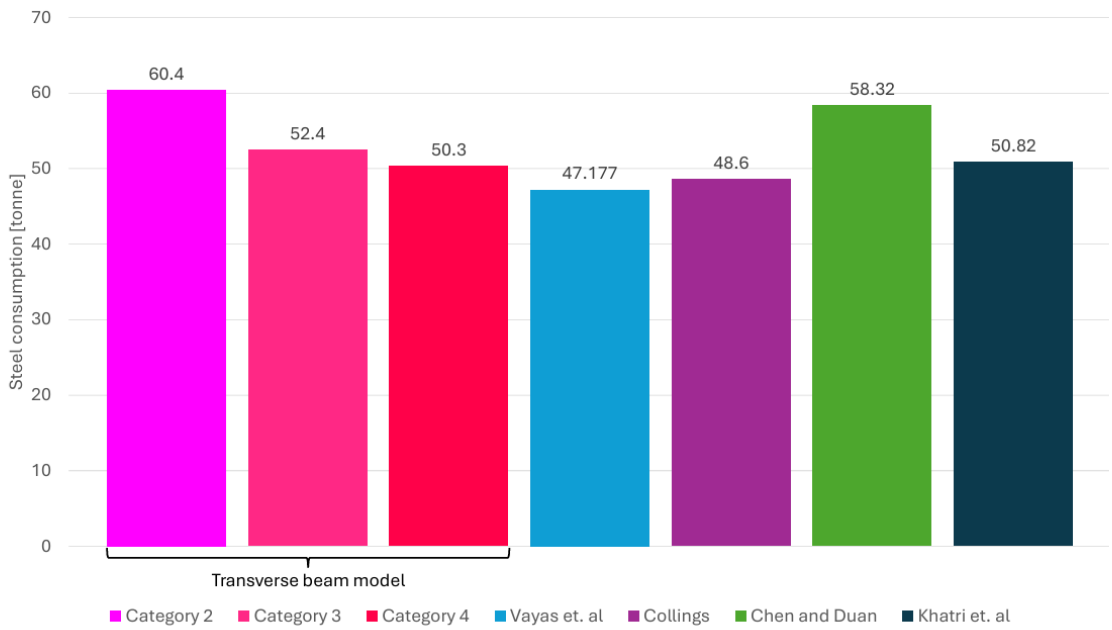

Figure 4.44: Steel consumption according to various empirical sources compared to the transverse beam model using different traffic categories.

It should be noted that the underlying assumptions in most of the empirical formulas are not fully compatible with the case study. For example, Vayas and Iliopoulos (2015) assumes a twin-girder bridge, whereas the case study concerns a multi-girder bridge with 4 I-girders, thus underestimating the steel consumption. Similarly, Chen and Duan (2013) assumes a bridge span of 30 m, which exceeds the 27 m span considered in the case study. In particular, the method yields a conservative estimate for traffic categories 3 and 4, while underestimating the consumption for traffic category 2.

Interestingly, Khatri et al. (2012) assumes an even longer span of 40 m but still predicts a lower steel tonnage (except for traffic category 4) than the updated transverse beam model. This suggests that the estimate is non-conservative and therefore the suitability for preliminary design depends on the traffic category relevant for the project. Collings (2013) is basing the amounts on a bridge with a smaller carriageway of 7.3 m, compared to the 12 m one used in the case study. Furthermore, Collings (2013) only uses traffic vehicles from Load Model 1 as specified in Eurocode, which may yield lower traffic loads than the ones received from the classification vehicles specified in TSFS.

Further differences in material consumption may arise from the limited construction height present in the case study, as the maximum girder depth caused the material consumption to be higher. This maximum height is not considered in any of the empirical estimates.

Overall, the empirical formulas provide an estimate of the steel consumption close to the ones based on the transverse beam model, proving the plausibility of the model. However, due to the assumptions made regarding boundary conditions and design codes, they are not suitable to accurately predict the steel consumption in preliminary design.

5 Conclusion and recommendations

This project aimed to find a suitable structural modeling technique to use in a preliminary design of a steel-concrete composite bridge. The first objective of finding a structural model to use in this design stage was accomplished, where the updated beam model was proven to yield results close to the reference case of the shell model. From the study, it was concluded that this modeling approach was accurate, simple, and fast, which are key components for a successful preliminary design process.

Secondly, the thesis aimed to investigate how the existing models could be improved. This was done by updating the transverse beam model supported by vertical springs by considering the load spreading angles when constructing the models. This was effectively implemented by varying the stiffnesses of the spring supports, as well as varying the stiffness of the beam element that represented the slab. It was concluded that a suitable load spreading angle for the specific case in this study was $\alpha = 55°$ for loads at the bridge cantilevers, whereas it was $\alpha = 65°$ for loads in the center of the bridge. It was also concluded that it was more efficient to vary the slab stiffness with the load-spreading angles than to consider stiffness variations for the spring supports.

Thirdly, utilizing the suggested updated model rather than the existing original model demonstrated that the bending moments could be successfully estimated in comparison with those of the shell model, with just a 1.6% difference on the conservative side. Whereas the shear forces were overestimated compared to the shell model by 26.3%, but still on the conservative side. The improvement of estimating the load effects was shown to generate a material reduction of up to 17.3% for bridges with heavy fatigue loading, whereas the difference got smaller for less fatigue-loaded bridges, but with a still overall material reduction.

Finally, a recommended workflow for both structural modeling and cross-sectional design of steel-concrete composite bridges was developed. These recommendations are illustrated in Figure 5.1 and 5.2.

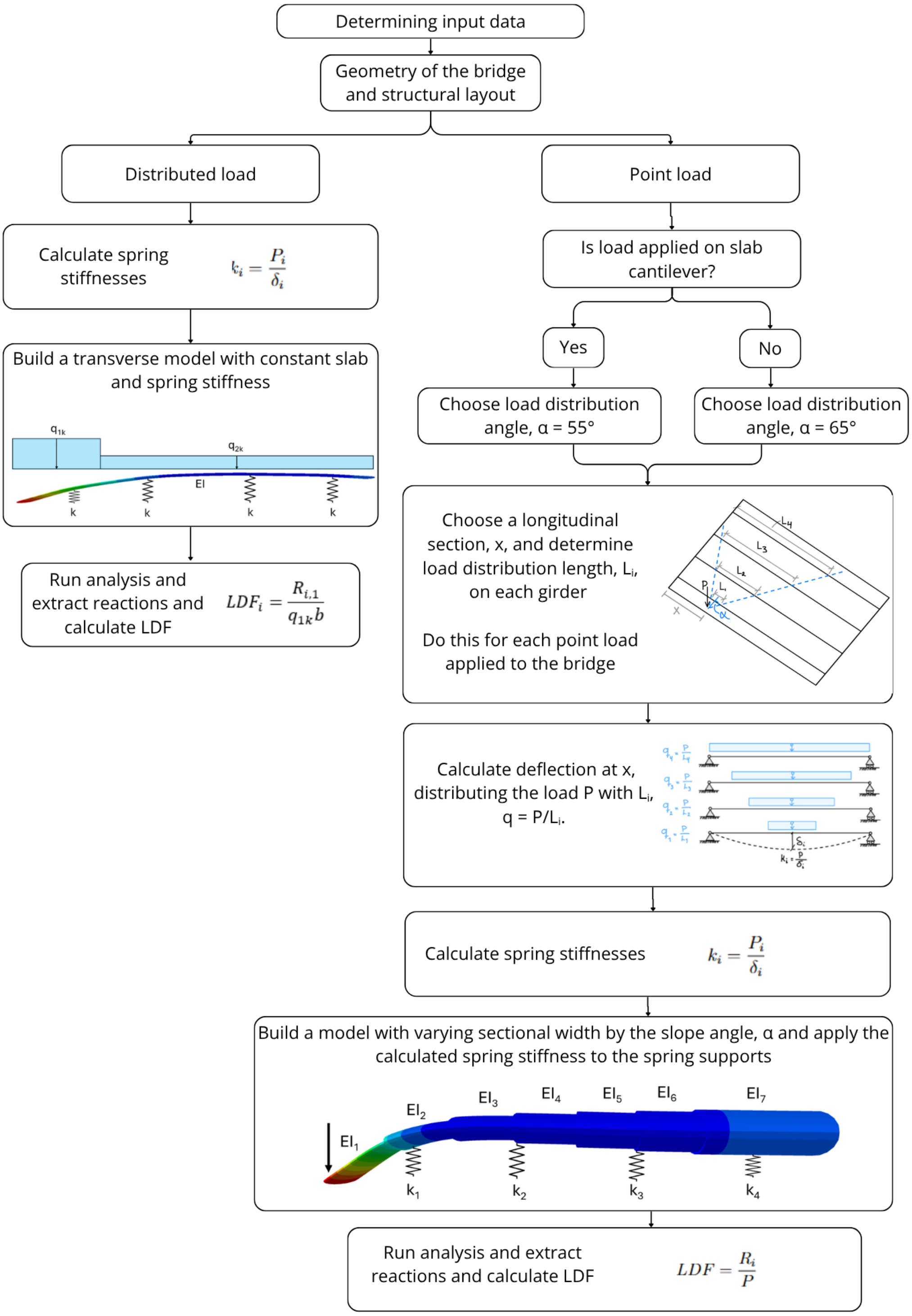

Figure 5.1: Workflow-chart for a proposed approach to determination of the load distribution factor.

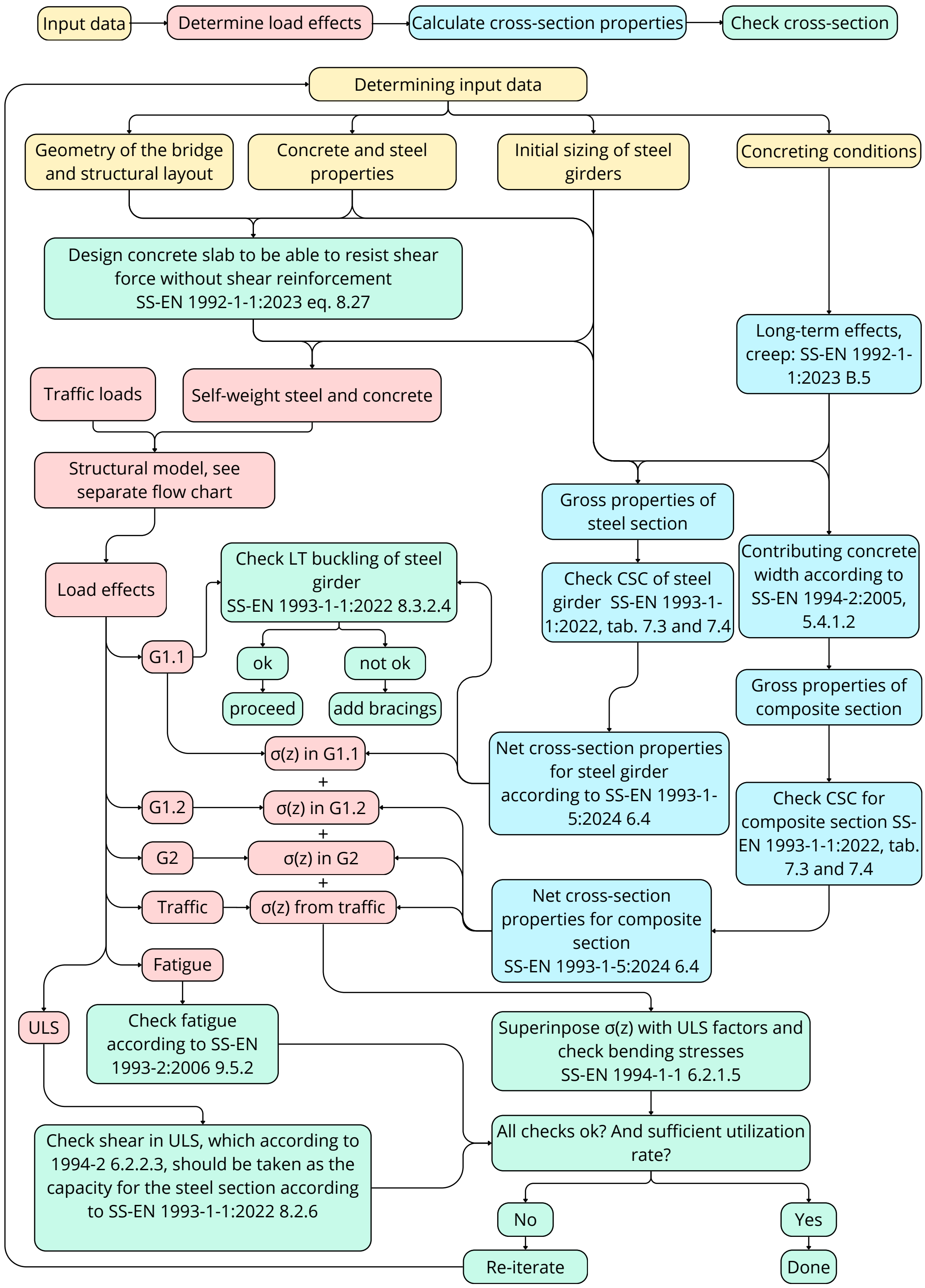

Figure 5.2: Flowchart for cross-section design and analysis.

6 Further studies

Recommended further studies involve both structural modeling and cross-sectional design. Firstly, for the structural modeling, it is recommended to analyze what effect the specific case in the case study had on the performance of the modeling approaches. This should be assessed by analyzing different cases, where the number of spans, span lengths, thickness of concrete slab, and number of girders should be varied to determine if these parameters have any effects on the results. Especially important is this for the analysis of whether the load spreading angles that were found in this thesis are still applicable for cases other than the one that was analyzed in this thesis.

Secondly, regarding the cross-section analysis, it would be interesting to analyze whether the material quantities could be further decreased by considering different steel qualities and plastic analysis. This is applicable where fatigue is not the governing limit state, since the change in steel quality does not affect the capacity in FLS. Another opportunity for improvement in terms of material reduction is by considering the use of different cross sections along the span of the bridge, instead of just considering the most conservative section, as was done in this thesis.

7 References

Al-Emrani, M., & Aygül, M. (2014, November). *Fatigue design of steel and composite bridges* (tech. rep.). Chalmers tekniska högskola. Göteborg.

Chen, W.-F., & Duan, L. (2013, September). *Bridge Engineering Handbook: Superstructure Design* (Second edition). Taylor & Francis Group.

Collings, D. (2013). *Steel-Concrete Composite Bridges - Designing with Eurocodes* (2nd Edition). ICE Publishing.

El Sarraf, R., Iles, D. C., Momtahan, A., Easey, D., & Hicks, S. J. (2013, September). *Steel-concrete composite bridge design guide*. NZ Transport Agency.

Ferreira, M. W., Real, M. d. V., Moura, M. W., & Santos, G. C. d. (2016). Determinação da distribuição do carregamento em pontes de concreto com elementos pré-moldados. *Congresso Brasileiro do Concreto*. https://www.researchgate.net/publication/337810919_DETERMINACAO_DA_DISTRIBUICAO_DO_CARREGAMENTO_EM_PONTES_DE_CONCRETO_COM_ELEMENTOS_PRE-MOLDADOS

FHWA. (2015). *Steel Bridge Design Handbook: Structural Behavior of Steel* (tech. rep.). Federal Highway Administration, U.S. Department of Transportation. www.steelbridges.org

Gocál, J., & Duršová, A. (2012). Optimisation of Transversal Disposition of Steel and Concrete Composite Road Bridges. *Procedia Engineering*, *40*, 125–130. https://doi.org/10.1016/J.PROENG.2012.07.067

ILES, D. C. (2014, March). *Composite Highway Bridge Design* (tech. rep.). The Steel Construction Institute. Berkshire. http://www.steel-sci.com

Jaeger, L. G., & Bakht, B. (1982). The grillage analogy in bridge analysis. *Canadian journal of civil engineering*, *9*(2), 224–235. https://doi.org/10.1139/L82-025

Khatri, V., Singh, P. K., & Maiti, P. R. (2012). Economical Design of Steel-Concrete Composite Bridge with MS and HPS. *International Journal of Engineering Research & Technology*, *1*(7). www.ijert.org

Lebet, J.-P., & Hirt, M. A. (2013). *Steel Bridges: Conceptual and Structural Design of Steel and Steel-Concrete Composite Bridges* (G. Couchman, Trans.). EPFL Press.

Ligocki Pedro, R. (2017). *Optimization of Steel-Concrete Composite I-Girder Bridges* [Doctoral dissertation, Federal University of Santa Catarina].

Mohan, T. J., Ramtekkar, G. D., & Bhatt, G. (2022). Comparison of Analytical and Finite element method of live load distribution in T Beam Girder Bridge. *ASPS Conference Proceedings*, *1*, 517–521. https://doi.org/10.38208/acp.v1.542

O'Brien, E. J., & Keogh, D. L. (1999). *Bridge deck analysis*. E.& F.N.Spon.

Pacoste, C., Plos, M., & Johansson, M. (2012). *Recommendations for finite element analysis for the design of reinforced concrete slabs* (tech. rep.). Stockholm. https://publications.lib.chalmers.se/records/fulltext/176734/local_176734.pdf

Parra Benítez, J. M., Benjumea, J. M., & Haach, V. G. (2022). Theoretical and computational simulation of the effect of the number of intermediate diaphragms on the live load distribution factors and structural response of a precast girder bridge.

Latin American Journal of Solids and Structures, *19*(5), 455–457. https://doi.org/10.1590/1679-78257120
Patel, B., & Patel, D. (2023). Grillage Analysis of I-Girder Bridge Deck Superstructure. *AIP Conference Proceedings*, *2855*(1). https://doi.org/10.1063/5.0168414
SIS. (2005a, January). *Eurocode 4: Design of composite steel and concrete structures-Part 1-1: General rules and rules for buildings* (tech. rep.). Swedish Standards Institute. www.sis.se
SIS. (2005b, March). *Eurocode 4: Design of composite steel and concrete structures - Part 2: General rules and rules for bridges* (tech. rep.). Swedish Standards Institute. www.sis.se
SIS. (2005c, July). *Eurocode 1: Actions on structures - Part 1-6: General actions - Actions during execution* (tech. rep.). Swedish Standards Institute. www.sis.se
SIS. (2006, October). *Eurocode 3: Design of steel structures - Part 2: Steel Bridges* (tech. rep.). Swedish Standards Institute. www.sis.se
SIS. (2022, November). *Eurocode 3: Design of steel structures - Part 1-1: General rules and rules for buildings* (tech. rep.). Swedish Standards Institute. www.sis.se
SIS. (2023a, March). *Eurocode 0: Basis of structural and geotechnical design* (tech. rep.). Swedish Standards Institute. www.sis.se
SIS. (2023b, December). *Eurocode 2: Design of concrete structures - Part 1-1: General rules and rules for buildings, bridges and civil engineering structures* (tech. rep.). Swedish Standards Institute. www.sis.se
SIS. (2024a, March). *Eurocode 1: Actions on structures - Part 2: Traffic loads on bridges and other civil engineering works* (tech. rep.). Swedish Standards institute. www.sis.se
SIS. (2024b, March). *Eurocode 3: Design of steel structures - Part 1-5: Plated structural elements* (tech. rep.). Swedish Standards Institute. www.sis.se
SIS. (2025a). *Eurocode 1: Actions on structures - Part 1-1: Specific weight of materials, self-weight of construction works and imposed loads on buildings* (tech. rep.). Swedish Standards Institute. www.sis.se
SIS. (2025b, February). *Eurocode 1: Actions on structures - Part 1-5: Thermal actions* (tech. rep.). Swedish Standards Institute. www.sis.se
SIS. (2025c, November). *Eurocode 3: Design of steel structures – Part 1-9: Fatigue* (tech. rep.). Swedish Standards Institute. www.sis.se
SIS. (2026, March). *Eurocode 1: Actions on structures - Part 1-4: Wind actions* (tech. rep.). Swedish Standards Institute. www.sis.se
Trafikverket. (2025, July). *TRVINFRA-00227 6.0 Bro och broliknande konstruktion Byggande Trafikverkets infrastrukturregelverk* (tech. rep.). www.trafikverket.se
Transportstyrelsen. (2018, September). *Transportstyrelsens föreskrifter och allmänna råd om tillämpning av eurokoder* (tech. rep.). Transportstyrelsen. www.transportstyrelsen.se
Vayas, I., Adamakos, T., & Iliopoulos, A. (2010). Spatial systems for modelling steel-concrete composite bridges — comparison of grillage systems and FE models. *Steel Construction*, *3*(2), 100–111. https://doi.org/10.1002/STCO.201010014

Vayas, I., & Iliopoulos, A. (2015, February). *Design of Steel-Concrete Composite Bridges to Eurocodes*. CRC Press.

Yuprasert, S., Maqsood, T., Venkatesan, S., & Chan, R. (2024). Load distribution factors for quick design and assessment in typical Australian bridges. *Australian Journal of Structural Engineering*, *25*(1), 1–19. https://doi.org/10.1080/13287982.2023.2255457

Appendix A: Calculation of LDF for the grillage and shell models

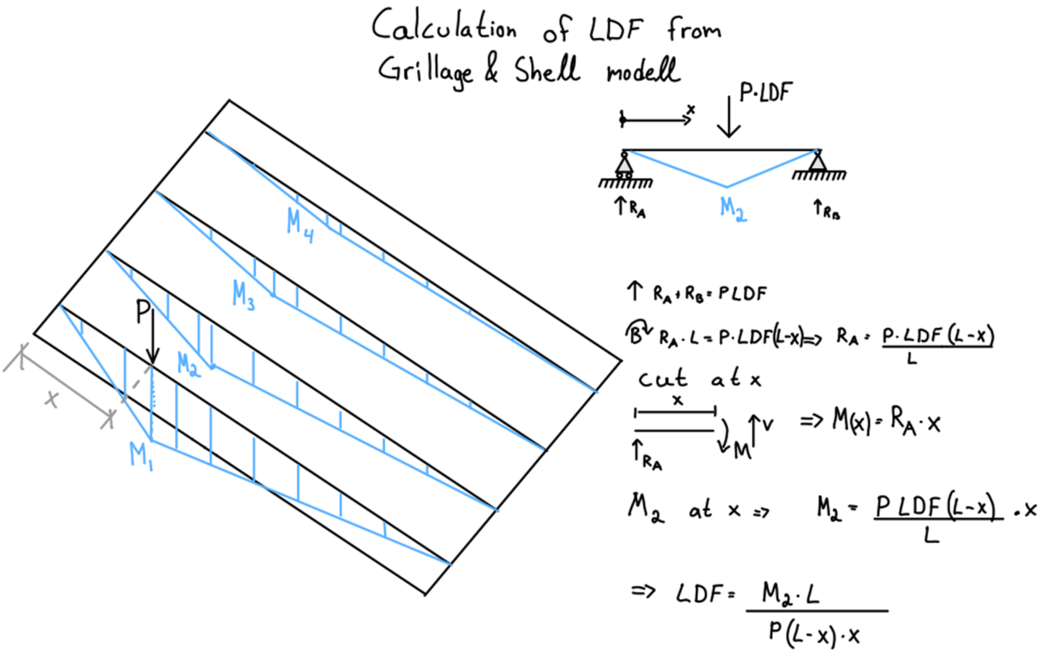

Figure A.1: Calculation of LDF for grillage and shell model.

Appendix B: Verification of shell model

B Verification of shell model

$t_w := 17\ mm$ $\quad h_w := 1025\ mm$

$t_{fo} := 25\ mm$ $\quad b_{fo} := 370\ mm$

$t_{fu} := 50\ mm$ $\quad b_{fu} := 650\ mm$

$t_{slab} := 230\ mm$ $\quad L := 27\ m$ $\quad b := 12\ m$

$\rho_{concrete} := 2500\ \frac{kg}{m^3}$ $\quad \rho_{steel} := 7850\ \frac{kg}{m^3}$ $\quad g = 9.807\ \frac{m}{s^2}$

$$g_{concrete} := t_{slab} \cdot b \cdot \rho_{concrete} \cdot g = 67.666\ \frac{kN}{m}$$

$$g_{steel} := g \cdot \rho_{steel} \cdot 4 \cdot \left(t_w \cdot h_w + t_{fo} \cdot b_{fo} + t_{fu} \cdot b_{fu}\right) = 18.222\ \frac{kN}{m}$$

$$g_{tot} := g_{concrete} + g_{steel} = 85.888\ \frac{kN}{m}$$

$$g_{construction} := b \cdot 1.48\ \frac{kN}{m^2} = 17.76\ \frac{kN}{m}$$

$$M_{max} := g_{tot} \cdot \frac{L^2}{8} = \left(7.827 \cdot 10^3\right)\ kN \cdot m \qquad M_{max.1} := \left(g_{tot} + g_{construction}\right) \cdot \frac{L^2}{8} = \left(9.445 \cdot 10^3\right)\ kN \cdot m$$

$$V_{max} := g_{tot} \cdot \frac{L}{2} = \left(1.159 \cdot 10^3\right)\ kN \qquad V_{max.1} := \left(g_{tot} + g_{construction}\right) \cdot \frac{L}{2} = \left(1.399 \cdot 10^3\right)\ kN$$

$$M_{brigade} := 7.829 \cdot 10^3\ kN \cdot m$$

$$V_{brigade} := 1.148 \cdot 10^3\ kN$$

$$\frac{M_{brigade}}{M_{max}} = 1.0003 \qquad \frac{V_{brigade}}{V_{max}} = 0.9901$$

Appendix C: Calculation of LDF using Courbon's method

C Courbons Method

C1Geometry

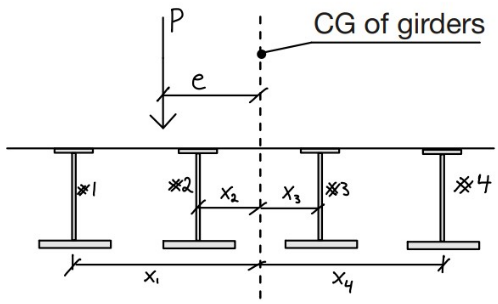

Total width

$w_{deck} := 12\ m$

Number of girders

$n_{beams} := 4$

Every beams position

Beam 1	Beam 2	Beam 3	Beam 4
$pos_1 := 1.5\ m$	$pos_2 := 4.5\ m$	$pos_3 := 7.5\ m$	$pos_4 := 10.5\ m$

Center of gravity for the beams

$$cog := \frac{pos_1 + pos_2 + pos_3 + pos_4}{4} = 6\ m$$

Every beams eccentricity to the center of gravity

Beam 1	Beam 2	Beam 3	Beam 4
$x_1 := cog - pos_1$	$x_2 := cog - pos_2$	$x_3 := cog - pos_3$	$x_4 := cog - pos_4$
$x_1 = 4.5\ m$	$x_2 = 1.5\ m$	$x_3 = -1.5\ m$	$x_4 = -4.5\ m$

C2 Load

Point load, P

$P := 100\ kN$

Position of load

$pos_p := 0.5\ m$

C3 Calculate the LDF's for the every beam

Eccentricity of load relative to center of gravity

$e_p := cog - pos_p = 5.5\ m$

Beam 1

$$\eta_{B1} := \frac{1}{n_{beams}} + \frac{x_1}{x_1^{\ 2} + x_2^{\ 2} + x_3^{\ 2} + x_4^{\ 2}} \cdot e_p \qquad \eta_{B1} = 0.8$$

Beam 2

$$\eta_{B2} := \frac{1}{n_{beams}} + \frac{x_2}{x_1^{\ 2} + x_2^{\ 2} + x_3^{\ 2} + x_4^{\ 2}} \cdot e_p \qquad \eta_{B2} = 0.433$$

Beam 3

$$\eta_{B3} := \frac{1}{n_{beams}} + \frac{x_3}{x_1^{\ 2} + x_2^{\ 2} + x_3^{\ 2} + x_4^{\ 2}} \cdot e_p \qquad \eta_{B3} = 0.067$$

Beam 4

$$\eta_{B4} := \frac{1}{n_{beams}} + \frac{x_4}{x_1^{\ 2} + x_2^{\ 2} + x_3^{\ 2} + x_4^{\ 2}} \cdot e_p \qquad \eta_{B4} = -0.3$$

Appendix D: Distribution of reaction forces for different longitudinal sections

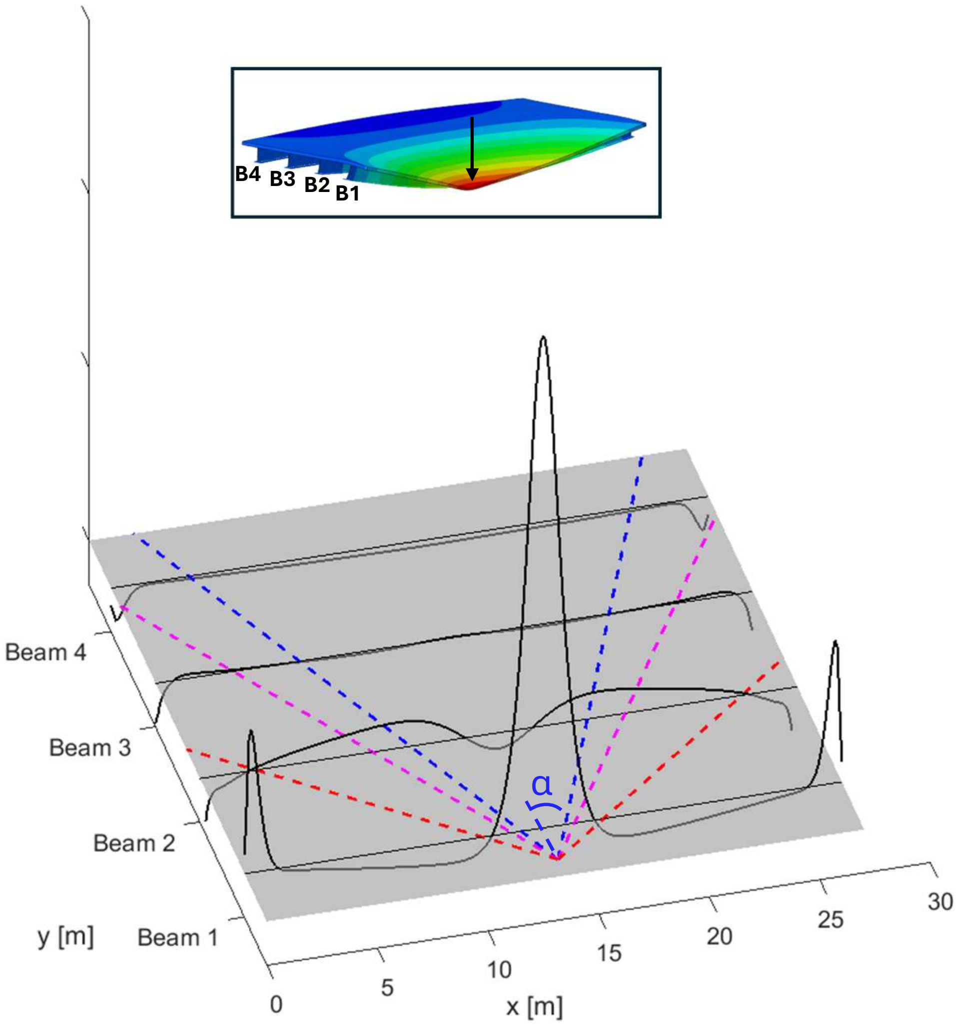

Figure D.1: Reaction force in each girder with a point applied on the cantilever edge, at $x = 10$ m.

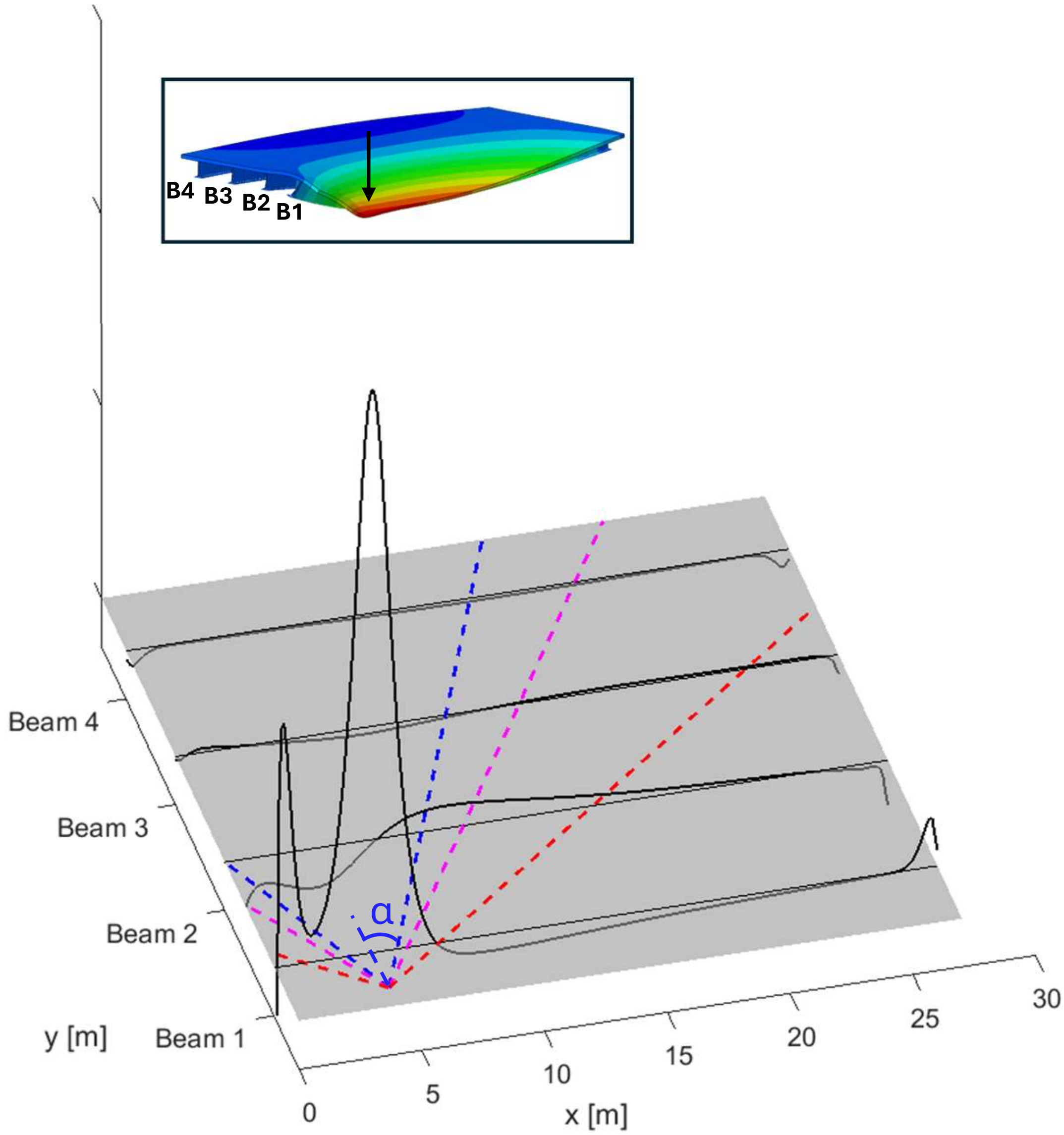

Figure D.2: Reaction force in each girder with a point load applied on the cantilever edge, at $x = 4$ m.

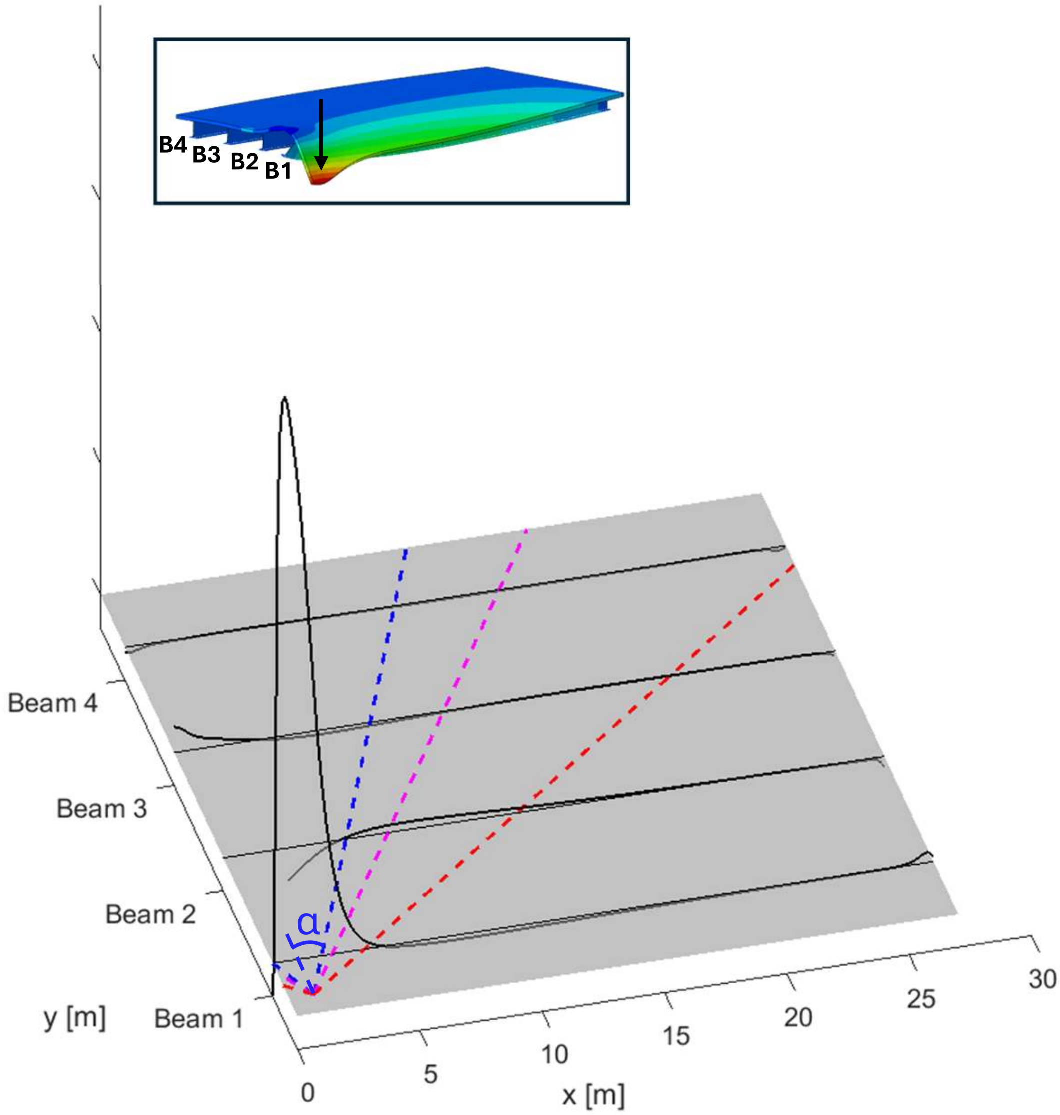

Figure D.3: Reaction force in each girder with a point load applied on the cantilever edge, at $x = 1$ m.

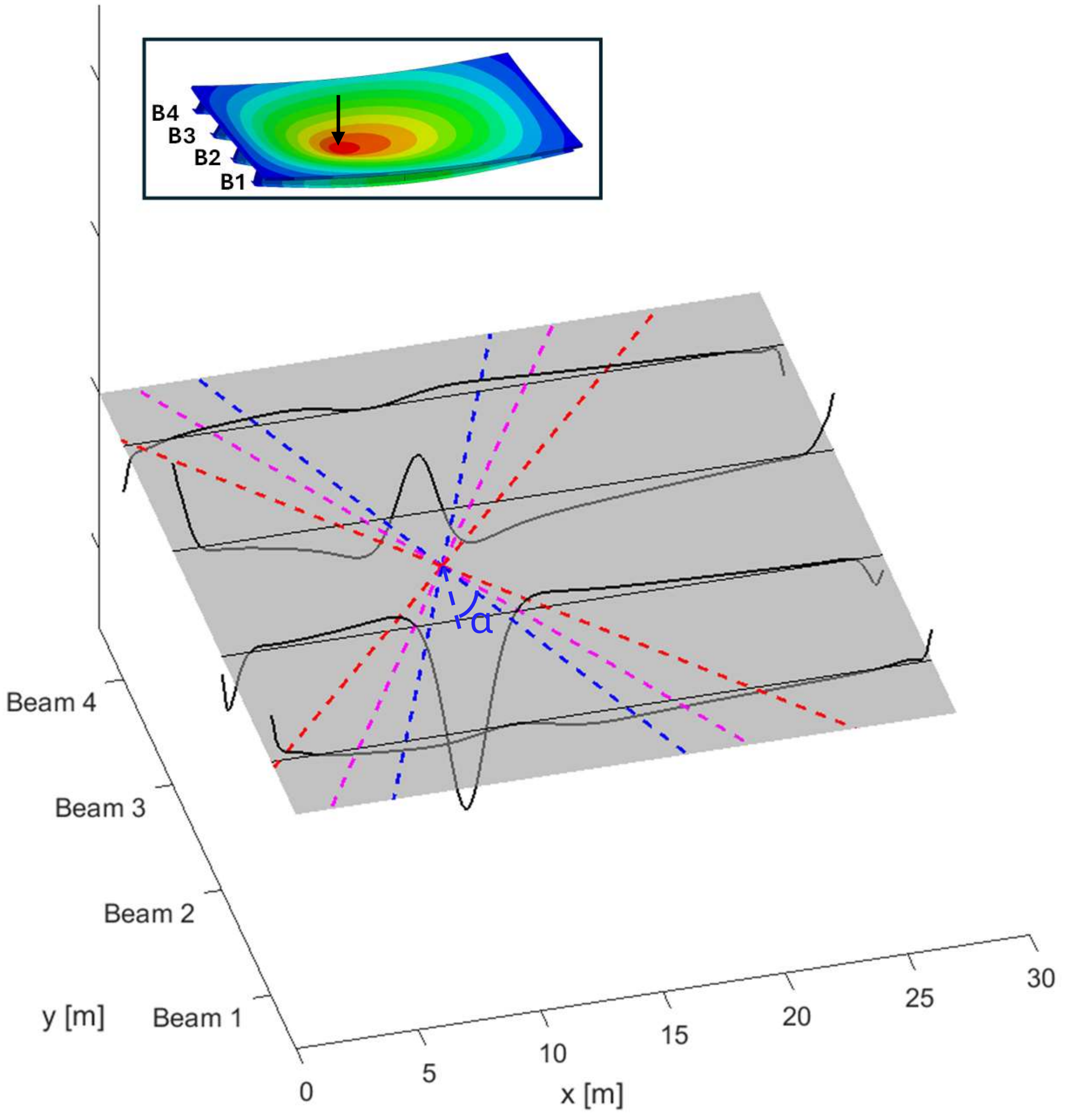

Figure D.4: Reaction force in each girder with a point load applied in the centre of the slab, at $x = 10$ m.

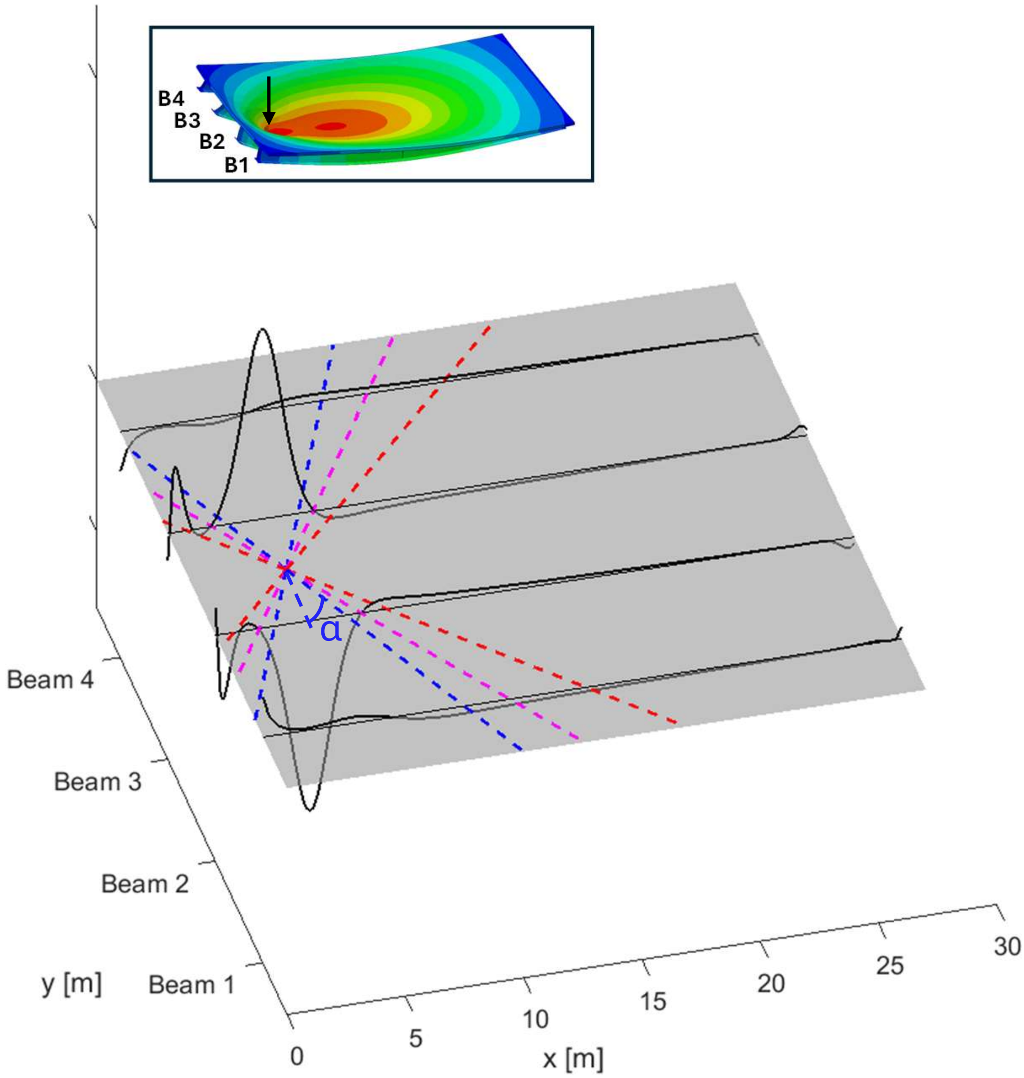

Figure D.5: Reaction force in each girder with a point load applied in the centre of the slab, at $x = 4$ m.

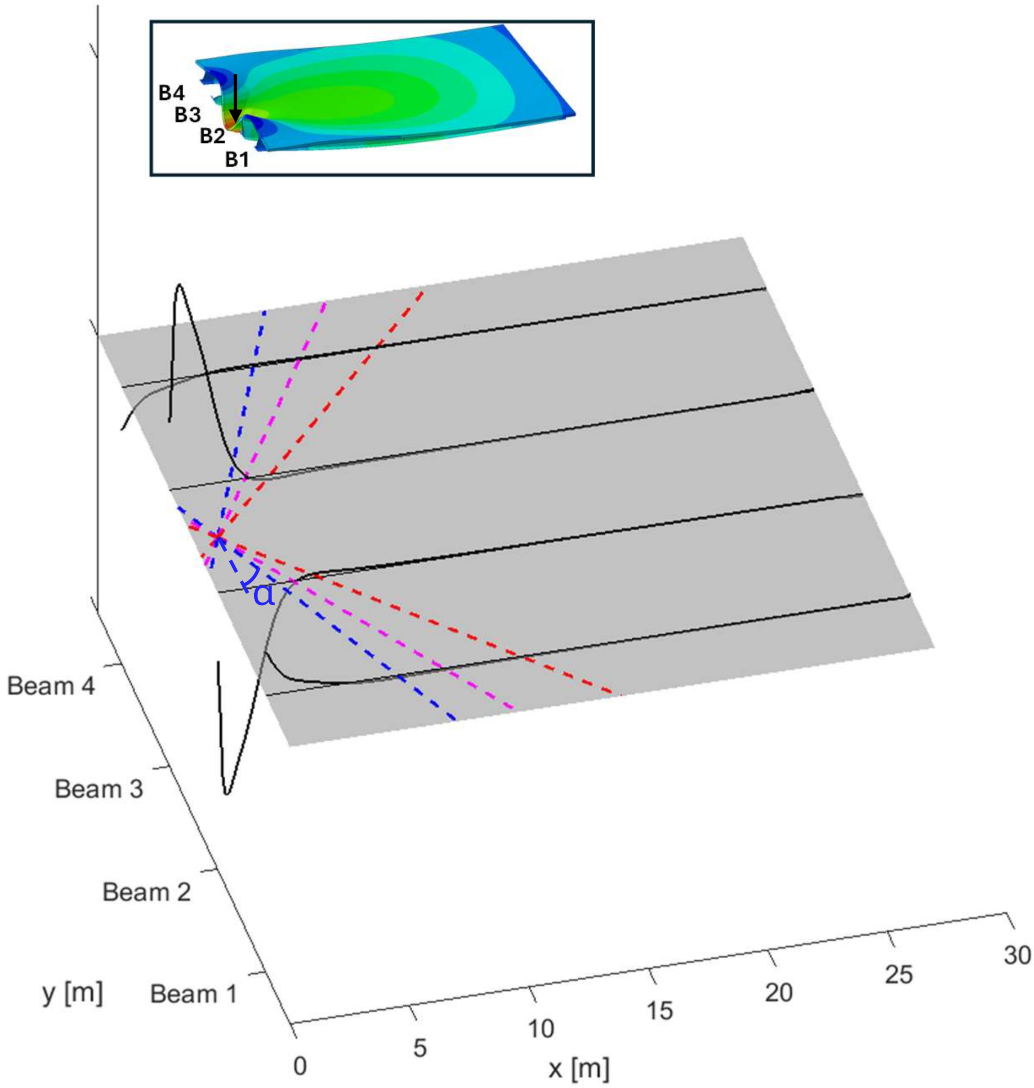

Figure D.6: Reaction force in each girder with a point load applied in the centre of the slab, at $x = 1$ m.

Appendix E: Design and analysis of concrete slab

E Design of concrete slab

The slab is designed with a sufficient thickness so that shear reinforcement is not required

Thickness of concrete slab

$t_c := 230 \ mm$

Characteristic compression strength of concrete C35/45

$f_{ck} := 35 \ MPa$

Reinforcement diameter

$\phi_{bar} := 20 \ mm$

Partial factor for shear and punching resistance of concrete without shear reinforcement

SS-EN 1992-1-1:2023 Table 4.3

$\gamma_v := 1.4$

Minimum concrete cover

Exposure class is chosen to XD1 according to the following table since that gives the biggest $c_{min.dur}$

General guidelines for selection of normal governing exposure classes for outdoor concrete surfaces (above the lowest ground water level and above the frost-free depth)

<table>
<tr><th rowspan="3"></th><th colspan="5">Chlorides</th></tr>
<tr><th rowspan="2">None</th><th colspan="2">Airborne</th><th colspan="2">Splash</th></tr>
<tr><th>De-icing salt</th><th>Sea water</th><th>De-icing salt</th><th>Sea water</th></tr>
<tr><td>Vertical</td><td>XC4 + XF1</td><td rowspan="3">XD1 + XF2</td><td rowspan="3">XS1 + XF2</td><td rowspan="3">XD1 + XF4</td><td rowspan="3">XS3 + XF4</td></tr>
<tr><td>Horizontal upper</td><td>XC4 + XF3</td></tr>
<tr><td>Horizontal under</td><td>XC3 + XF1</td></tr>
</table>

Exposure class is set as XD1: According to *TSFS 2018:57 Table 12.1* $c_{min.dur}$ should be set as:

$c_{min.dur} := 30 \ mm$

Minimum cover for bond $c_{min.b}$ according to *SS-EN 1992-1-1:2023 6.5.2.3:*

$c_{min.b} := \phi_{bar} = 20 \ mm$

According to *SS-EN 1992-1-1:2023 eq 6.2* c_{min} is calculated as:

$c_{min} := \max\left(c_{min.dur}, c_{min.b}, 10 \ mm\right) = 30 \ mm$

Allowance for deviation according to *SS-EN 1992-1-1:2023 Table 6.7, prescribing execution in tolerance class 2*

$\Delta c_{dev} := 5\ mm$

Nominal concrete cover thickness according to *SS-EN 1992-1-1:2023 eq 6.1*

$c_{nom} := c_{min} + \Delta c_{dev} = 35\ mm$

Effective depth

$d := t_c - c_{nom} - \frac{\phi_{bar}}{2} = 185\ mm$

The distribution width of the shear forces is determined according to "Recommendations for finite element analysis for the
design of reinforced concrete slabs" (Pacoste et al., 2012). Since the distribution is dependent on the different load models, a distribution width is calculated separately for LM1, Transportstyrelsen Classification vehicles and LM2.

Dimension of wheel in transverse direction

$c_{TypF} := 300\ mm$

$c_{LM1} := 320\ mm$

$c_{LM2} := 600\ mm$

Dimension of wheel in longitudinal direction

$b_{TypF} := 200\ mm$

$b_{LM1} := 220\ mm$

$b_{LM2} := 350\ mm$

Critical section for shear force

$y_{cs.TypF} := \frac{c_{TypF} + d}{2} = 242.5\ mm$

$y_{cs.LM1} := \frac{c_{LM1} + d}{2} = 252.5\ mm$

$y_{cs.LM2} := \frac{c_{LM2} + d}{2} = 392.5\ mm$

Minimum distribution that is possible

$$w_{min.TypF} := min\left(7 \cdot d + b_{TypF} + t_c, 10 \cdot d + 1.3 \cdot y_{cs.TypF}\right) = 1725\ mm$$

$$w_{min.LM1} := min\left(7 \cdot d + b_{LM1} + t_c, 10 \cdot d + 1.3 \cdot y_{cs.LM1}\right) = 1745\ mm$$

$$w_{min.LM2} := min\left(7 \cdot d + b_{LM2} + t_c, 10 \cdot d + 1.3 \cdot y_{cs.LM2}\right) = 1875\ mm$$

Set width of slab as minimum distribution width at critical section

$$b_{c.TypF} := w_{min.TypF} = 1.725\ m$$

$$b_{c.LM1} := w_{min.LM1} = 1.745\ m$$

$$b_{c.LM2} := w_{min.LM2} = 1.875\ m$$

1st order of inertia for a unit width of slab

$$S_{c.trans.TypF} := b_{c.TypF} \cdot \frac{t_c}{2} \cdot \frac{t_c}{4} = 0.011\ m^3$$

$$S_{c.trans.LM1} := b_{c.LM1} \cdot \frac{t_c}{2} \cdot \frac{t_c}{4} = 0.012\ m^3$$

$$S_{c.trans.LM2} := b_{c.LM2} \cdot \frac{t_c}{2} \cdot \frac{t_c}{4} = 0.012\ m^3$$

2nd moment of inertia for a unit width of slab

$$I_{c.trans.x.TypF} := \frac{b_{c.TypF} \cdot t_c^{\ 3}}{12} = 0.002\ m^4$$

$$I_{c.trans.x.LM1} := \frac{b_{c.LM1} \cdot t_c^{\ 3}}{12} = 0.002\ m^4$$

$$I_{c.trans.x.LM2} := \frac{b_{c.LM2} \cdot t_c^{\ 3}}{12} = 0.002\ m^4$$

Longitudinal reinforcement area assumed to be 1% of concrete area

$$A_{sl.TypF} := 1\% \cdot b_{c.TypF} \cdot t_c = 0.004\ m^2$$

$$A_{sl.LM1} := 1\% \cdot b_{c.LM1} \cdot t_c = 0.004\ m^2$$

$$A_{sl.LM2} := 1\% \cdot b_{c.LM2} \cdot t_c = 0.004\ m^2$$

Smallest value of upper sieve size for the coarsest fraction of aggregates, in this case set as_

$D_{lower} := 32\ mm$

Parameter describing the failure zone roughness according to *SS-EN 1992-1-1:2023 8.2.1 (4)*

$d_{dg} := min\left(16\ mm + D_{lower}, 40\ mm\right) = 40\ mm$

Reinforcement ratio

$$\rho_{l.TypF} := \frac{A_{sl.TypF}}{b_{c.TypF} \cdot d} = 0.012$$

$$\rho_{l.LM1} := \frac{A_{sl.LM1}}{b_{c.LM1} \cdot d} = 0.012$$

$$\rho_{l.LM2} := \frac{A_{sl.LM2}}{b_{c.LM2} \cdot d} = 0.012$$

Shear capacity without shear reinforcement

Shear capacity without shear reinforcement according to *SS-EN 1992-1-1:2023 eq. 8.27*

$$\tau_{Rd.c.TypF} := \frac{0.66}{\gamma_v} \cdot \left(100 \cdot \rho_{l.TypF} \cdot \frac{f_{ck}}{MPa} \cdot \frac{d_{dg}}{d}\right)^{\left(\frac{1}{3}\right)} \cdot MPa \qquad \tau_{Rd.c.TypF} = 0.995\ MPa$$

$$\tau_{Rd.c.LM1} := \frac{0.66}{\gamma_v} \cdot \left(100 \cdot \rho_{l.LM1} \cdot \frac{f_{ck}}{MPa} \cdot \frac{d_{dg}}{d}\right)^{\left(\frac{1}{3}\right)} \cdot MPa \qquad \tau_{Rd.c.LM1} = 0.995\ MPa$$

$$\tau_{Rd.c.LM2} := \frac{0.66}{\gamma_v} \cdot \left(100 \cdot \rho_{l.LM2} \cdot \frac{f_{ck}}{MPa} \cdot \frac{d_{dg}}{d}\right)^{\left(\frac{1}{3}\right)} \cdot MPa \qquad \tau_{Rd.c.LM1} = 0.995\ MPa$$

ULS partial factors

$\gamma_G := 1.35$ $\qquad \gamma_{G.favorable} := 1$ $\qquad \gamma_Q := 1.5$

$\gamma_{G.pave} := 1.1 \cdot \gamma_G = 1.485$ $\qquad$ *TSFS 2018:57 5 kap. 4 §*

Maximum Shear force from transverse Brigade model

$V_{Ed.G1.1.trans} := 11.2\ kN$

$V_{Ed.G1.2.trans} := -2.33\ kN$

$V_{Ed.G2.trans} := 6.88\ kN$

$V_{Ed.LM1.Boogie.trans} := 148\ kN$

$V_{Ed.LM1.UDL.trans} := 9.7\ kN$

$V_{Ed.TypF.Boogie.trans} := 114.5\ kN$

$V_{Ed.Tra.TypF.UDL.trans} := 2.6\ kN$

$V_{Ed.LM2.Boogie.trans} := 180\ kN$

$V_{Ed.LM1.Trans} := V_{Ed.LM1.Boogie.trans} + V_{Ed.LM1.UDL.trans} = 157.7\ kN$

$V_{Ed.TypF.Trans} := V_{Ed.TypF.Boogie.trans} + V_{Ed.Tra.TypF.UDL.trans} = 117.1\ kN$

$V_{Ed.LM2.Trans} := V_{Ed.LM2.Boogie.trans} = 180\ kN$

$$V_{Ed.ULS.TypF} := \gamma_G \cdot V_{Ed.G1.1.trans} + \gamma_{G.favorable} \cdot V_{Ed.G1.2.trans} + \gamma_{G.favorable} \cdot V_{Ed.G1.2.trans} + \gamma_Q \cdot \left(V_{Ed.TypF.Trans}\right)$$

$V_{Ed.ULS.TypF} = 186.11\ kN$

$$V_{Ed.ULS.LM1} := \gamma_G \cdot V_{Ed.G1.1.trans} + \gamma_{G.favorable} \cdot V_{Ed.G1.2.trans} + \gamma_{G.favorable} \cdot V_{Ed.G1.2.trans} + \gamma_Q \cdot \left(V_{Ed.LM1.Trans}\right)$$

$V_{Ed.ULS.LM1} = 247.01\ kN$

$$V_{Ed.ULS.LM2} := \gamma_G \cdot V_{Ed.G1.1.trans} + \gamma_{G.favorable} \cdot V_{Ed.G1.2.trans} + \gamma_{G.favorable} \cdot V_{Ed.G1.2.trans} + \gamma_Q \cdot \left(V_{Ed.LM2.Trans}\right)$$

$V_{Ed.ULS.LM2} = 280.46\ kN$

Maximum shear stress:

$$\tau_{Ed.trans.TypF} := \frac{V_{Ed.ULS.TypF} \cdot S_{c.trans.TypF}}{I_{c.trans.x.TypF} \cdot b_{c.TypF}}$$

$$\tau_{Ed.trans.TypF} = 0.704\ MPa$$

$$\tau_{Ed.trans.LM1} := \frac{V_{Ed.ULS.LM1} \cdot S_{c.trans.LM1}}{I_{c.trans.x.LM1} \cdot b_{c.LM1}}$$

$$\tau_{Ed.trans.LM1} = 0.923\ MPa$$

$$\tau_{Ed.trans.LM2} := \frac{V_{Ed.ULS.LM2} \cdot S_{c.trans.LM2}}{I_{c.trans.x.LM2} \cdot b_{c.LM2}}$$

$$\tau_{Ed.trans.LM2} = 0.976\ MPa$$

Check utilization ratio

$$\eta_{V.trans} := \max\left(\frac{\tau_{Ed.trans.TypF}}{\tau_{Rd.c.TypF}}, \frac{\tau_{Ed.trans.LM1}}{\tau_{Rd.c.LM1}}, \frac{\tau_{Ed.trans.LM2}}{\tau_{Rd.c.LM2}}\right) = 0.98$$

$$Check_{shear.slab} := \text{if}\left(\eta_{V.trans} < 1, \text{“Ok”}, \text{“NOT OK”}\right) = \text{“Ok”}$$

Appendix F: Design and analysis of cross-sections

F1 Input Data
F1.1 Geometry
Plan view

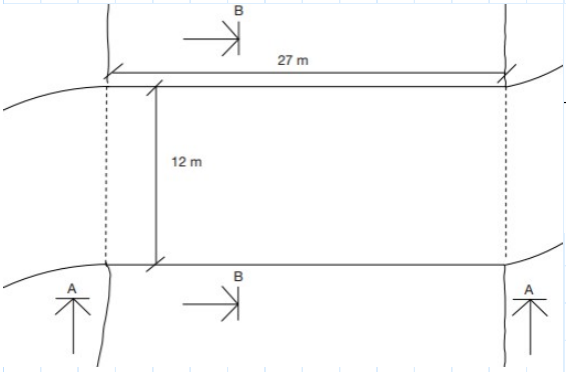

Elevation A-A

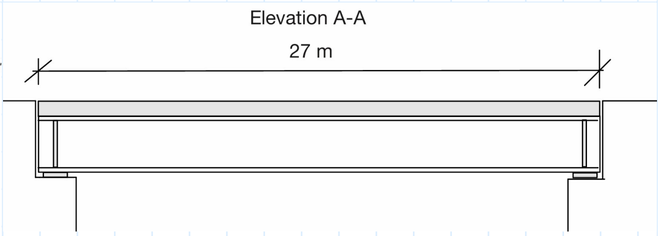

Section B-B

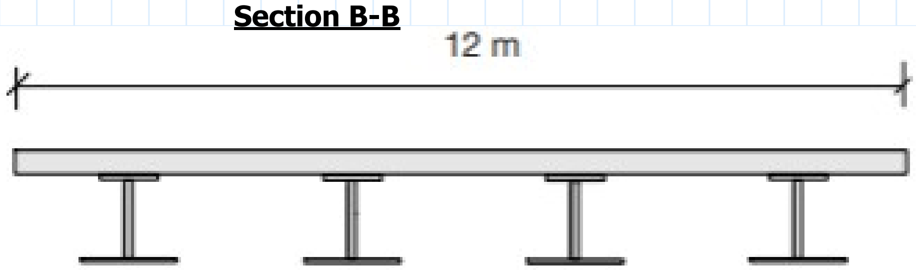

Geometry of cross section

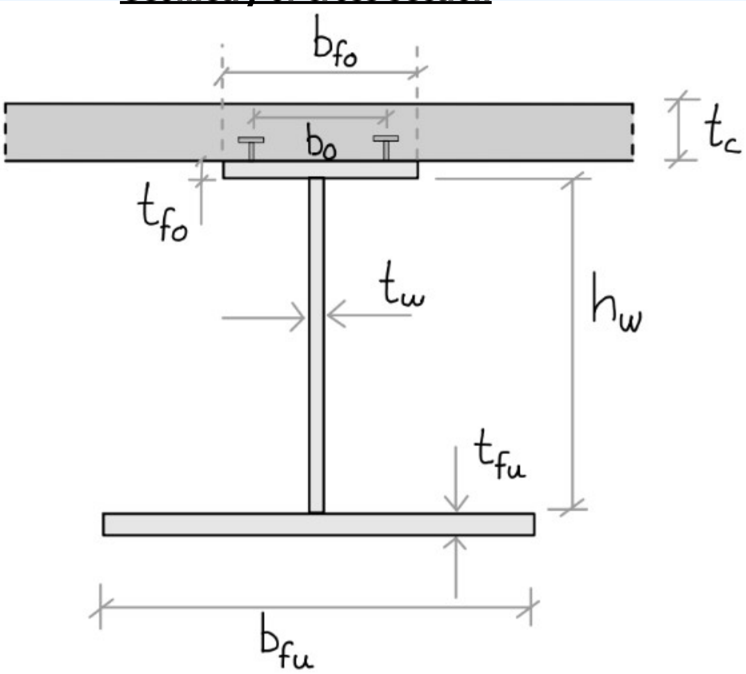

Geometry of concrete slab

Width of deck

$w_{deck} := 12\ m$

Slab thickness

$t_c := 230\ mm$

$A_c := w_{deck} \cdot t_c$

$u_c := 2 \cdot \left(w_{deck} + t_c\right)$

Maximum construction height

$h_{max} := 1330\ mm$

Geometry of steel girder

Span length

$L_{span} := 27\ m$

Spacing Girders

$cc_{long} := 3\ m$

Number of girders

$n_{girder} := 4$

Over flange width:

$b_{fo} := 655\ mm$

Web thickness:

$t_w := 14\ mm$

Under flange width:

$b_{fu} := 1100\ mm$

The thickness of the flanges is set to the minimum thickness that ensures CSC 3 according to SS-EN 1993-1-1:2022 tab. 7.4, rounded up to nearest integer.

$$t_{fo} := \mathrm{Ceil}\left(\frac{\frac{b_{fo} - t_w}{2}}{14 \cdot 0.814}, 1\ mm\right) = 29\ mm$$

$$t_{fu} := \mathrm{Ceil}\left(\frac{\frac{b_{fu} - t_w}{2}}{14 \cdot 0.814}, 1\ mm\right) = 48\ mm$$

Height of the web is set to the highest possible within the construction height

$h_w := h_{max} - t_c - t_{fo} - t_{fu} = 1023\ mm$

Total height of steel section

$h_{steel} := t_{fo} + h_w + t_{fu} = 1100\ mm$

Total area steel section

$A_{steel} := b_{fu} \cdot t_{fu} + t_w \cdot h_w + b_{fo} \cdot t_{fo} = 0.086\ m^2$

Composite section

Total height of composite section

$h_{tot} := t_{fu} + h_w + t_{fo} + t_c = 1.33\ m$

Studs

Diameter of studs

$\phi_{studs} := 22\ mm$

Longitudinal cc spacing of studs according to *SS-EN 1994-2:2005 6.6.5.7 (4)* minimum distance is 5d

$cc_{studs} := 150\ mm$ > $5 \cdot \phi_{studs} = 110\ mm$ ok!

Number of studs placed transversally *SS-EN 1994-2:2005 6.6.5.7 (4)* minimum distance in transverse direction is 2.5d. Therefore, assure that the number of studs yield in a sufficient transversal spacing

$n_{studs.width} := 2$

Distance between studs

$b_0 := 335\ mm$

Distance between edge of flange and edge of a stud should not be less than 25 mm according to *SS-EN 1994-2:2005 6.6.5.6 (2)*

$e_D := \frac{b_{fo} - b_0}{2} - \frac{\phi_{studs}}{2} = 149\ mm$ >25 mm ok!

F1.2 Partial factors

$\gamma_{M0} := 1$ *SS-EN 1993-1-1:2022, 8.1*

$\gamma_{M1} := 1$ *SS-EN 1993-1-1:2022, 8.1*

$\gamma_C := 1.5$ *SS-EN 1992-1-1:2023 Table 4.3*

Partial factors for fatigue assessment

$\gamma_{Mf} := 1.35$ *SS-EN 1993-1-9:2025 Table 5.1*

$\gamma_{Ff} := 1$ *SS-EN 1993-2:2006 9.3 (1)*

F1.3 Material properties

Concrete C35/45

Characteristic compressive strength

$f_{ck} := 35\ MPa$

Mean compressive strength

$f_{cm.28} := 43\ MPa$

Factor to take into account the difference between cylindric strength and the strength of a structural member

$$\eta_{cc} := min\left(\left(\frac{40\ MPa}{f_{ck}}\right)^{\left(\frac{1}{3}\right)}, 1\right) = 1$$

Design compressive strength *SS-EN 1992-1-1:2023 eq. 5.4*

$$f_{cd} := \eta_{cc} \cdot \frac{f_{ck}}{\gamma_C} = 23.333\ MPa$$

Density dry

$$\rho_{c.dry} := 2500\ \frac{kg}{m^3}$$

Density wet

$$\rho_{c.wet} := 2600\ \frac{kg}{m^3}$$

Poisons ratio

$$\upsilon_c := 0.2$$

Mean modulus of elasticity

$$E_{cm} := 34\ GPa$$

Shear modulus

$$G_c := \frac{E_{cm}}{2\ (1+\upsilon_c)} = 14.167\ GPa$$

Coefficient for strength development in concrete (assumes Class CN)
SS-EN 1992-1-1:2023 chap. B.5 (4)

$$\alpha_{SC} := 0$$

Steel S355

Yield strength SS-EN 10025-2:2019 Tab. 6

$$f_y(t) := \begin{cases} 355\ MPa & \text{if } t \le 16\ mm \\ 345\ MPa & \text{else if } 16\ mm < t \le 40\ mm \\ 335\ MPa & \text{else if } 40\ mm < t \le 63\ mm \\ 325\ MPa & \text{else if } 63\ mm < t \le 80\ mm \end{cases}$$

ε according to SS-EN 1993-1-1:2022 eq 5.1

$$f_{y.fo} := f_y(t_{fo}) = 345\ MPa \qquad \varepsilon_{fo} := \sqrt{\frac{235 \cdot MPa}{f_{y.fo}}}$$

$$f_{y.w} := f_y(t_w) = 355\ MPa \qquad \varepsilon_w := \sqrt{\frac{235 \cdot MPa}{f_{y.w}}}$$

$$f_{y.fu} := f_y(t_{fu}) = 335\ MPa \qquad \varepsilon_{fu} := \sqrt{\frac{235 \cdot MPa}{f_{y.fu}}}$$

Density

$$\rho_{steel} := 7850\ \frac{kg}{m^3}$$

Poisons ratio

$$\upsilon_{steel} := 0.3$$

Modulus of elasticity

$$E_s := 210\ GPa$$

Shear modulus

$$G_s := \frac{E_s}{2\ (1+\upsilon_{steel})} = 80.769\ GPa$$

F1.4 Concreting conditions

Relative humidity

$$RH := 80\%$$

Age of concrete at considered moment [days]

$$t := 120 \cdot 365$$

Age of concrete at loading [days]

$t_0 := 10$

F1.5 Fatigue input data

Gross weight of lorries in slow moving lane according to TRVINFRA-00227 Krav Version 6.0 Tab. 7.2-7

$Q_{m1} := 445\ kN$

Total amount of lorries per year according to SS-EN 1991-2:2024 tab. 6.7 assuming traffic category 2

$N_{Obs} := 0.5 \cdot 10^6$

F2 Loads

F2.1 G1.1

Self weight of steel girder

$g_{k.a} := \left(t_{fo} \cdot b_{fo} + t_w \cdot h_w + t_{fu} \cdot b_{fu}\right) \cdot g \cdot \rho_{steel}$ $\qquad g_{k.a} = 6.629\ \frac{kN}{m}$

Self weight of wet concrete

$g_{k.c.wet.tot} := t_c \cdot w_{deck} \cdot \rho_{c.dry} \cdot g$ $\qquad g_{k.c.wet.tot} = 67.666\ \frac{kN}{m}$

Formwork on, including formwork (0.5kN/m2), extra weight for wet concrete (1kN/m3*tc) and construction loads (0.75kN/m2)

$q_{cc.on} := 0.5\ \frac{kN}{m^2} + 1\ \frac{kN}{m^3} \cdot t_c + 0.75\ \frac{kN}{m^2}$ $\qquad q_{cc.on} = 1.48\ \frac{kN}{m^2}$

F2.2 G1.2

Formwork removal

$q_{cc.off} := -q_{cc.on}$ $\qquad q_{cc.off} = -1.48\ \frac{kN}{m^2}$

F2.3 G2

Pavement on bridge deck

From "rambeskrivning: typbeläggning 4bIA according to Råd brobyggande 4b1A should be used. Råd brobyggande tab. G.3-1 gives the following:

4. 2 x Tätskicktsmatta a 10mm

Thickness	Specific Weight
$t_{matta} := 2 \cdot 10\ mm$	$\gamma_{matta} := 22\ \frac{kN}{m^3}$

b. Skyddsbetong 70mm

Thickness	Specific Weight acc. to SS-EN1991-1-2025 tab. A.1 un-reinforced concrete
$t_{skydd.btg} := 70\ mm$	$\gamma_{skydd.btg} := 24\ \frac{kN}{m^3}$

I. ABb>11 B/70/100mm

Thickness

$t_{ABb.11} := 50\ mm$

Specific Weight acc. to SS-EN 1991-1-2025 tab. A.6 Asfaltbetong

$\gamma_{ABb.11} := 25\ \frac{kN}{m^3}$

a. ABb>16 B/70/100mm

Thickness

$t_{ABb.16} := 40\ mm$

Specific Weight acc. to SS-EN 1991-1-2025 tab. A.6 Asfaltbetong

$\gamma_{ABb.16} := 25\ \frac{kN}{m^3}$

$$g_{pavement.k} := t_{matta} \cdot \gamma_{matta} + t_{skydd.btg} \cdot \gamma_{skydd.btg} + t_{ABb.11} \cdot \gamma_{ABb.11} + t_{ABb.16} \cdot \gamma_{ABb.16}$$

$$g_{pavement.k} = 4.37\ \frac{kN}{m^2}$$

F2.4 Traffic loads

Traffic loads are implemented by adopting LM1 and LM2 as per SS-EN 1991-2-2024 chapter 6.3.2 and 6.3.3, respectively. Also, the "typfordon" as per TSFS 2018:57 chapter 11 are considered.

F2.5 Fatigue loads

Fatigue loads are implemented by fatigue load model 3 (FLM3) since the simplified λ method is used for fatigue assessment which requires FLM 3 (SS-EN 1993-2:2006 9.2.2 (1)). FLM 3 is defined in SS-EN 1991-2-2024 chapter 6.6.7

F2.6 Temperature loads

As shown by the shell model, the temperature loads gave minor effects and can be neglected in this stage.

F2.7 Shrinkage loads

As shown by the shell model, the shrinkage loads gave minor effects and can be neglected in this stage.

F3. Cross sectional properties

F3.1 Long-term effects, Creep

Effect of elevated or reduced concrete temperatures

Assumes concrete temperature to 20 degrees

$t_{0.T} := t_0 = 10$ *SS-EN 1992-1-1:2023 chap. B.5 (4)*

Adjusted time based on early strength development

$$t_{0.adj} := \max\left(t_{0.T} \cdot \left(\frac{9}{2 + t_{0.T}^{1.2}} + 1\right)^{\alpha_{SC}}, 0.5\right) = 10$$

SS-EN 1992-1-1:2023 eq. B.17

Function describing effect of concrete strength on creep

$$\beta_{bc.fcm} := \frac{1.8}{\left(\frac{f_{cm.28}}{MPa}\right)^{0.7}} = 0.129$$ SS-EN 1992-1-1:2023 eq. B.7

Function describing development of creep over time

$$\beta_{bc.t\_t0} := \ln\left(\left(\frac{30}{t_{0.adj}} + 0.035\right)^2 \left(t - t_0\right) + 1\right)$$ SS-EN 1992-1-1:2023 eq. B.8

Basic creep function

$$\varphi_{bc} := \beta_{bc.fcm} \cdot \beta_{bc.t\_t0}$$ SS-EN 1992-1-1:2023 eq. B.6

$$\alpha_{fcm} := \left(\frac{35}{\frac{f_{cm.28}}{MPa}}\right)^{0.5} = 0.902$$ SS-EN 1992-1-1:2023 eq. B.16

$$h_n := \frac{2 \cdot A_c}{u_c} = 225.675\ mm$$ SS-EN 1992-1-1:2023 eq. B.15

$$\beta_h := min\left(1.5 \cdot \frac{h_n}{mm} + 250 \cdot \alpha_{fcm}, 1500 \cdot \alpha_{fcm}\right) = 564.06$$ SS-EN 1992-1-1:2023 eq. B.15

$$\gamma_{t0.adj} := \frac{1}{2.3 + \frac{3.5}{\sqrt{t_{0.adj}}}} = 0.294$$ SS-EN 1992-1-1:2023 eq. B.14

$$\beta_{dc.t\_t0} := \left(\frac{t - t_0}{\beta_h + t - t_0}\right)^{\gamma_{t0.adj}}$$ SS-EN 1992-1-1:2023 eq. B.13

$$\beta_{dc.t0} := \frac{1}{0.1 + t_{0.adj}^{\ 0.2}} = 0.594$$ SS-EN 1992-1-1:2023 eq. B.12

$$\beta_{dc.RH} := \frac{1 - \frac{RH}{100}}{\sqrt[3]{0.1 \cdot \frac{\frac{h_n}{mm}}{100}}} = 1.629$$ SS-EN 1992-1-1:2023 eq. B.11

$$\beta_{dc.fcm} := \frac{412}{\left(\frac{f_{cm.28}}{MPa}\right)^{1.4}} = 2.128$$ SS-EN 1992-1-1:2023 eq. B.10

Drying creep coefficient

$\varphi_{dc} := \beta_{dc.fcm} \cdot \beta_{dc.RH} \cdot \beta_{dc.t0} \cdot \beta_{dc.t\_t0} = 2.05$ *SS-EN 1992-1-1:2023 eq. B.9*

Total creep coefficient

$\varphi_L := \varphi_{bc} + \varphi_{dc} = 3.72$

Modular ratio

Short-term modular ratio

$n_0 := \frac{E_s}{E_{cm}} = 6.176$

Long-term modular ratio

$\psi_L := 0.55$ *SS-EN 1994-2:2005 5.4.2.2 (2)*

$n_L := n_0 \cdot (1 + \psi_L \cdot \varphi_L) = 18.815$ *SS-EN 1994-2:2005 eq. 5.6*

F3.2 Contributing concrete width

The contributing width of concrete is determined by considering the effect of shear lag according to *SS-EN 1994-2:2005, chapter 5.4.1.2*

SS-EN 1994-2:2005 5.4.1.2 (4): In global analysis, the effective width is calculated in mid-span and assumed to be constant over the whole length

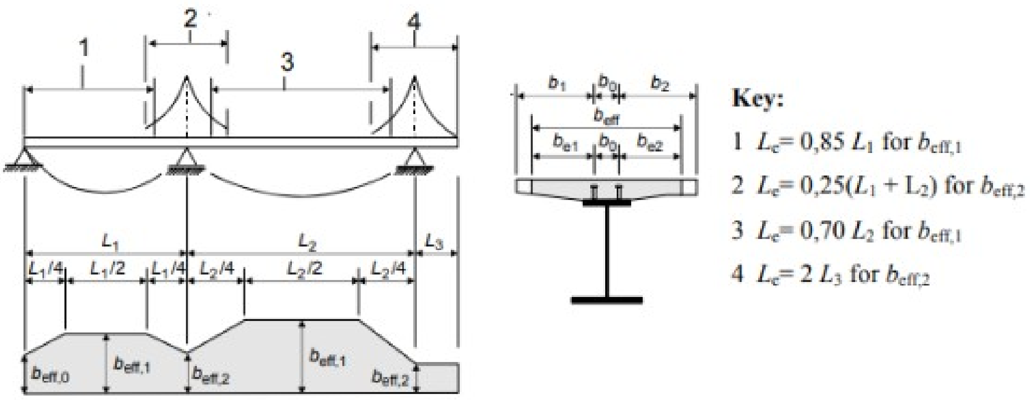

Figure 5.1: Equivalent spans, for effective width of concrete flange

Equivalent spans

$L_{e.mid} := 0.7 \cdot L_{span} = 18.9\ m$ *SS-EN 1994-2:2005 fig. 5.1*

Width between studs

$b_0 = 335\ mm$

Available width between girders

$$b_{avalible} := \frac{cc_{long} - b_0}{2} = 1.333\ m$$

Effective width on each side at mid span

$$b_{ei.mid} := min\left(b_{avalible}, \frac{L_{e.mid}}{8}\right) = 1.333\ m$$ SS-EN 1994-2:2005 5.4.1.2 (5)

Total effective width at mid span

$$b_{eff.mid} := b_0 + 2 \cdot b_{ei.mid} = \left(3 \cdot 10^3\right)\ mm$$ SS-EN 1994-2:2005 eq. 5.4

F3.3 Gross cross-sectional properties of steel girder

Area over flange

$$A_{fo} := b_{fo} \cdot t_{fo} = 0.019\ m^2$$

Area web

$$A_w := t_w \cdot h_w = 0.014\ m^2$$

Area under flange

$$A_{fu} := b_{fu} \cdot t_{fu} = 0.053\ m^2$$

Moment of inertia o.f.

$$I_{fo} := \frac{b_{fo} \cdot t_{fo}^{\ 3}}{12}$$

Moment of inertia web

$$I_w := \frac{t_w \cdot h_w^{\ 3}}{12}$$

Moment of inertia u.f.

$$I_{fu} := \frac{b_{fu} \cdot t_{fu}^{\ 3}}{12}$$

Lever arm over flange

$$z_{a.fo} := \frac{t_{fo}}{2} = 0.015\ m$$

Lever arm web

$$z_{a.w} := t_{fo} + \frac{h_w}{2} = 0.541\ m$$

Lever arm under flange

$$z_{a.fu} := t_{fo} + h_w + \frac{t_{fu}}{2} = 1.076\ m$$

Total height steel girder

$$h_a := t_{fo} + h_w + t_{fu} = \left(1.1 \cdot 10^3\right)\ mm$$

Total area steel girder

$$A_{a.tot} := A_{fo} + A_w + A_{fu} = 0.086\ m^2$$

Neutral axis of steel girder

$$z_{a.tp.gross} := \frac{A_{fo} \cdot z_{a.fo} + A_w \cdot z_{a.w} + A_{fu} \cdot z_{a.fu}}{A_{fo} + A_w + A_{fu}} = 752.805\ mm$$

Moment of inertia of steel girder (gross cross section)

$$I_{a.y.gross} := I_{fo} + A_{fo} \cdot \left(z_{a.tp.gross} - z_{a.fo}\right)^2 + I_w + A_w \cdot \left(z_{a.tp.gross} - z_{a.w}\right)^2 + I_{fu} + A_{fu} \cdot \left(z_{a.tp.gross} - z_{a.fu}\right)^2$$

$$I_{a.y.gross} = 0.018\ m^4$$

F3.4 Check of cross sectional class of steel girder

Cross sectional classes (CSC) are checked according to *SS-EN 1993-1-1:2022, tab. 7.3 and 7.4*
In this case, only elastic capacity will be considered, therefore the cross section is only checked whether it is in class 3 or higher or in class 4

$$\varepsilon_w := \sqrt{\frac{235 \cdot MPa}{f_{y.w}}} = 0.814 \qquad \varepsilon_{fo} := \sqrt{\frac{235 \cdot MPa}{f_{y.fo}}}$$

$$\psi_a := \frac{-\left(h_w + t_{fo} - z_{a.tp.gross}\right)}{z_{a.tp.gross} - t_{fo}} = -0.413$$

$$CSC_{w.a} := \text{if } \psi_a > -1 \;\; \Big\| \; \text{if } \frac{h_w}{t_w} < \frac{38\ \varepsilon_w}{0.608 + 0.343 \cdot \psi_a + 0.049 \cdot \psi_a^{\ 2}} \;\|\; 3 \;\; \text{else} \;\|\; 4 \;\; \text{else if } \psi_a \le -1 \;\; \Big\| \; \text{if } \frac{h_w}{t_w} < 60.5 \cdot \varepsilon_w \cdot \left(1 - \psi_a\right) \;\|\; 3 \;\; \text{else} \;\|\; 4$$

$$CSC_{fo.a} := \text{if } \frac{\frac{b_{fo} - t_w}{2}}{t_{fo}} \le 14\ \varepsilon_{fo} \;\|\; 3 \;\; \text{else} \;\|\; 4$$

Cross sectional class of over flange $CSC_{fo.a} = 3$ Minimum (only check if CSC<=3)

Cross sectional class of web $CSC_{w.a} = 4$

F3.5 Net cross-sectional properties of steel girder

Properties in CSC <4

Moment of inertia of steel girder

$I_{a.y.CSC3} := I_{a.y.gross} = 0.018\ m^4$

Neutral axis

$z_{a.NA.CSC3} := z_{a.tp.gross} = 752.805\ mm$

Properties in CSC 4

$b\_ := h_w$

Compression part of web SS-EN 1993-1-5:2024 Tab. 6.1

$$b_{c.} := \frac{b\_}{1 - \psi_a} = 723.805\ mm$$

Tension part of web SS-EN 1993-1-5:2024 Tab. 6.1

$b_t := h_w - b_{c.} = 299.195\ mm$

Material property ε_w depending on f_y and defined above

$\varepsilon_w = 0.814$

Buckling factor according to SS-EN 1993-1-5:2024 Tab. 6.1

$$k_{sigma} := \text{if } 0 > \psi_a > -1 \;\; \| \; k_{sigma} \leftarrow 7.81 - 6.29 \cdot \psi_a + 9.78 \cdot \psi_a^{\,2} \;\; \text{else if } -1 > \psi_a \geq -3 \;\; \| \; k_{sigma} \leftarrow 5.98 \cdot (1 - \psi_a)^2$$

$k_{sigma} = 12.081$

Slenderness of the web according to SS-EN 1993-1-5:2024 eq. 6.4

$$\lambda_p := \frac{\frac{b\_}{t_w}}{28.4 \cdot \varepsilon_w \cdot \sqrt{k_{sigma}}} = 0.91$$

Reduction factor according to to SS-EN 1993-1-5:2024 eq. 6.2

$$\rho := \text{if } \lambda_p \leq 0.5 + \sqrt{0.085 - 0.055 \cdot \psi_a} \;\; \| \; \rho \leftarrow 1 \;\; \text{else if } \lambda_p > 0.5 + \sqrt{0.085 - 0.055 \cdot \psi_a} \;\; \| \; \rho \leftarrow \frac{\lambda_p - 0.055 \cdot (3 + \psi_a)}{\lambda_p^{\,2}}$$

Effective width according to SS-EN 1993-1-5:2024 Tab. 6.1

$$b_{eff.w} := \frac{\rho \cdot b\_}{1 - \psi_a} = 0.671 \; m$$

Dividing the effective with into one upper and one lower parts according to SS-EN 1993-1-5:2024 Tab. 6.1

$b_{e1.w} := 0.4 \cdot b_{eff.w} = 268.461 \; mm$

$b_{e2.w} := 0.6 \cdot b_{eff.w} = 402.691 \; mm$

Calculate neutral axis of effective cross section

$A_{fo} = \left(1.9 \cdot 10^4\right) mm^2$ $\qquad z_{a.fo} = 0.015 \; m$

$A_{e1.w} := b_{e1.w} \cdot t_w = \left(3.758 \cdot 10^3\right) mm^2$ $\qquad z_{a.e1} := t_{fo} + \frac{b_{e1.w}}{2}$

$A_{e2.w} := b_{e2.w} \cdot t_w = \left(5.638 \cdot 10^3\right) mm^2$ $\qquad z_{a.e2} := t_{fo} + b_{c.} - \frac{b_{e2.w}}{2}$

$A_{t.w} := b_t \cdot t_w = \left(4.189 \cdot 10^3\right) mm^2$ $\qquad z_{a.w.t} := t_{fo} + b_{c.} + \frac{b_t}{2} = 902.402 \; mm$

$A_{fu} = 0.053 \; m^2$ $\qquad z_{a.fu} = 1.076 \; m$

$A_{a.eff} := A_{fo} + A_{e1.w} + A_{e2.w} + A_{t.w} + A_{fu} = 0.085\ m^2$

$z_{a.NA.eff} := \dfrac{A_{fo} \cdot z_{a.fo} + A_{e1.w} \cdot z_{a.e1} + A_{e2.w} \cdot z_{a.e2} + A_{t.w} \cdot z_{a.w.t} + A_{fu} \cdot z_{a.fu}}{A_{a.eff}} = 756.509\ mm$

Calculate moment of inertia for effective cross section

$I_{fo} = \left(1.331 \cdot 10^6\right)\ mm^4$

$\Delta z_{fo.eff} := z_{a.NA.eff} - z_{a.fo} = 742.009\ mm$

$I_{e1} := \dfrac{t_w \cdot b_{e1.w}^{\ 3}}{12} = \left(2.257 \cdot 10^7\right)\ mm^4$

$\Delta z_{e1.eff} := z_{a.NA.eff} - z_{a.e1} = 593.278\ mm$

$I_{e2} := \dfrac{t_w \cdot b_{e2.w}^{\ 3}}{12} = \left(7.618 \cdot 10^7\right)\ mm^4$

$\Delta z_{e2.eff} := z_{a.NA.eff} - z_{a.e2} = 205.049\ mm$

$I_{w.t} := \dfrac{t_w \cdot b_t^{\ 3}}{12} = \left(3.125 \cdot 10^7\right)\ mm^4$

$\Delta z_{t.eff} := z_{a.NA.eff} - z_{a.w.t} = -145.894\ mm$

$I_{fu} = \left(1.014 \cdot 10^7\right)\ mm^4$

$\Delta z_{fu.eff} := z_{a.NA.eff} - z_{a.fu} = -319.491\ mm$

$$I_{a.eff} := I_{fo} + A_{fo} \cdot \Delta z_{fo.eff}^{\ 2} + I_{e1} + A_{e1.w} \cdot \Delta z_{e1.eff}^{\ 2} + I_{e2} + A_{e2.w} \cdot \Delta z_{e2.eff}^{\ 2} + I_{w.t} + A_{t.w} \cdot \Delta z_{t.eff}^{\ 2} + I_{fu} + A_{fu} \cdot \Delta z_{fu.eff}^{\ 2}$$

$I_{a.eff} = \left(1.764 \cdot 10^{10}\right)\ mm^4$

Sectional properties for the steel section

$$I_{a.y} := \begin{array}{l} \text{if } CSC_{w.a} \le 3 \\ \quad \| \ I_{a.y.gross} \\ \text{else if } CSC_{w.a} = 4 \\ \quad \| \ I_{a.eff} \end{array} = 0.018\ m^4$$

$$z_{a.NA} := \begin{array}{l} \text{if } CSC_{w.a} \le 3 \\ \quad \| \ z_{a.tp.gross} \\ \text{else if } CSC_{w.a} = 4 \\ \quad \| \ z_{a.NA.eff} \end{array} = 0.757\ m$$

F3.6 Gross sectional properties of composite section

The composite section's properties is determined in with long term concrete properties

Lever arms

$z_c := \frac{t_c}{2} = 0.115\ m$

$z_{fo} := t_c + \frac{t_{fo}}{2} = 0.245\ m$

$z_w := t_c + t_{fo} + \frac{h_w}{2} = 0.771\ m$

$z_{fu} := t_c + t_{fo} + h_w + \frac{t_{fu}}{2} = 1.306\ m$

Effective area of contributing concrete, adjusted with long term modular ratio

$$A_{c.ekv.L} := \frac{b_{eff.mid}}{n_L} \cdot t_c = 0.037\ m^2$$

Effective moment of inertia of contributing concrete, adjusted with long term modular ratio

$$I_{c.ekv.L} := \frac{\frac{b_{eff.mid}}{n_L} \cdot t_c^{\ 3}}{12}$$

Neutral axis

$$z_{tp.L} := \frac{A_{c.ekv.L} \cdot z_c + A_{fo} \cdot z_{fo} + A_w \cdot z_w + A_{fu} \cdot z_{fu}}{A_{c.ekv.L} + A_{fo} + A_w + A_{fu}} = 723.621\ mm$$

Total moment of inertia of the composite section, long term conditions

$$I_{y.L.gross} := I_{c.ekv.L} + A_{c.ekv.L} \cdot \left(z_{tp.L} - z_c\right)^2 + I_{fo} + A_{fo} \cdot \left(z_{tp.L} - z_{fo}\right)^2 + I_w + A_w \cdot \left(z_{tp.L} - z_w\right)^2 + I_{fu} + A_{fu} \cdot \left(z_{tp.L} - z_{fu}\right)^2$$

$$I_{y.L.gross} = 0.037\ m^4$$

Total area of the composite section, long term conditions

$$A_{tot.L.gross} := A_{fo} + A_w + A_{fu} + A_{c.ekv.L} = 0.123\ m^2$$

F3.7 Cross sectional class of composite section

According to SS-EN 1994-2:2005 5.5.1 (3) the steel flange can be seen as being in more favorable class when it is attached to the reinforced concrete slab. Therefore, only the web is checked.

Cross sectional classes (CSC) are checked according to *SS-EN 1993-1-1:2022, tab. 7.3 and 7.4*
In this case, only elastic capacity will be considered, therefore the cross section is only checked whether it is in class 3 or higher or in class 4

Elastic stress distribution

$$\psi_{comp} := \frac{-\left(t_c + h_w + t_{fo} - z_{tp.L}\right)}{z_{tp.L} - t_c - t_{fo}} = -1.202 \qquad \varepsilon_w = 0.814$$

$$CSC_{w.comp} := \text{if } \psi_{comp} > -1$$
$$\quad \text{if } \frac{h_w}{t_w} < \frac{38\ \varepsilon_w}{0.608 + 0.343 \cdot \psi_{comp} + 0.049 \cdot \psi_{comp}^{\ 2}}$$
$$\quad\quad 3$$
$$\quad \text{else}$$
$$\quad\quad 4$$
$$\text{else if } \psi_{comp} \le -1$$
$$\quad \text{if } \frac{h_w}{t_w} < 60.5 \cdot \varepsilon_w \cdot \left(1 - \psi_{comp}\right)$$
$$\quad\quad 3$$
$$\quad \text{else}$$
$$\quad\quad 4$$

Cross sectional class of web $\qquad CSC_{w.comp} = 3$

F3.8 Net cross sectional properties of composite section

Since all parts are in at least CSC 3, the net cross sectional properties is equal to the gross one

Net moment of inertia of composite section

$$I_{y.L} := I_{y.L.gross} = 0.037\ m^4$$

Net area of composite section

$$A_{tot.L} := A_{tot.L.gross} = 0.123\ m^2$$

F4 Cross section analysis
F4.1 Analysis in G1.1
F4.1.1 Calculate stresses in bending

$g_{k.G1.1} := 22.243 \ \frac{kN}{m}$ Self weight of concrete, form work and construction loads

$g_{k.a} = 6.629 \ \frac{kN}{m}$ Self weight of steel

$$M_{Ed.G1.1} := \frac{\left(g_{k.a} + g_{k.G1.1}\right) \cdot L_{span}^{\ 2}}{8} = \left(2.631 \cdot 10^{3}\right) \ kN \cdot m$$

Stresses in the steel girder in stage G1.1

Top

$$\sigma_{a.G1.1.top} := \frac{M_{Ed.G1.1}}{I_{a.y}} \cdot \left(-z_{a.NA}\right) = -112.844 \ MPa$$

Bottom

$$\sigma_{a.G1.1.bot} := \frac{M_{Ed.G1.1}}{I_{a.y}} \cdot \left(h_{steel} - z_{a.NA}\right) = 51.237 \ MPa$$

F4.1.2 Check bending stresses in stage G1.1

ULS combination factor

$\gamma_G := 1.35$

Check utilization rates steel section

$$\eta_{b.G1.1.top} := \frac{\left|\gamma_G \cdot \sigma_{a.G1.1.top}\right|}{f_{y.fo}} = 0.442 \qquad \eta_{b.G1.1.bot} := \frac{\left|\gamma_G \cdot \sigma_{a.G1.1.bot}\right|}{f_{y.fu}} = 0.206$$

$$\eta_{b.G1.1} := \max\left(\eta_{b.G1.1.top}, \eta_{b.G1.1.bot}\right) = 0.442$$

$$Check_{b.G1.1} := \text{if}\left(\eta_{b.G1.1} < 1, \text{“Ok”}, \text{“NOT OK”}\right) = \text{“Ok”}$$

F4.1.3 Lateral torsional stability

In the construction stage, before the concrete is cured the self weight of the fresh concrete is carried solely by the steel girders. According to *SS-EN 1994-2:2005 6.4.1 (1)* the steel flange can be assumed to be stabilized by the concrete slab when it is hardened. However, this does not apply when the concrete is fresh, requiring a check of lateral torsional buckling

cc distance between bracings $cc_{bracings} := 13.5\ m$

To verify the lateral tortional stability of the girders, they are analyzed by the "simplified approach" in *SS-EN 1993-1-1:2022 8.3.2.4* which suggests that the an equivalent compression flange should be analyzed as a strut.

Effective area according to SS-EN 1993-1-1:2022 8.3.2.4 (4):

$$A_{eff.c} := A_{fo} + \frac{1}{2} \cdot A_w = 0.026\ m^2$$

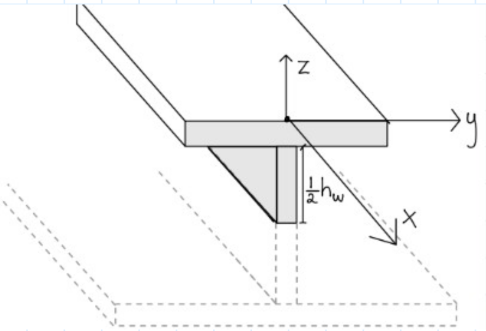

Max width of flange for CSC 3 according to SS-EN 1993-1-1:2022 tab 7.4

$$b_{max} := 2 \cdot (14 \cdot \varepsilon_{fo} \cdot t_{fo}) + t_w = 0.684\ m$$

Effective width:

$$b_{eff.c.} := min(b_{max}, b_{fo}) = 655\ mm$$

Effective moment of inertia around LT buckling axis (z):

$$I_{eff.z.c} := \frac{t_{fo} \cdot b_{eff.c.}^{\ 3}}{12} + \frac{\frac{h_w}{2} \cdot t_w^{\ 3}}{12} = (6.792 \cdot 10^{-4})\ m^4$$

Critical length:

$$L_{cr.c} := cc_{bracings} = 13.5\ m$$

Critical Euler load

$$N_{cr.c.z} := \frac{\pi^2 \cdot E_s \cdot I_{eff.z.c}}{L_{cr.c}^{\ 2}} = (7.724 \cdot 10^3)\ kN$$

Relative slenderness

$$\lambda_{c.z} := \sqrt{\frac{A_{eff.c} \cdot \max(f_{y.w}, f_{y.fo})}{N_{cr.c.z}}} = 1.096$$

SS-EN 1993-1-1:2022 eq 8.25

Min and max flange thicknesses

$$t_{f.max} := \max(t_{fo}, t_{fu}) = 48\ mm$$
$$t_{f.min} := min(t_{fo}, t_{fu}) = 29\ mm$$

Height of cross section

$$h := t_{fo} + h_w + t_{fu} = \left(1.1 \cdot 10^3\right)\ mm$$

Correction factor

$$\beta_c := min\left(\sqrt{\frac{0.06 \cdot \frac{h}{t_{f.max}}}{\lambda_{c.z} + \frac{t_{f.max}}{t_{f.min}}}}, 1\right) = 0.707$$

SS-EN 1993-1-1:2022 eq. 8.87:

Slenderness correction factor

$k_c := 0.94$

SS-EN 1993-1-1:2022 tab. 8.6:

Modified slenderness

$\lambda_{c.z.mod} := k_c \cdot \beta_c \cdot \lambda_{c.z} = 0.729$

SS-EN 1993-1-1:2022 eq 8.86:

Imperfection factor, curve d:

$\alpha := 0.76$

SS-EN 1993-1-1:2022 tab. 8.2

Buckling curve

$$\phi := 0.5 \cdot \left(1 + \alpha \cdot \left(\lambda_{c.z.mod} - 0.2\right) + {\lambda_{c.z.mod}}^2\right) = 0.966$$

SS-EN 1993-1-1 eq. 8.74:

$$\chi_{c.z} := min\left(\frac{1}{\phi + \sqrt{\phi^2 - {\lambda_{c.z.mod}}^2}}, 1\right) = 0.625$$

SS-EN 1993-1-1 eq. 8.73:

Bending resistance

$$W_{a.y} := min\left(\frac{I_{a.y}}{z_{a.NA}}, \frac{I_{a.y}}{h_{steel} - z_{a.NA}}\right) = 0.023\ m^3$$

Lateral tortional buckling capacity

$$M_{b.Rd.LT} := \chi_{c.z} \cdot W_{a.y} \cdot \frac{min\left(f_{y.fo}, f_{y.w}, f_{y.fu}\right)}{\gamma_{M1}} = 4.879\ MN \cdot m$$

SS-EN 1993-1-1 eq. 8.84

Bending moment form Brigade analysis construction stage

Check capacity

$$\eta_{b.G1.1.LT} := \frac{M_{Ed.G1.1}}{M_{b.Rd.LT}} = 0.539$$

$$Check_{b.G1.1.LT} := \text{if}\left(\eta_{b.G1.1.LT} < 1, \text{“Ok”}, \text{“NOT OK”}\right) = \text{“Ok”}$$

F4.2 Analysis in G1.2

F4.2.1 Calculate stresses in bending

Load effects obtained from Brigade analysis

$M_{Ed.G1.2} := -421\ kN \cdot m$

Stresses in the steel girder in stage G1.2

Steel stresses in top

$$\sigma_{a.G1.2.top} := \frac{M_{Ed.G1.2}}{I_{y.L}} \cdot \left(t_c - z_{tp.L}\right) = 5.57\ MPa$$

Steel stresses in bottom

$$\sigma_{a.G1.2.bot} := \frac{M_{Ed.G1.2}}{I_{y.L}} \cdot \left(h_{tot} - z_{tp.L}\right) = -6.843\ MPa$$

Stresses in concrete slab in stage G2

$$\sigma_{concrete.G1.2} := \frac{1}{n_L} \frac{M_{Ed.G1.2}}{I_{y.L}} \cdot \left(-z_{tp.L}\right) = 0.434\ MPa$$

F4.3 Analysis in G2

F4.3.1 Calculate stresses in bending

Load effects obtained from Brigade analysis

$M_{Ed.G2} := 1243\ kN \cdot m$

Stresses in the steel girder in stage G2

Steel stresses in top

$$\sigma_{a.G2.top} := \frac{M_{Ed.G2}}{I_{y.L}} \cdot \left(t_c - z_{tp.L}\right) = -16.447\ MPa$$

Steel stresses in bottom

$$\sigma_{a.G2.bot} := \frac{M_{Ed.G2}}{I_{y.L}} \cdot \left(h_{tot} - z_{tp.L}\right) = 20.204\ MPa$$

Stresses in concrete slab in stage G2

$$\sigma_{concrete.G2} := \frac{1}{n_L} \frac{M_{Ed.G2}}{I_{y.L}} \cdot \left(-z_{tp.L}\right) = -1.281\ MPa$$

F4.4 Analysis of traffic loads

F4.4.1 Calculate stresses in bending

Load effects obtained from Brigade analysis

$M_{Ed.Tra.Char} := 6031 \; kN \cdot m$

Stresses in the steel girder in stage G2

Steel stresses in top

$$\sigma_{a.Tra.Char.top} := \frac{M_{Ed.Tra.Char}}{I_{y.L}} \cdot \left(t_c - z_{tp.L}\right) = -79.799 \; MPa$$

Steel stresses in bottom- tension

$$\sigma_{a.Tra.Char.bot} := \frac{M_{Ed.Tra.Char}}{I_{y.L}} \cdot \left(h_{tot} - z_{tp.L}\right) = 98.028 \; MPa$$

Stresses in concrete slab in stage G2

$$\sigma_{concrete.Tra.Char} := \frac{1}{n_L} \frac{M_{Ed.Tra.Char}}{I_{y.L}} \cdot \left(-z_{tp.L}\right) = -6.218 \; MPa$$

F4.5 Check bending in ULS

F4.5.1 Combination factors

$\gamma_G = 1.35$ $\quad$ $\gamma_{G.favorable} := 1$

$\gamma_{G.pave} := 1.1 \cdot \gamma_G = 1.485$ $\quad$ *TSFS 2018:57 5 kap. 4 §*

$\gamma_Q := 1.5$

F4.5.2 Total bending stresses in ULS

Final compressive stresses in concrete

$$\sigma_{concrete.tot.c} := \gamma_{G.pave} \cdot \sigma_{concrete.G2} + \gamma_{G.favorable} \cdot \sigma_{concrete.G1.2} + \gamma_Q \cdot \sigma_{concrete.Tra.Char}$$

$\sigma_{concrete.tot.c} = -10.795 \; MPa$

Final top stresses in steel girder

$$\sigma_{a.tot.top} := \gamma_{G.pave} \cdot \sigma_{a.G2.top} + 1 \cdot \sigma_{a.G1.2.top} + \gamma_G \cdot \sigma_{a.G1.1.top} + \gamma_Q \cdot \sigma_{a.Tra.Char.top}$$

$\sigma_{a.tot.top} = -290.891 \; MPa$

Final bottom stresses in steel girder

$$\sigma_{a.tot.bot} := \gamma_{G.pave} \cdot \sigma_{a.G2.bot} + 1 \cdot \sigma_{a.G1.2.bot} + \gamma_G \cdot \sigma_{a.G1.1.bot} + \gamma_Q \cdot \sigma_{a.Tra.Char.bot}$$

$\sigma_{a.tot.bot} = 239.371 \; MPa$

F4.5.3 Check bending capacity of cross section in ULS

Bending capacity of steel section according to SS-EN 1994-1-1 6.2.1.5 (2)

$$\eta_{b.steel.top} := \left| \frac{\sigma_{a.tot.top}}{f_{y.fo}} \right| = 0.843 \qquad \eta_{b.steel.bot} := \left| \frac{\sigma_{a.tot.bot}}{f_{y.fu}} \right| = 0.715$$

$$\eta_{b.steel} := \max\left(\eta_{b.steel.top}, \eta_{b.steel.bot}\right) = 0.843$$

$$Check_{b.steel} := \text{if}\left(\eta_{b.steel} < 1, \text{“Ok”}, \text{“NOT OK”}\right) = \text{“Ok”}$$

Bending capacity of concrete slab according to SS-EN 1994-1-1 6.2.1.5 (2)

$$\eta_{b.concrete} := \frac{\left|\sigma_{concrete.tot.c}\right|}{f_{cd}} = 0.463$$

$$Check_{b.concrete} := \text{if}\left(\eta_{b.concrete} < 1, \text{“Ok”}, \text{“NOT OK”}\right) = \text{“Ok”}$$

F4.6 Check shear in ULS

According to SS-EN 1994-2 6.2.2.3, the shear buckling resistance should be taken as the resistance of the steel section. Also, since the sectional properties should be taken as those of just the steel girder, shear is only checked for the steel section in ULS and does not require multiple stages-super positioning of stresses

Shear force from Brigade analysis

$$V_{Ed.G1.1} := \left(g_{k.a} + g_{k.G1.1}\right) \cdot \frac{L_{span}}{2} = 389.778\ \boldsymbol{kN}$$

$$V_{Ed.G1.2} := -62.18\ \boldsymbol{kN}$$

$$V_{Ed.G2} := 183.6\ \boldsymbol{kN}$$

$$V_{Ed.Tra.Char} := 939.6\ \boldsymbol{kN}$$

$$V_{Ed.ULS} := \gamma_G \cdot V_{Ed.G1.1} + 1 \cdot V_{Ed.G1.2} + \gamma_{G.pave} \cdot V_{Ed.G2} + \gamma_Q \cdot V_{Ed.Tra.Char} = \left(2.146 \cdot 10^3\right)\ \boldsymbol{kN}$$

Check risk of shear buckling (SB)

$\eta := 1.2$ *SS-EN 1993-1-5:2024, 7.1 (2)*

$A_v := \eta \cdot h_w \cdot t_w$ *SS-EN1993-1-1 2022 8.2.6 e)*

$$SB := \text{if } \frac{h_w}{t_w} < 72\,\frac{\varepsilon_w}{\eta} \;\; \| \text{“No risk of SB”} \;\; \text{else} \;\; \| \text{“Risk of SB”} = \text{“Risk of SB”}$$

SS-EN 1993-1-5:2024, 7.1 (2)

Determining shear buckling coefficient

Assume no longitudinal stiffeners and transverse stiffeners at supports:

$$\lambda_w := \frac{h_w}{86.4 \cdot t_w \cdot \varepsilon_w}$$

SS-EN 1993-1-5:2024 eq. 7.5

Factor of contribution from web to shear buckling resistance *SS-EN 1993-1-5:2024 tab. 7.1*

Assume rigid end posts:

$$\chi_w := \text{if } \lambda_w < \frac{0.83}{\eta} \;\; \| \eta \;\; \text{else if } \frac{0.83}{\eta} \le \lambda_w < 1.08 \;\; \| \frac{0.83}{\lambda_w} \;\; \text{else if } \lambda_w \ge 1.08 \;\; \| \frac{1.37}{0.7+\lambda_w} = 0.798$$

Shear capacity

$$V_{Rd} := \text{if } SB = \text{“No risk of SB”}$$

$$\quad V_{pl.Rd} \leftarrow \frac{A_v \cdot \frac{f_{y.w}}{\sqrt{3}}}{\gamma_{M0}}$$ *SS-EN1993-1-1:2022 eq. 8.23*

$$\quad V_{Rd} \leftarrow V_{pl.Rd}$$

$$\text{else if } SB = \text{“Risk of SB”}$$

$$\quad V_{bw.Rd} \leftarrow \frac{\chi_w \cdot f_{y.w} \cdot h_w \cdot t_w}{\sqrt{3} \cdot \gamma_{M1}}$$ *SS-EN 1993-1-5:2024 eq. 7.2*

$$\quad V_{bf.Rd} \leftarrow 0\ kN$$ *Assume no contribution from flanges*

$$\quad V_{b.Rd} \leftarrow min\left(V_{bw.Rd} + V_{bf.Rd}, \frac{\eta \cdot f_{y.w} \cdot h_w \cdot t_w}{\sqrt{3} \cdot \gamma_{M1}}\right)$$ *SS-EN 1993-1-5:2024 eq. 7.1*

$$\quad V_{Rd} \leftarrow V_{b.Rd}$$

$V_{Rd} = (2.344 \cdot 10^3)\ kN$

Check shear capacity utilization ratio

$$\eta_{V.ULS} := \frac{V_{Ed.ULS}}{V_{Rd}} = 0.916$$

$$Check_{shear} := \text{if}\left(\eta_{V.ULS} < 1, \text{“Ok”}, \text{“NOT OK”}\right) = \text{“Ok”}$$

F4.7 Fatigue Analysis

Fatigue is is checked in the following regions, where each region is denoted with A-D

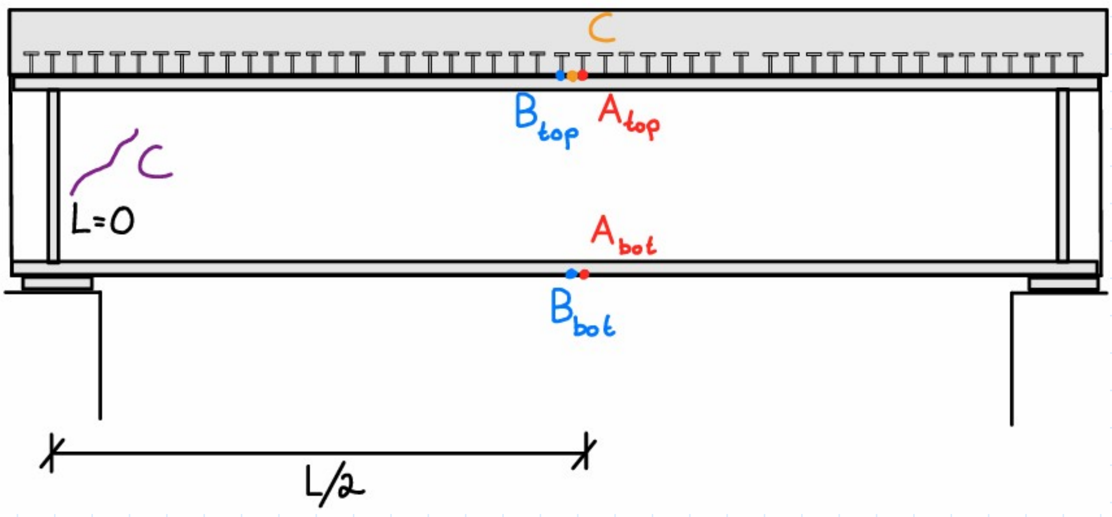

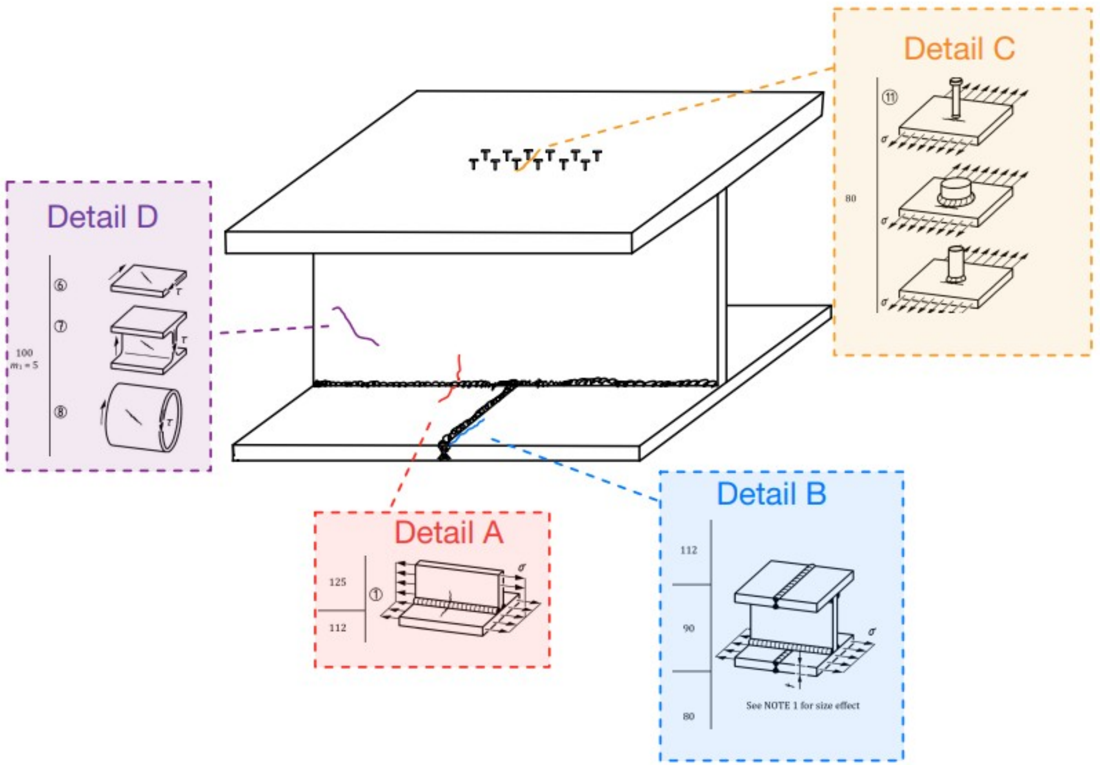

The fatigue assessment is performed firstly by the use of the damage equivalence factor λ according to *SS-EN 1993-2:2006 9.5.2*

Length of influence line according to SS-EN 1993-2:2006 9.5.2 (2) since simply supported:

$L_i := L_{span} = 27\ m$

Factor for damage effect of traffic

$\lambda_1 := \max\left(2.55 - 0.7\ \frac{L_i - 10\ m}{70\ m}, 1.85\right) = 2.38$ *SS-EN 1993-2:2006 Figure 9.5*

Reference values according to *SS-EN 1993-2:2006 9.5.2 (3)*

$Q_0 := 480\ kN$ $N_0 := 0.5 \cdot 10^6$

Factor for traffic volume, according to *SS-EN 1993-2:2006 eq. 9.10*

$\lambda_2 := \frac{Q_{m1}}{Q_0} \cdot \left(\frac{N_{Obs}}{N_0}\right)^{\left(\frac{1}{5}\right)} = 0.927$

Factor for design life of bridge (120 years) according to *SS-EN 1993-2:2006 Table 9.2*

$\lambda_3 := 1.037$

Factor for traffic on other lanes according to *TSFS 2018:57 3§ 14*

$\lambda_4 := 1$

Maximum λ value according to *SS-EN 1993-2:2006 Figure 9.6*

$\lambda_{max} := \max\left(2.5 - 0.5 \cdot \frac{L_i - 10\ m}{15\ m}, 2\right) = 2$

Calculate λ factor according to *SS-EN 1993-2:2006 eq. 9.9*

$\lambda := min\left(\lambda_1 \cdot \lambda_2 \cdot \lambda_3 \cdot \lambda_4, \lambda_{max}\right) = 2$

Partial factors for fatigue assessment

$\gamma_{Mf} = 1.35$ *SS-EN 1993-1-9:2025 Table 5.1*

$\gamma_{Ff} = 1$ *SS-EN 1993-2:2006 9.3 (1)*

F4.7.1 Check for fatigue in steel girder flange to web weld, detail A

125	① 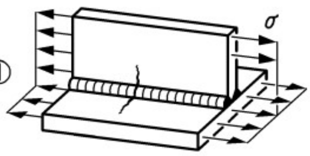		① Automatic or fully mechanized butt welds, welded from both sides, without stop-starts	None.
112			as aforementioned, but with stop-starts	

Detail category 1, *SS-EN 1993-1-9:2025 Table 10.3*

$\Delta\sigma_{c.A} := 112\ MPa$

Maximum bending moment from Brigade analysis, moment in mid-span

$M_{max.fat} := 2232\ kN \cdot m$

Calculate stresses at the section between web and flange

$$\Delta\sigma_{A.top} := \frac{M_{max.fat}}{I_{y.L}} \cdot \left(t_c + t_{fo} + h_w - z_{tp.L}\right) = 33.407\ MPa$$

$$\Delta\sigma_{A.bot} := \frac{M_{max.fat}}{I_{y.L}} \cdot \left(z_{tp.L} - t_c - t_{fo}\right) = 27.798\ MPa$$

Equivalent stress range

$$\Delta\sigma_{E.A.top} := \lambda \cdot \Delta\sigma_{A.top} = 66.814\ MPa$$

$$\Delta\sigma_{E.A.bot} := \lambda \cdot \Delta\sigma_{A.bot} = 55.595\ MPa$$

Check for fatigue

$$\eta_{fat.A.top} := \frac{\gamma_{Ff} \cdot \gamma_{Mf} \cdot \Delta\sigma_{E.A.top}}{\Delta\sigma_{c.A}} = 0.805 \qquad \eta_{fat.A.bot} := \frac{\gamma_{Ff} \cdot \gamma_{Mf} \cdot \Delta\sigma_{E.A.bot}}{\Delta\sigma_{c.A}} = 0.67$$

$$\eta_{fat.A} := \max\left(\eta_{fat.A.top}, \eta_{fat.A.bot}\right) = 0.805$$

$$\text{if}\left(\eta_{fat.A} < 1, \text{“ok!”}, \text{“NOT OK!”}\right) = \text{“ok!”}$$

F4.7.2 Check for fatigue in steel girder flange, detail B

Detail category [a]	Constructional detail		Symbol	Description	Supplementary Requirements
112	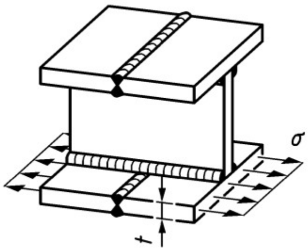 See NOTE 1 for size effect	⑦ 		⑦ Flange and web splices in plate girders, welded from both sides, ground flush	⑦⑧⑨: No application to full cross-section joint. Splices should be welded before assembly of girder. Longitudinal weld should be checked using Table 10.3 ⑦: see ①. ⑧: see ②. ⑨: see ③.
90		⑧ 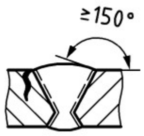		⑧ as aforementioned, but as-welded with flank angle ≥ 150°	
80		⑨ 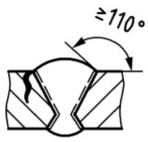		⑨ as aforementioned, but as-welded, with flank angle ≥ 110°	

Detail category 9, *SS-EN 1993-1-9:2025 Table 10.3 ground flush*

$\Delta\sigma_{c.B\_} := 112\ MPa$

Size effect over flange

$$k_{s.fo} := \left(\frac{25}{\frac{t_{fo}}{mm}}\right)^{0.2}$$

Size effect under flange

$$k_{s.fu} := \left(\frac{25}{\frac{t_{fu}}{mm}}\right)^{0.2}$$

Corrected $\Delta\sigma_{c.B}$

$$\Delta\sigma_{c.B.fo} := k_{s.fo} \cdot \Delta\sigma_{c.B\_} = 108.724\ MPa$$

$$\Delta\sigma_{c.B.fu} := k_{s.fu} \cdot \Delta\sigma_{c.B\_} = 98.301\ MPa$$

Maximum bending moment from Brigade analysis, moment in mid-span

$$M_{max.fat} = \left(2.232 \cdot 10^{3}\right)\ kN \cdot m$$

Calculate stresses at bottom fiber in bottom flange

$$\Delta\sigma_{B.fu} := \frac{M_{max.fat}}{I_{y.L}} \cdot \left(t_c + t_{fo} + h_w + t_{fu} - z_{tp.L}\right) = 36.279\ MPa$$

Calculate stresses at top fiber in top flange

$$\Delta\sigma_{B.fo} := \frac{M_{max.fat}}{I_{y.L}} \cdot \left(z_{tp.L} - t_c\right) = 29.533\ MPa$$

Equivalent stress range

$\Delta\sigma_{E.B.fu} := \lambda \cdot \Delta\sigma_{B.fu} = 72.558\ MPa$ $\Delta\sigma_{E.B.fo} := \lambda \cdot \Delta\sigma_{B.fo} = 59.065\ MPa$

Check for fatigue

$$\eta_{fat.B.top} := \frac{\gamma_{Ff} \cdot \gamma_{Mf} \cdot \Delta\sigma_{E.B.fo}}{\Delta\sigma_{c.B.fo}} = 0.733 \qquad \eta_{fat.B.bot} := \frac{\gamma_{Ff} \cdot \gamma_{Mf} \cdot \Delta\sigma_{E.B.fu}}{\Delta\sigma_{c.B.fu}} = 0.996$$

$\eta_{fat.B} := \max\left(\eta_{fat.B.top}, \eta_{fat.B.bot}\right) = 0.996$ $\text{if}\left(\eta_{fat.B} < 1, \text{“ok!”}, \text{“NOT OK!”}\right) = \text{“ok!”}$

F4.7.3 Check for fatigue in steel girder top flange around studs , detail C

80	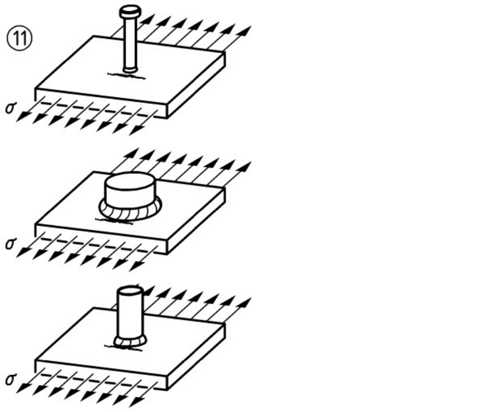		⑪ Plates, flanges or webs subject to normal stress with small attachment (such as welded shear stud, bushings etc.) of any shape at their surfaces Note: It applies ℓ ≤ 50mm for small attachments. See ⑦ for definition of ℓ.	Δσ should be calculated using normal stress in parent metal neglecting the small attachment.
ª Slope parameter of fatigue resistance curve should be set $m_1 = 3$ unless otherwise stated in detail category.				

Detail category 11, *SS-EN 1993-1-9:2025 Table 10.3*

$\Delta\sigma_{c.C} := 80\ MPa$

Maximum bending moment from Brigade analysis, moment in mid-span

$M_{max.fat} = \left(2.232 \cdot 10^{3}\right)\ kN \cdot m$

Calculate stresses at top fiber in over flange

$$\Delta\sigma_{C} := \frac{M_{max.fat}}{I_{y.L}} \cdot \left(z_{tp.L} - t_{c}\right) = 29.533\ MPa$$

Equivalent stress range

$\Delta\sigma_{E.C} := \lambda \cdot \Delta\sigma_{C} = 59.065\ MPa$

Check for fatigue

$$\eta_{fat.C} := \frac{\gamma_{Ff} \cdot \gamma_{Mf} \cdot \Delta\sigma_{E.C}}{\Delta\sigma_{c.C}} = 0.997$$

$\text{if}\left(\eta_{fat.C} < 1, \text{“ok!”}, \text{“NOT OK!”}\right) = \text{“ok!”}$

F4.7.4 Check fatigue in the shear of web, detail D

100 $m_1 = 5$	⑥ ⑦ ⑧ 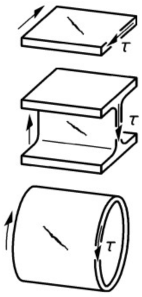 	Rolled or extruded products subject to shear stress: ⑥ to ⑧ same description as for ① to ③	For shear loads in webs of any section class, Formula (8.25) of EN 1993-1-1:2022 should be used to calculate Δτ.	⑥, ⑦ and ⑧: Requirements as for ① to ③ in detail category 125.
For ① to ⑧ made of weathering steel the next lower detail category of Figure 8.1 should be used, but not higher than Detail Category 140. For ① to ⑧ with hot dip galvanizing the next lower detail category of Figure 8.1 should be used, but not higher than Detail Category 140.				

Detail category, Detail 7 SS-EN 1993-1-9:2025

$\Delta\tau_{c.D} := 100\ MPa$

Neutral axis of steel section

$z_{a.NA} = 756.509\ mm$

Height steel section

$h_{steel} = 1.1\ m$

Effective equivalent area of concrete

$A_{c.ekv.L} = 0.037\ m^2$

1st order of inertia (long term) for the section above N.A.

$$S_{upper} := A_{fo} \cdot \left(z_{a.NA} - \frac{t_{fo}}{2}\right) + t_w \cdot \left(z_{a.NA} - t_{fo}\right) \cdot \frac{\left(z_{a.NA} - t_{fo}\right)}{2} = \left(1.78 \cdot 10^7\right)\ mm^3$$

2nd moment of inertia (long term) for the section between top flange and concrete slab

$I_{a.y} = 0.018\ m^4$

Maximum shear force from brigade analysis of the fatigue load combinations

$\Delta V_{fat.max} := 404.9\ kN$

Calculate shear stresses

$$\Delta\tau_D := \frac{\Delta V_{fat.max} \cdot S_{upper}}{I_{a.y} \cdot t_w} = 29.185\ MPa$$

Equivalent stress range

$\Delta\tau_{E.D} := \lambda \cdot \Delta\tau_D = 58.371\ MPa$

Check for fatigue

$$\eta_{fat.D} := \frac{\gamma_{Ff} \cdot \gamma_{Mf} \cdot \Delta\tau_{E.D}}{\Delta\tau_{c.D}} = 0.788$$

$\text{if}\left(\eta_{fat.D} < 1, \text{“ok!”}, \text{“NOT OK!”}\right) = \text{“ok!”}$

F5 Summary of utilization ratios and material quantities

F5.1 Cross sectional class (CSC) of sections

Steel girder web

$CSC_{w.a} = 4$

Steel top flange

$CSC_{fo.a} = 3$

Composite section web

$CSC_{w.comp} = 3$

F5.2 Utilization ratios

Bending in G1.1

Top

$\eta_{b.G1.1.top} = 0.442$

Bottom

$\eta_{b.G1.1.bot} = 0.206$

LT buckling in stage G1.1

$\eta_{b.G1.1.LT} = 0.539268$ with a bracing cc of $cc_{bracings} = 13.5\ m$

Concrete stresses in bending

$\eta_{b.concrete} = 0.463$

Steel stresses in bending ULS

Top

$\eta_{b.steel.top} = 0.843$

Bottom

$\eta_{b.steel.bot} = 0.715$

Shear capacity in ULS

$\eta_{V.ULS} = 0.916$

Fatigue

Detail A

Top

$\eta_{fat.A.top} = 0.805$

Bottom

$\eta_{fat.A.bot} = 0.67$

Detail B

Top

$\eta_{fat.B.top} = 0.733$

Bottom

$\eta_{fat.B.bot} = 0.99646$

Detail C

$\eta_{fat.C} = 0.997$

Detail D

$\eta_{fat.D} = 0.788$

F5.3 Total material quantities

Concrete

$ton_{concrete} := t_c \cdot w_{deck} \cdot \rho_{c.dry} \cdot L_{span}$

$ton_{concrete} = 186.3\ tonne$

Steel

$ton_{steel} := n_{girder} \cdot \left(A_{steel} \cdot \rho_{steel} \cdot L_{span}\right)$

$ton_{steel} = 73.01\ tonne$

Appendix G: Estimates of steel consumption using empirical formulas

G Steel consumption from empirical estimates

G1 Empirical formulas (Vayas et. al, 2015)

OBS: For twin-girder bridges!

$L := 27\ m$ $\qquad b_c := 12\ m$

$L_{eq} := 1.4 \cdot L = 37.8\ m$ For isostatic spans (statically determinate spans)

$$g_{vayas} := \left(63 + 0.9\ \frac{L_{eq}^{\ 1.2}}{m^{1.2}} \left(1.34 - \frac{b_c}{40\ m}\right) + \frac{L_{eq}}{4\ m}\right) \frac{kg}{m^2} = 145.609\ \frac{kg}{m^2}$$

$G_{vayas} := g_{vayas} \cdot L \cdot b_c = 47.177\ tonne$

G2 Steel weight from graph (Collings, 2013)

Approximately 100-150 kg/m2

$$G_{collings} := 150\ \frac{kg}{m^2} \cdot L \cdot b_c = 48.6\ tonne$$

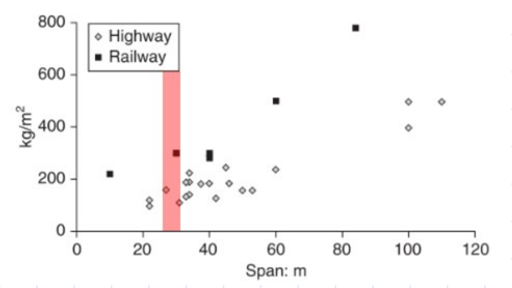

G3 Steel weight from graph (Chen and Duan, 2013)

OBS: For 30 m span!

Approximately 140-180 kg/m2

$$G_{chen.duan} := 180\ \frac{kg}{m^2} \cdot L \cdot b_c = 58.32\ tonne$$

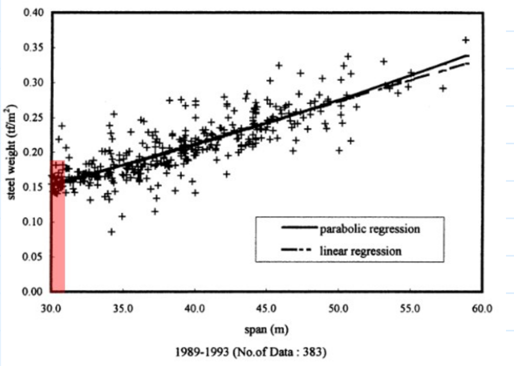

G4 Steel weight from graph (Khatri et al., 2012)

OBS: For 40 m span!

$D := 1.1\ m$

$\frac{L}{D} = 24.545$

Approximately 14 tons per girder

$G_{Khatri} := 14\ ton \cdot 4 = 50.802\ tonne$

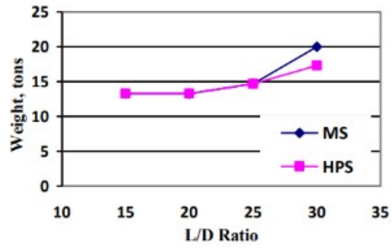

(a) Weights for 40 m span girder

DEPARTMENT OF ARCHITECTURE AND CIVIL ENGINEERING
CHALMERS UNIVERSITY OF TECHNOLOGY
Gothenburg, Sweden 2026
www.chalmers.se

AVANCEZ
1829

CHALMERS
UNIVERSITY OF TECHNOLOGY